UCLouvain

epl

École polytechnique de Louvain

Development of porous biodegradable polymer materials for biological applications

Author: **Marie GOFFIN**
Supervisors: **Sophie DEMOUSTIER, Alain JONAS**
Readers: **Quentin PAPELOER, Evelyne VAN RUYMBEKE**
Academic year 2021–2022
Biomedical Engineering

Abstract

Porous biodegradable organic materials are ideal scaffolds for cell colonization. The ability to 3D print them into any shape offers even more opportunities for tissue engineering and organ rehabilitation. However, one challenge is to provide easy access to 3D printable materials that result in pores with well-controlled sizes, using only biocompatible and sustainable processes.
In this work, a method for the preparation of porous PLLA was described, starting from miscible mixtures of PLLA and a water-soluble polymer (PEG). The composition of the mixture, the molar mass of PEG, the isothermal crystallization temperature, and the crystallization time were the four parameters studied. During its crystallization, PLA repels PEG outside its crystals, leading to the formation of aggregates of PEG within and between PLLA spherulites, from which pores can be formed by dissolving PEG in water. The crystallization and morphology of the semi-crystalline mixture were studied, as well as the evaluation of porosity after dissolution of PEG.
All parameters were found to affect both crystalline morphology and porosity. PEG diffuses out of the spherulites more rapidly and accumulates at their interface at lower molar mass, higher PEG content and higher crystallization temperature; at which the viscosity is higher. However, if the PEG content is too high, the resulting porosity makes the film brittle. The pore size at the surface did not vary much, but the porosity at depth still needs to be investigated. In addition, it remains difficult to establish a protocol with the various parameters that must be chosen to obtain a very accurate porosity.
This work succeed in showing the effect of PEG and important processing parameters on PLA crystallization and porosity. However, the mechanical properties still need to be studied for future perspectives.

Acknowledgements

First of all, I would like to thank my supervisors Prof. Alain Jonas and Prof. Sophie Demoustier for their support and availability throughout the year. They always took the time to organize regular meetings and always encouraged me without putting pressure on me. Their knowledge helped me a lot to complete this work. Thank you for your support, patience, and confidence.

I am particularly grateful to Quentin Papeloer, who was always present and helpful, even before I started my work. Our exchanges were always very constructive and encouraged me throughout my work. He allowed me to progress in a positive and motivating atmosphere. Thank you for your good mood and for the detailed and rapid feedbacks.

I also thank Delphine Magnin for her assistance and help concerning the SEM and Sabine Bebelman for its availability to train me on the FTIR. I also express my gratitude to all the members of the laboratory who provided me with the necessary material or helped me in one way or another.

Many thanks also to Prof. Evelyne Van Ruymbeke for the time you spent reading this work, I hope you will find it enjoyable and interesting.

Last but not least, I also greatly thank my family and friends, especially Alix who accompanied me during these five years. We went through all the emotions together, to finally succeed with great memories.

To all, I offer my thanks, respect and gratitude. I wish you all the best.

Contents

Acronyms

ATR Attenuated Total Reflectance.

DSC Differential Scanning Calorimetry.

FTIR Fourier Transform Infrared Spectroscopy.

LA Lactic acid.

LM Low Magnification.

$\mathbf{M}_n$ Number-average molar mass.

$\mathbf{M}_w$ Weight-average molar mass.

MD Medical Device.

MM Molar mass.

PCL Poly(caprolactone).

PDLA Poly(D-lactic acid).

PEG Poly(ethylene glycol).

PEO Poly(ethylene oxide).

PET Poly(ethylene terephthalate).

PGA Poly(glycolic acid).

PLA Poly(lactic acid).

PLLA Poly(L-lactic acid).

POM Polarized Optical Microscopy.

PP Poly(propylene).

PS Poly(styrene).

ROP Ring-Opening Polymerization.

SEI Secondary Electron Imaging.

SEM Scanning Electron Microscopy.

$\mathbf{T}_c$ Crystallization temperature.

T_g Glass transition temperature.

T_m Melting temperature.

T_{cc} Cold crystallization temperature.

TE Tissue Engineering.

TGA Thermogravimetric analysis.

T°_m Thermodynamic melting temperature.

Chapter 1

Introduction

In the past decades, tissue engineering (TE) has emerged as an important new topic in biomedicine. It has shown great promise in providing biological alternatives to harvested tissues, implants, and prostheses. TE is based on the idea of isolating cells from a patient, growing their population in a cell culture, and seeding them onto a scaffold. The resulting tissue-engineered construct is then transplanted to the same patient to take over the function of the damaged tissue. This requires a highly porous artificial extracellular matrix to host the cells and control their growth and tissue regeneration in three dimensions. It is also desirable to synchronize the degradation of the scaffold with its replacement by a natural tissue made of cells. Therefore, scaffolds must meet many requirements: they must be biocompatible both in bulk and in degraded form, and should have appropriate mechanical properties to provide the correct stress environment for the new tissues. Physical integrity and stability are necessary to support the sterilization process and to be stored for a specified period of time. In addition, porosity and permeability are required to allow cells and nutrients penetration, and they must have appropriate surface structure and chemistry for cell attachment [1]. The external geometry, surface topography (i.e., roughness, hydrophobicity, etc.), and microstructure of the scaffold (i.e., pore size, porosity, and interconnectivity of pores) affect the interactions between cells and the scaffold. Therefore, the first step of tissue engineering begins with the fabrication of a three-dimensional porous scaffold in addition to the selection of the appropriate material.

On the one hand, metals and ceramics have contributed to great advances in the field of orthopedic tissue replacement. However, they are not biodegradable and their processability is limited [2]. On the other hand, polymers have gained interest and are probably the most versatile materials used in the fabrication of biomedical devices. Polymers are easier to process and allow proper control of architectural parameters in scaffold fabrication (i.e., pore size and shape, porosity, pore connectivity, and surface area), which are key elements for seeding, migration, growth, mass transfer, and tissue formation [3]. Manipulating their physicochemical properties (i.e., microstructure, degradation rate, mechanical properties, porosity, etc.) makes them even more interesting.

There are numerous fabrication techniques for developing polymer-based porous scaffolds: 3D printing, solvent-based techniques such as solvent casting, gas foaming, phase separation, and others. In recent years, 3D printing has become an emerging technology that is attracting a lot of interest due to its ability to produce scaffolds that can be very well controlled in terms of their mechanical and morphological properties [3].

Natural polymers such as polysaccharides and proteins have been used to repair nerves, skin, cartilage, and bone. Although they most closely simulate the natural cellular environment, significant batch-to-batch variation in biological tissue isolation limits their applications. Their poor mechanical performance is also a common drawback. To address these problems, many synthetic polymers, such as polyesters and others, have been developed [1].

Synthetic biodegradable polylactones such as polylactic acid (PLA), polyglycolic acid (PGA), polycaprolactone (PCL), and their copolymers are widely used because of their excellent biocompatibility and are approved by the Food and Drug Administration ([4]. These biodegradable synthetic polymers are most commonly used in TE. They degrade by water absorption and hydrolysis, as well as by enzymatic cleavage of the polymer chain.

PLA is the most commonly used synthetic biomaterial in various biomedical applications, due to its renewability, biodegradability, biocompatibility, mechanical strength, and processability in 3D printing. Although it has good mechanical properties comparable to those of conventional petroleum-based polymers (e.g., polystyrene (PS), polyethylene terephthalate (PET), and polypropylene (PP)), PLA has some drawbacks, such as its low crystallization rate, low hydrophobicity, low impact strength, and slow degradation rate. A very common and cost-effective approach to overcome the above limitations of PLA is polymer blending. By controlling the ratio of PLA to secondary blended polymer, or by introducing functional nanoparticles, the development of PLA blend systems could expand the applications of PLA in commodities and engineering [5].

Polyethylene glycol (PEG) is widely used in biomedical applications due to its high biocompatibility, satisfactory safety, hydrophilicity, etc. It is frequently used in polymer blends, especially with PLA. It not only affects the physical and mechanical properties, but also the surface properties such as hydrophobicity. In addition, PEG has been used as a porogen in many works. For example, when a solvent is evaporated, two phases are completely separated, and porous structures are formed by removing PEG in water.

This thesis aims to develop a methodology to fabricate porous polymeric materials for future biomedical applications. Based on previous research and the work of Q.Papeloer, this work investigates blends of PLA and PEG.
The thesis is divided into six chapters, including the introduction. Chapter 2 provides a comprehensive overview of what has already been done in the field and what should be investigated further. It includes two sections on the polymers used in this framework, namely PLA and PEG. For each of these polymers, the properties and applications are described to understand their interest in this work. Another section deals with the improvement of the properties of the polymers, leading to a section on PLA/PEG blends, where the work and the discoveries already made about these polymers in a blend are presented. A last section explains the different steps in the crystallization process of a polymer, which are essential to understand the work.
Next, the context, objectives, and overall strategy are presented in Chapter 3. Then, the experimental sections will include the description of the materials, sample preparation, and characterization techniques used in Chapter 4: Fourier Transform Infrared Spectroscopy (FTIR), Polarized Optical Microscopy (POM), and Scanning Electron Microscopy (SEM). Chapter 5 contains the experimental results obtained based on the previous chapter. These results are then discussed and analyzed. Appendices 6 are provided as additional support to this chapter. The conclusions and perspectives conclude this thesis in Chapter 6.

Chapter 2

State of the Art

2.1 PLA

2.1.1 Overview

Polylactic acid (PLA) is a synthetic biodegradable and aliphatic polyester derived from lactic acid produced from natural resources such as corn starch or sugar cane.
PLA products can be recycled after use either by remelting and reprocessing the material or by hydrolysis to lactic acid, which occurs naturally in our body. Compared to other biopolymers, the production of PLA has numerous advantages [6]:

- **Eco-friendly**: PLA is derived from renewable resources (e.g., corn, wheat, rice), biodegradable, recyclable, compostable and its production consumes carbon dioxide.
- **Biocompatibility**: in biomedical applications, the material should not produce toxic or carcinogenic effects and the degradation products should not interfere with tissue healing. PLA hydrolyzes to constituent easily excreted when implanted in living organisms. Plus, PLA degradation by-products are non-toxic (at a lower composition) making it a natural choice for biomedical applications. The FDA has also approved PLA for direct contacting with biological fluids [7].
- **Processability**: PLA has better thermal processability compared to other biocompatible polymers such (e.g., PCL and PEG). It can be processed by injection molding, film extrusion, blow molding, thermoforming, fiber spinning, and film forming.

However, there are limitations in some applications:

- **Toughness**: PLA is a rather brittle material with less than 10% elongation at break. Its poor toughness limits its use in applications that require plastic deformation at high stress level.
- **Slow degradation rate**: degradation rate depends on the crystallinity of the polymer and other parameters, the degradation is done through hydrolysis of backbone ester groups and can be catalyzed by enzymes. A slow degradation rate can be a barrier with respect to the disposability for biomedical applications.
- **Hydrophobicity**: the hydrophobicity of PLA results in low cell affinity and may induce an inflammatory response from the host.
- **Lack of reactive side-chain groups**: PLA is an inert material with no reactive side-groups. Needs for chemical and physical modification are therefore frequent to improve its properties as well as to control surface properties (i.e., hydrophobicity, roughness, reactive groups).

Lactic acid (LA) is the most abundant hydroxycarboxylic acid due to its versatile uses in the food, pharmaceutical and textile industries, and as a monomer for PLA production [8]. Lactic acid can exists in two enantiomers: L- and D-lactic acid (Figure 2.1).

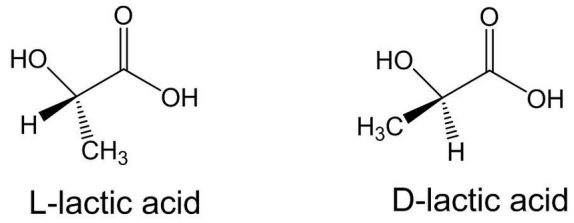

Figure 2.1: Enantiomers of lactic acid [9]

It can be produced by chemical synthesis or fermentation. About 90% of the total lactic acid produced worldwide is produced by bacterial fermentation. On the one hand, chemical synthesis of lactic acid provide the racemic mixture of D-and L-lactic acid. On the other hand, interest in fermentative production of lactic acid has increased due to the prospect of environmental friendliness and the use of renewable resources instead of petrochemicals [2].

Due to the chirality of LA, PLA can occur in three stereoisomers: Poly (L-lactide) (PLLA), Poly (D-lactide) (PDLA), and Poly (D,L-lactide) (PDLLA). Isotactic and optically active PLLA and PDLA are crystalline, while atactic and optically inactive PDLLA is amorphous. L-isomer is the main form of PLA obtained from biological sources by plant fermentation. The raw materials are very cheap and the degradation of PLLA is harmless, while D-lactic acid is harmful to the human body and more expensive [10]. Therefore, PLLA is the main stereoisomer used, PDLA is generally used only for research.

PLA can be synthesized from LA by various polymerization process including: polycondensation, ring opening polymerization or by direct methods such as azeotopic dehydration and enzymatic polymerization (Figure 2.2).

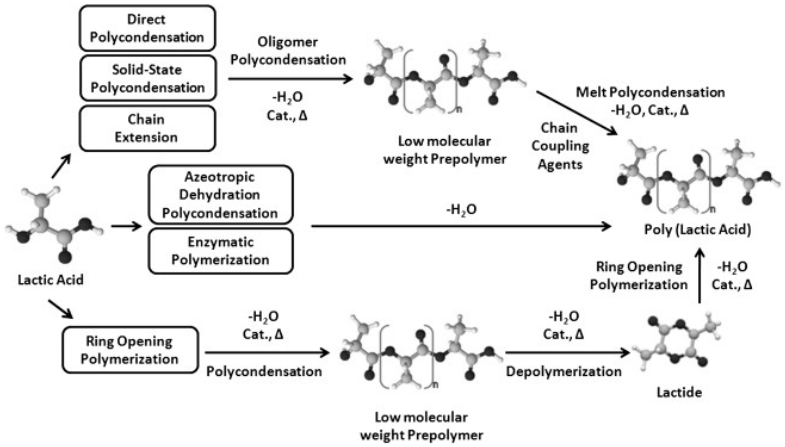

Figure 2.2: Synthesis processes of PLA [11]

Ring-opening polymerization: ring-opening polymerization (ROP) of lactide is the most common method to produce high molar mass (MM) PLA (M_w > 100 000 g/mol) [12] by controlling the residence time and temperatures in combination with the type and concentration of catalyst. The process is carried out in three steps: polycondensation, depolymerization and ring-opening polymerization (Figure 2.2).

Direct Polycondensation: the presence of both a hydroxyl and a carboxyl group in lactic acid allows direct conversion to polyester through a polycondensation reaction [4]. It has fewer manufacturing steps, lower cost, and is easier to handle compared to ROP. In this process, solvents and/or catalysts are used and it is carried out under high vacuum and high temperature to remove the water produced during condensation. However, conventional condensation polymerization of lactic acid does not sufficiently increase the molar mass sufficiently, resulting in a maximum M_n of 3000 for the polycondensation of aqueous DL-lactic acid and up to 6500 g/mol for pure L-lactide [4]. In a solvent-free system, it is difficult to achieve high molar mass. Therefore, the use of coupling agents or esterification-promoting adjuvants is required, adding cost and complexity.

Azeotopic dehydration: in the azeotopic dehydration, removal of water is easier and high MM PLA can be reached. PLA is synthesized by heavy metal catalysed ROP of lactide from fermentative LA. However, traces of heavy metal residues remain, which are unfavorable for certain applications.

Enzymatic polymerization: enzymatic polymerization is an environmentally friendly process and can provide adequate control of the polymerization process. Compared to the above chemical processes, extremely pure monomers and high temperatures are not required to avoid side reactions. Fine-structured polymers can be synthesized from low-cost raw materials by a specific enzymatic reaction, which is a very interesting alternative to other methods [13]. In most of the recently published works, enzymatic polymerization via ROP is the preferred synthesis method. The highest molar mass of enzymatically synthesized PLA grades (M_n 78 100 g/mol) was obtained by Mälberg et al. [14].

2.1.2 Physical properties

The properties of PLA depend on the isomers, processing temperature, annealing time, and molar mass. The stereochemistry and thermal history affect the crystallinity and directly the properties in general. The physical and mechanical properties of PLA affect the stability, processability, degradation, miscibility with other polymers, aging and other requirements depending on the application [6].

Crystallinity

PLA exists in crystalline, amorphous, and mesophasic phases. The content of each phase depends on the thermal history, average molar mass, and chirality of the monomers, as mentioned in the overview of PLA. As depicted in Figure 2.3, during the crystallization process of semicrystalline polymers, spherulites are formed with clusters of crystalline lamellae comprising chain segments in an extended straight conformation, separated by amorphous regions with unaligned chain segments. This structure forms fibrillar stacks emanating more or less radially from the spherulite center.

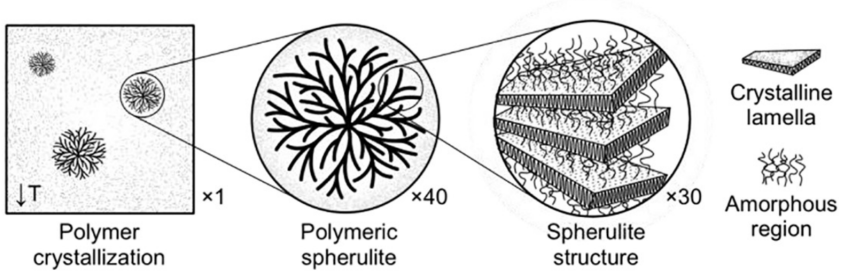

Figure 2.3: Structure of polymeric spherulites of a semicrystalline polymer. Approximate magnifications are given for reference. Adapted from [15].

In the crystal, PLA exists as a polymer helix with an orthorhombic unit cell. Depending on thermal and/or mechanical treatment, PLA exhibits polymorphism as the crystals can grow in three structural forms, namely α, β and γ (less common), which are characterized by different helical conformations and cell symmetries. While the α form grows upon melt or cold crystallization, the β form develops by mechanical stretching of the more stable α form at elevated temperature. Since the α form is the most stable phase, it is the predominant crystal structure. It is formed during crystallization at temperatures above 120°C or can be formed by crystallization from a solution. Conversely, crystallization at temperatures around 100-120°C leads to the formation of $\alpha^{'}$-crystals. The crystalline $\alpha^{'}$ form has a similar molecular geometry to the α form, but is present in a loose packing of crystalline fibers. These are metastable at the temperature at which they form, but convert to a stable α-form when heated at their stability limit of about 150°C [16].

Thermal properties

Depending on stereochemistry and thermal history, PLA can be either amorphous or semi-crystalline. The glass transition temperature (T_g) affects physical properties (e.g., density, heat capacity, rheological and mechanical properties). It determines the upper use temperature for most commercial applications of amorphous PLAs. In fact, T_g is the most important parameter because above this temperature significant changes in the chain mobility of the polymer occur. Above T_g, amorphous PLA goes from glassy to rubbery and behaves like a viscous liquid upon further heating. Below T_g, flexibility decreases and PLA behaves like glass.
For semi-crystalline PLAs, both T_g ($\sim$ 58°C) and T_m ($\sim$ 130°–230°C, depending on the structure) are significant. The dramatic changes in polymer chain motion that occur at these transition temperatures result in changes in the physical properties of the polymer. They are strongly influenced by optical purity, primary structure, thermal history, and molar mass. Thermal analysis of PLA based on the number average molar mass and the type of isomer (D, L, and DL) indicated that the T_g of PLA increases as a function of molar mass. Table 2.1 summarizes the thermal properties of the different stereoisomers of PLA [8].

	PLLA	**PDLLA**
T_m **[°C]**	170-200	amorphous - no melting point
T_g **[°C]**	55-65	50-60

Table 2.1: Thermal properties of PLA [17]

The kinetics of melt crystallization of PLA were studied in detail, and the isothermal crystallization rates were determined over a wide temperature range from 70 to 165°C. From these analyzes, the crystal growth rate () can be plotted as a function of crystallization temperature, showing the temperature range over which the polymer can crystallize in a reasonable time. It is well known that, according to crystallization theory, the crystal growth rate exhibits a bell-shaped dependence on temperature. Indeed, for many polymers, including nylon-6, PET, and isotactic PS, it has been reported that the value of G increases with T_c. After reaching the maximum, it then decreases with increasing T_c. However, PLLA shows a discontinuity in the growth rate, as shown in Figure 2.4. The spherulitic growth rate curve shows a first maximum at about 105°C and a second at about 130°C. The occurrence of this discontinuity is not associated with a change in nucleation rate or spherulite morphology, but was attributed to a sudden acceleration in spherulite growth. It results from the different growth rates of α- and $\alpha^{'}$-crystals [16].

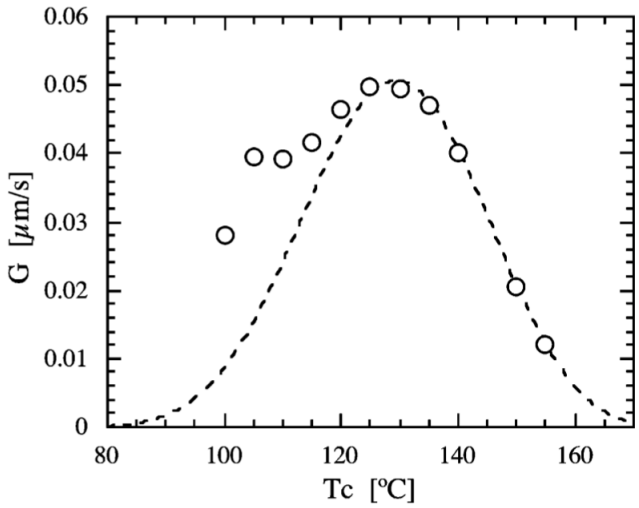

Figure 2.4: Radius growth rate G of the spherulite of PLLA as a function of crystallization temperature (T_c). The broken line indicates the theoretical curve fitted for the temperature above 120 °C based on the Hoffmann-Lauritzen analysis from [18]

The theoretical bell-shaped curve can be obtained by the following equation :

$$G = G_0 \exp\left(\frac{-B_1}{T_c - T_0}\right) \exp\left(\frac{-B_2}{T_m^\circ - T_c}\right)$$

With $B_1 = -U^*/R$, $-U^*$ is the activation energy for segment diffusion to the site of crystallization, R the gas constant. B_2 depends on the nucleation constant, T_c and the thermodynamic melting temperature (T°_m) [18].

Solubility

PLA is soluble in most chlorinated solvents (i.e., chloroform, methylene chloride, 1,1,2-trichloroethane and dichloroacetic acid). At room temperature, PLA can be partially dissolved in ethylbenzene, toluene, acetone, tetrahydrofuran, and is soluble in these when heated to boiling temperatures. However, the solubility of PLA depends on its degree of crystallinity. Amorphous polymers are soluble in various organic solvents (e.g., acetone, acetonitrile, and methylene chloride). Crystalline PLA can only be dissolved at high temperatures in dichloromethane or benzene because the chains are more compact and the solvent has difficulty penetrating between them. Nevertheless, polymers based on LA are not soluble in water, in alcohols (e.g., methanol, ethanol, propylene glycol), or in unsubstituted hydrocarbons such as hexane and heptane [6].

Degradation

The location of the medical device (MD) in the case of implantation plays an important role in implant degradation. Large devices in areas of poor vascularization can degrade and exceed the body's ability to remove degradation products, resulting in an acidic environment that further catalyzes degradation [6]. PLA is able to degrade naturally in situ, reducing surgical intervention. For implantable medical devices, the biodegradable polymer should retain its mechanical properties until it is no longer needed in the body after implantation. The rate of degradation of PLA is therefore a critical feature, as during this process the yield strain, the yield stress, and the elongation to failure decrease. The degradation of PLA occurs in two phases:

1. **Hydrolysis**: random non-enzymatic chain scission of the ester groups along the backbone of the polymer leads to a decrease in MM. The rate of hydrolysis is determined by its rate constant, water concentration, acid or base catalyst, temperature and morphology.

2. **Enzymatic degradation**: random cleavage of low MM polymers by microorganisms to produce carbon dioxide and water.

These mechanisms are controlled by four basic parameters: rate constant, water concentration, diffusion coefficient of chain fragments within the polymer, and the solubility of degradation products [19]. The rate of degradation is determined by all factors affecting the reactivity of the polymer with water and catalysts, especially polymer composition, MM, crystallinity, etc. A major challenge is that the hydrolysis reaction of PLA is autocatalytic due to the carboxyl end groups, unlike other polymers such as PET. Stabilization strategies such as reducing the residual monomer content, lowering the water content, adding basic buffer salts (e.g. $CaCO_3$) or functionalizing the PLA end group are therefore important [8].

The MM has a significant effect on degradation. A high MM PLA degrades within 2 to 8 years, leading to inflammation and infection in vivo. A shorter MM is therefore desirable, and studies have shown that PLA implants can maintain their mechanical properties for as long as is required for fracture healing [6].

Highly crystalline polymers can last for several months, degrading after a few years, while low-crystalline polymers can degrade within a few weeks. The crystalline domains of PLA are more resistant to hydrolysis than the amorphous domains because access of water molecules to the chains within the rigid crystalline domains is limited [20]. As shown in Figure 2.5, in phase A, chain cleavages of amorphous chains allow crystalline lamellae to form. The more mobile polymer chains reorganize to form crystalline lamellae, and the formation of the crystalline phase continues in stage B. In the final stage C, the amorphous phase, which lies between the crystalline lamellae, is degraded and loses its mechanical properties.

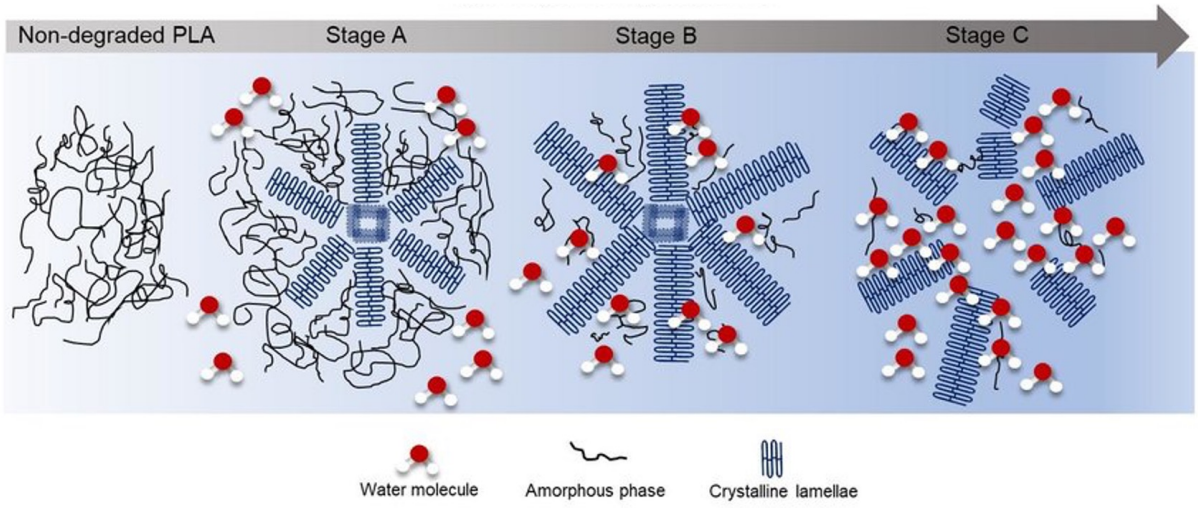

Figure 2.5: Schematic of the hydrolysis of PLA. Stage A: chain scissions of amorphous chains and formation of crystalline lamellae. Stage B: reorganization of polymer chain into crystalline lamellae. Stage C: degradation of the amorphous phase [21].

2.1.3 Mechanical properties

Semi-crystalline polymers have regular repeating units that allow the chains to fold into dense regions that give them higher tensile strength and modulus compared to amorphous polymer. Therefore, semi-crystalline PLA is preferred over amorphous polymer when higher mechanical properties are required.

As shown in Table 2.2, PLLA has high tensile strength and low elongation at break. Consequently, it has a high modulus and is more interesting for load-bearing applications such as orthopedic sutures and fixations, compared to amorphous polymers. Besides, PDLLA is amorphous and has lower tensile strength and higher elongation, but much faster degradation time, which is attractive for drug delivery systems.
PLA has higher tensile strength and modulus than other polyesters (e.g., PCL, PGA, etc.). However, its toughness is quite low, with less than 10% elongation at break, which can lead to failure under high stress as plastic deformation occurs.

	PLLA	**PDLLA**
Elastic modulus [GPa]	2.7-4.14	1-3.45
Tensile strength [MPa]	15.5-150	27.6-50
Elongation at break [%]	3.0-10	2.0-10.0

Table 2.2: Mechanical properties of PLA [17]

2.1.4 Biomedical applications

PLA is environmentally friendly and highly versatile. Its diversification in many application is due to simple modifications of its physical and chemical structure and the ability to blend or copolymerize it with other polymeric or non-polymeric components to achieve the desired behavior. Due to its renewability, biodegradability, processability and mechanical properties, it is increasingly used in various applications. In addition, production costs for PLA manufacturing processes are decreasing [22].

Tissue engineering is the most recent and one of the most exciting inter- and multidisciplinary research areas where the use of PLA has increased exponentially over time [6]. As a scaffold, it acts as an extracellular matrix to which cells can adhere and grow to restore functional tissue. The pore diameter is important for cell growth, vascularization and diffusion of nutrients. The degradation of PLA makes it very interesting as a support material, leaving a perfect patch of natural neo-tissue. Depending on porosity, chemical composition, and crystallinity, degradation can take anywhere from 10 months to 4 years. Three-dimensional porous scaffold made of PLA for culturing muscle tissue, bone or cartilage are being increasingly studied. The high strength of PLLA allows the fabrication of 3D mesh structures with different geometries thanks to 3D printing. This technology is a promising way to create complex devices based on patient-specific anatomical data and computer design. Combining stem cells with custom-printed PLA 3D scaffolds is on the rise in regenerative medicine. However, 3D printing is subject to several technological limitations, and a balance must be found between physical/mechanical properties and biodegradation rates.

2.2 PEG

Since the 1950s, PEGs have been widely used as release and cleaning aids, matrices for embedding, lubricants for medical devices, food additives, and as carriers in dermatological applications, tablets, pills, etc. Later, PEG was explored as a steric stabilizer capable of evading the host immune system, and the concept of PEGylation for protein and drug delivery was introduced [23]. Although other alternatives to PEG such as sodium alginate and dextran have emerged, PEG is still used as the polymer of choice.

PEG is a is a water-soluble, biocompatible, non-polar, crystalline thermoplastic polyether composed of ethylene glycol (EG) units (Figure 2.6). PEG with high MM can also be called polyethylene oxide (PEO), which refers to polymers with a molar mass greater than 20 000

g/mol. This FDA-approved polymer is popular due to its adaptable properties and well-known safety profile.

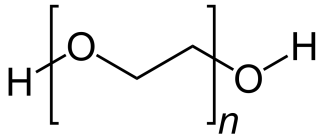

Figure 2.6: Polyethylene glycol structure

2.2.1 Physical properties

PEG has high flexibility, biocompatibility, amphiphilicity, and hydration capacity. The biocompatibility and lack of immunogenicity make PEG an important polymer for biomedical applications. PEG is indeed inert in the biological environment with low protein adsorption, low cell activation and adhesion, and negligible inflammation. Moreover, PEG reduces the risk of particle aggregation in vivo and during storage through steric stabilization. It can also prevent interactions with blood components as well as protein interactions such as enzymatic degradation due to the formation of a *"conformational cloud"*, created by the highly flexible polymer chains, which have a large total number of possible conformations. The molar mass and graf conformations (i.e., brush-shaped or mushroom-shaped) influence the efficiency of this steric hindrance cloud [24]. In most cases, PEG is used in the preparation of polymer blends to modify their surface and mechanical properties. Let us summarize the main thermal properties and solubility.

Thermal properties

The molar mass commonly used in biomedical applications ranges from a few hundred to about 20 000 g/mol. Low MM such as PEG 100 to PEG 700 are liquid at room temperature, while those between 1000 and 2000 are soft solids. PEGs with MM above 2000 g/mol are hard crystalline solids with a melting point of about 63°C. The T_g of PEG increases with MM, while the T_m decreases. For instance, the T_g of PEG 4000 and 20 000 g/mol ranges from -34°C to -22°C with a melting point of 67°C to 51°C. Low melting points are critical, for example, in blends produced by hot melt extrusion. By blending or copolymerizing with PEG with different molar masses, the glass transition temperature and melting point can be influenced depending on the application [23].

Solubility and surface properties

The high polarity of PEG increases its hydrophilicity and thus its solubility in water, which is very different from that of other polymers with similar structures. PEG is soluble in water, ethanol, and many organic solvents (e.g., acetonitrile, benzene, and dichloromethane), while it is insoluble in diethyl ether and hexane [23]. Its hydrophilicity can significantly reduce the contact angle of hydrophobic materials. Moore et al.[25] showed a 34° and 50° decrease in contact angle by coating PEG on glass and gold plates, respectively. PEG is electrically neutral over a wide pH range and can block the electrostatic interactions between substrate and protein. In addition, it can be prepared with a wide range of terminal functional groups.

2.3 Improvement of PLA properties

PLA has many limitations. PLA's hydrophobicity and low elongation at break makes it unsuitable for drug delivery or in environment with high mechanical strength (e.g., bone transplantation). This can be improved by adding modified additives during synthesis, by blending with other polymers or other methods [22].

2.3.1 Bulk modifications

Bulk modifications can be divided into chemical and physical modifications. Blending and plasticizing are physical modifications, while crosslinking and copolymerization are chemical modifications.

A simple and widely used modification method is **blending** PLA with plasticizers, olefin polymers/fibers, inorganic materials, natural polymers, or biodegradable polyesters; this significantly changes both physical and mechanical properties. Tensile properties (i.e., tensile strength, elastic modulus, and elongation at break) and thermal stability have been reported to be improved by stereocomplexing enantiomeric PLA (i.e., PLLA and PDLA) with low or high MM [22]. Plasticizers are widely used to improve the processability, flexibility, and extensibility of polymers. Among them, ester-type plasticizers such as glycerol, sorbitol, glucose and citrates are used. The monomer LA itself is one of the best plasticizers for PLA, but it migrates quickly on the polymer surface. Therefore, high MM plasticizers (e.g., PEG) are required for low mobility to avoid migration into the PLA matrix. So far, PEG, citrate and oligomeric lactic acid were the most commonly used plasticizers that gave the best results [6].

Copolymerization is a direct and effective method that starts simultaneously with the polymerization reaction. Depending on the synthesis method and structure, different block copolymers can be formed: diblock, triblock or multiblock. The carboxylic and hydroxyl groups in LA allow copolymerization with a wide range of monomers (e.g., ϵ-caprolactone (CL), ethylene oxide (EO), ethylene glycol (EG), etc.) [26]. The addition of a polyester backbone to PLA can lower the crystallinity and melting point, so it is important to make the right choice of polymer depending on the application and desired properties. In particular, the hydrophilicity of PLA can be improved by copolymerization with PEG [27].

2.3.2 Surface modifications

While bulk properties can initially determine the suitability of the material for an application, surface properties are critical to the function of many biomedical devices. Surface modification focuses on properties such as roughness, hydrophobicity, and surface morphology. The goal of biomaterial surface modification is to create a specific chemical and physical environment that induces a favorable cellular response in the tissue. In tissue integration, macro, micro, and even nanoscale features that allow cells to adhere, proliferate, and migrate in their environment are essential [28].
The introduction of functional groups, coatings, or plasma treatments are good examples of surface modifications. Park et al.[29] used oxygen plasma treatment and hydrophilic acrylic acid grafting on the surface of electrospun PLLA nanofiber scaffolds. The properties were significantly different from those of the unmodified nanofiber scaffolds, with higher oxygen to carbon ratios and lower contact angles. This improved **hydrophilicity** increased the affinity of the cells with the surface.
PEG/PEO coatings have been investigated as an anti-fouling coating for implants to reduce protein adsorption to surfaces in contact with blood, which is beneficial for stents and other applications.

Microscopic topography and porosity are also critical to promote cell adhesion and nutrient infiltration into an implant, while ensuring that the tissue is mechanically interlocked with the device. Various conventional fabrication techniques techniques can be used to introduce **porosity**.
Among them, solvent-casting particulate leaching is currently a popular method for preparing polymer scaffolds in TE because it is simple and inexpensive. The polymer is dissolved in an organic solvent, and then porogen particles (e.g., water-soluble salts) are mixed with the polymer solution. The solution is then transferred into a mold (e.g., a Petri dish), which determines the shape of the membrane. Evaporation of the solvent produces a porogen-polymer composite, which is finally washed to remove the particles in water. The final porosity, pore size, and interconnectivity can be controlled by proper selection of the polymer, porogen, and their composition [30].
In gas foaming technique, the polymer is formed into solid discs at high temperature. The discs are then exposed to high-pressure carbon dioxide gas for several days to form pores before the pressure is reduced back to atmospheric levels. The main advantage of this method is that chemical solvents no longer need to be used, eliminating the leaching step in the manufacturing process. However, it is difficult to ensure pore connectivity and control pore sizes due to gas formation. Moreover, the application of high temperatures during disc formation prohibits the use of bioactive molecules in the scaffolds [31].

2.4 PLA/PEG blend

PLA is an attractive material for use in tissue engineering, but the surface properties of scaffolds based on it are not ideal for cell adhesion and growth. The applications of PLA have been limited due to its brittleness, hydrophobicity, poor heat resistance, slow degradation rate, etc. As mentioned previously, these limitations can be improved by copolymerization, blending, and plasticization. Polymer blending is a suitable physical modification method to achieve new properties of different polymers.
PEG has good miscibility with PLA because the terminal hydroxyl groups in PEG molecules can react with the carboxyl groups in PLA. PEG in a blend can affect the physical, mechanical and surface properties. The terminal hydroxyl groups of PEG increase the hydrophilicity of the blended polymer, greatly improving the biocompatibility of the material for culturing cells [32]. Numerous studies have reported the benefits of PEG on the properties of PLA and its potential for the preparation of porous PLLA membranes.

Sheth et al.[33] have shown that PLA/PEG blends can be miscible to partially miscible. When the content of PEG increases from 10 to 50 wt%, phase separation occurs and the polymers crystallize independently.
Sungsanit et al.[34] used PEG 1000 g/mol to plasticize PLLA. They observed that the crystallinity, elongation at break, and impact strength of PLLA/PEG blends increased, while the glass transition temperature, tensile strength, and modulus decreased with increasing PEG content. They also found that the PEG phase separated from the PLLA/PEG blends when the PEG content exceeded 10 wt%. In addition, Wang et al. [35] performed a thermal analysis and concluded that PLA and PEG form miscible blends in compositions of less than 50/50.
Baiardo et al.[36] plasticized PLA with PEGs from 400 to 10 000 g/mol and found that the solubility limit and plasticization efficiency of PEG in PLA decreased with the increase of PEG MM. Lower MM PEG could reduce the T_g more significantly. In addition, they found that the elongation at break increased sharply when the T_g of the blend was close to room temperature, while the tensile strength and modulus decreased rapidly with increasing PEG content.
In the following subsections, the thermal, mechanical and surface properties of PLA/PEG blends from different studies are described.

2.4.1 Thermal properties

Athanasoulia et al.[37] showed by **thermal transition** in DSC analysis that at higher PEG (M_n = 10 000 g/mol) content (30 and 40 wt%), the crystallization of PLA was enhanced. The plasticizer increased the mobility of polymer chains and accelerated the crystallization rate by reducing the energy required for chain folding during crystallization. Melted PEG chains penetrate into the non-crystalline region of PLLA, increasing chain mobility and chain rearrangement while reducing the T_g of the blend.

Thermogravimetric analysis (TGA) allows determination of the **thermal stability** of the blends by looking at the weight loss as a function of temperature. The addition of PEG (10 to 50 wt%) decreases the initial decomposition temperature of the PLA/PEG blend, which could be due to the lower initial decomposition temperature of PEG. The lubrication of PLLA molecules becomes the main mechanism that facilitates the thermal decomposition. The thermal degradation process shows a two-step degradation, one step for the decomposition of stereocrystals of the PLLA phase, and another for the PEG degradation (Figure 2.7). While the decomposition of the PLA component takes place at lower temperatures, the decomposition of PEG shifts to a higher temperature with increasing PEG content in the mixture. Thus, the addition of PEG plasticizer makes PLA more sensitive to thermal stability, facilitates the thermal degradation of PLA, and reduces the thermal stability of PLA. However, the temperature range in which this occurs (above 300 °C) is not reached during the processing step [35].

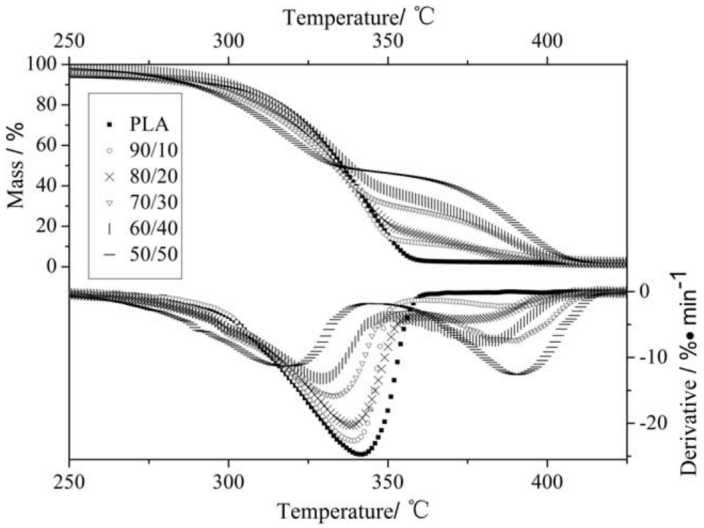

Figure 2.7: The TGA curves and DTG curves of PLA and the PLA/PEG blends at 10°C/min (taken from[35]).

Chen et al.[38] used PDLA-PEG-PDLA /PLLA blends and observed the crystal morphologies at different temperatures and times to better understand the crystallization behavior of the PLLA blends. They investigated the effect of the molar mass of PEG on the crystal morphologies of the mixtures when the crystallization time was increased from 5 minutes to 4 hours at 140°C and 180°C, respectively (Figure 2.8). They concluded that PEG increases the slow crystallization rate of pure PLLA below 1 hour, and when the crystallization time is 4 hours, the crystal growth is almost complete. Moreover, the size of PLA crystals increases with increasing molar mass of PEG. However, when the molar mass of PEG exceeds 6000 g/mol, the molecular chain is easily entangled, which causes resistance to crystallization.

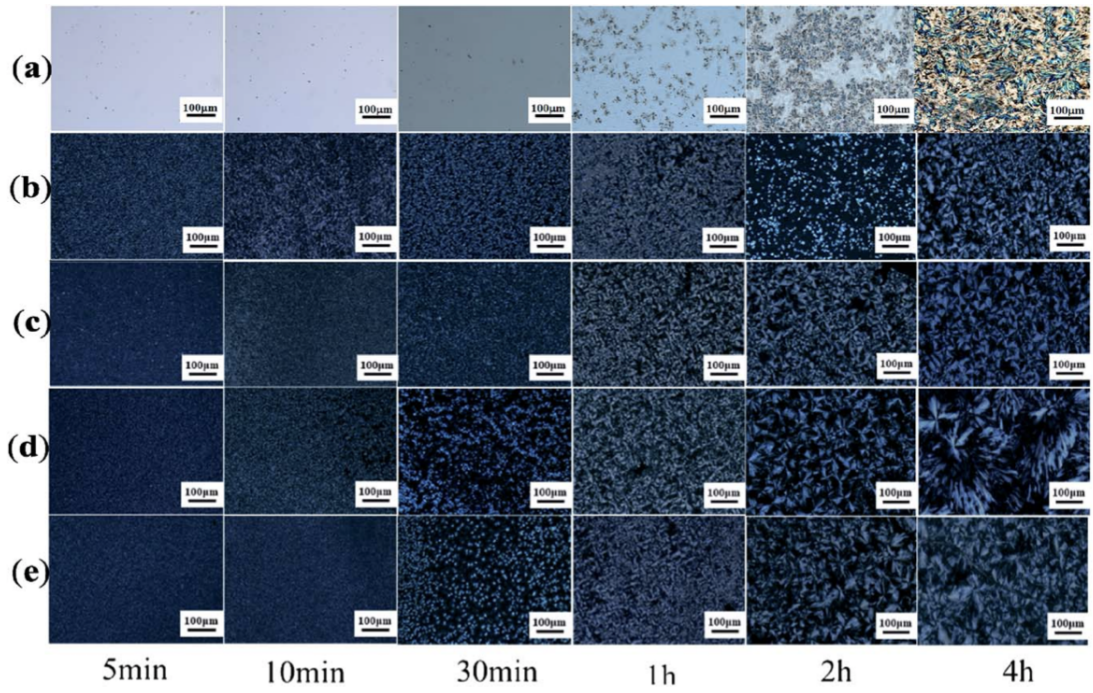

Figure 2.8: POM photos of PDLA–PEG–PDLA/PLLA blends with different molar mass of PEG at 140°C: (a) pure PLLA; (b) PEG2000; (c) PEG4000; (d) PEG6000; and (e) PEG8000 (taken from [38]).

Zhang et al.[39] compared PCL/PLA, PEO/PLA, and PEG /PLA bilayer films and showed that both low molar mass PEG (M_w = 3500 g/mol) and high molar mass PEO (M_w = 150 000 g/mol) could increase the mobility of PLA chain segments and thus accelerate the spherulitic growth rate of PLA (Figure 2.9). Moreover, the **spherulitic growth rate** for PEG/PLA bilayer film was higher than that of PEO due to the shorter chain length. The temperature with the maximum spherulitic growth rate for each curve shifted to a lower temperature, which is related to the increasing miscibility of the covering polymer layers with PLA. The lowest temperature at which the spherulitic growth rates of PLA can be well measured shifted to 65°C with the addition of PEG or PEO, while neat PLA did not crystallize at this low temperature.

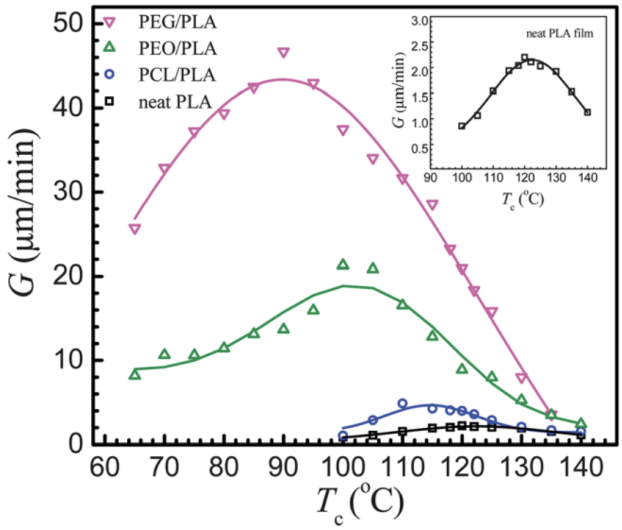

Figure 2.9: Changes in the spherulitic growth rate as functions of T_c for the neat PLA film and PCL/PLA, PEO/PLA and PEG/PLA double-layer films. Inset shows the result for neat PLA film (taken from [39]).

2.4.2 Mechanical properties

Tensile tests show that incorporation of PEG into the PLLA matrix significantly decreases the tensile strength and elastic modulus of the blends at PEG content greater than 20 wt% [37]. Plasticizers weaken the intermolecular interactions of the polymer and impart flexibility to the PLLA, leading to a decrease in tensile modulus with the increase in PEG content. The blends are thus able to increase the free volume between the polymer chains, improving the mobility of the polymer chains with respect to each other.
Figure 2.10 shows an increase in elongation at break for PEG content from 10 to 30 wt%. The fracture behavior of PLA changes from brittle to ductile due to the plasticization of PEG, which can improve the segmental mobility of PLA chains and increase the plastic deformation of PLA. At 40 wt% PEG, a significant decrease is due to the lack of cohesion between the polymer matrix and PEG, which can lead to phase separation and increase brittleness. This decrease is due to crystallization of the PEG component and phase separation at a high PEG content. In addition, PEG has a greater tendency to migrate to the polymer surface at higher concentrations, which can lead to an uneven plasticizing effect and difficulty in plastic deformation.
Although elongation at break increases with PEG content, the optimum mechanical property is achieved by blending PLA with 30 wt% PEG [35].

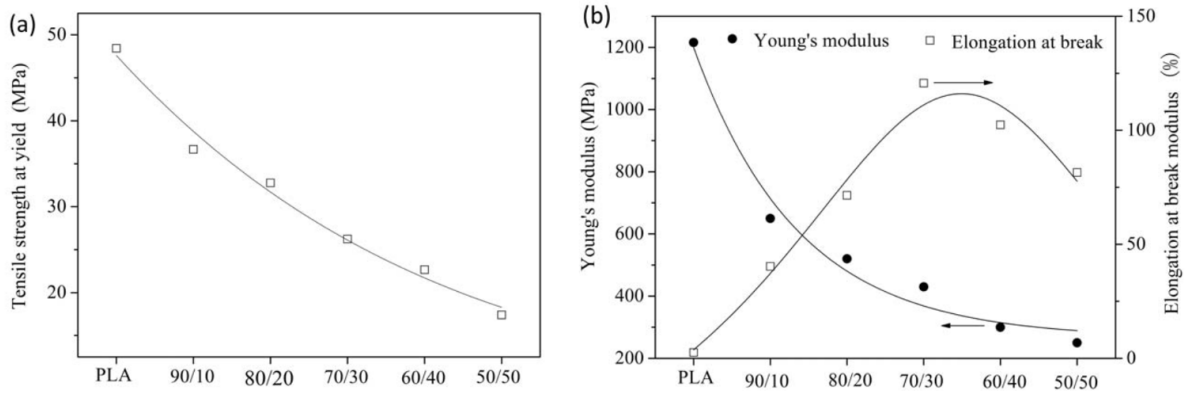

Figure 2.10: The tensile property of PLA and PLA/PEG blends (taken from [35]).

2.4.3 Porosity

Tsuji et al.[40] prepared porous PLLA films by water extraction of PEG from solution-cast PLLA and PEG blend films. Low molar mass (M_w = 1000 g/mol) and high molar mass PEG (M_w = 10 000 g/mol) films were used. The maximum pore size was larger for porous films prepared from high molecular MM PEG when compared with the same mixing ratio of PLLA/PEG before water extraction. A maximum pore size of $\sim$ 100 micrometers and 20 micrometers was obtained for high and low MM PEG, respectively (Figure 2.11). Porosity and pore size appear to be controlled by the content of PEG and its molar mass.

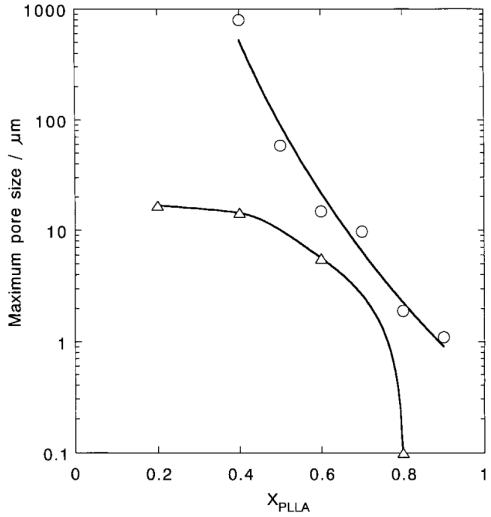

Figure 2.11: Maximum pore size of water-extracted, dried blend films of PLLA-PEO(H) (△) and PLLA-PEO(L) (O) as a function of the PLLA ratio in the blend (taken from [40]).

Nakane et al.[41] studied the properties and structures of blend films of PLLA and low MM PEG (400 g/mol) prepared by a solvent casting method. They found that the blend films PEG 20 wt% and PEG 40 wt% exhibited a **porous structure** with a pore diameter of 3-5 and 7-8 micrometers, respectively (Figure 2.12). SEM microscopic image of the cross-section of a PLLA/PEG sample (80/20 wt%) showed that the pores were homogeneously present throughout the film, i.e., from the surface to the center. After immersion in distilled water, the shape of the pore has become more complex due to the removal of the PEG area.

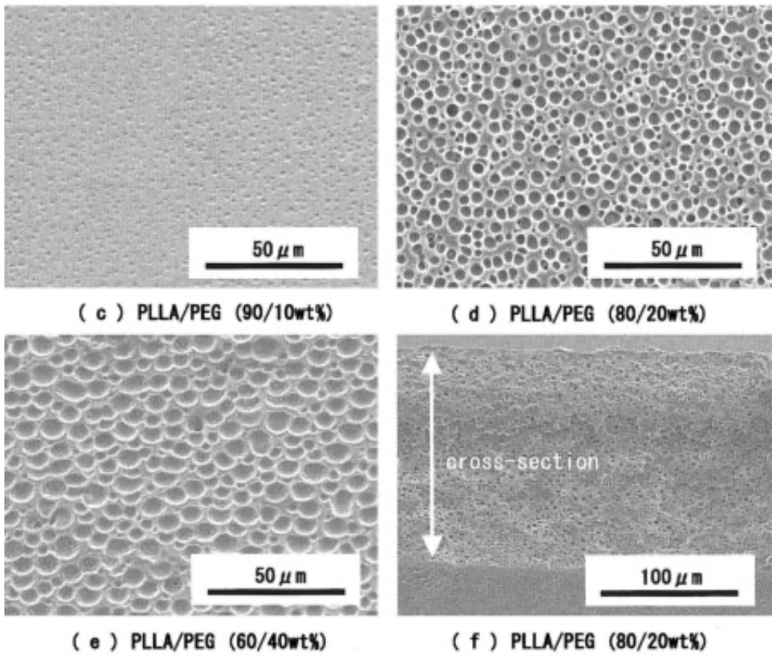

Figure 2.12: SEM micrographs of as-cast PLLA/PEG blend films (adapted from [40]).

Selvam et al.[30] reported the preparation of PLLA membranes (mpPLLAm) with channelized pores using the PEG solvent-cast/particulate leaching technique. Phase separation of the mixture into PLLA-rich and PEG -rich phases was suggested to be the cause of the characteristic pore morphology. This phase separation could be caused by the slow evaporation rate of the

co-solvent. The pore density of the membrane could be controlled by varying the blending ratio of the two polymers. The results show that the prepared mpPLLAm was permeable to glucose, L-tryptophan and dextran with effective pore diameters in the range of 1-4 micrometers. This is very promising for use in tissue engineering of biomaterial grafts for clinical applications.

Nashekina et al.[32] investigated the effect of different isomeric forms of PLA and PEG with terminal amino groups to obtain **porous** biocompatible films for human mesenchymal stem cells cultivation. Using solvent molding methods, PLA was mixed with high MM (15 000 g/mol) and low MM (6000 g/mol) PEG. After evaporation of the solvent (chloroform), the resulting mixture was incubated in water to dissolve the PEG phase. The samples obtained from the mixture of PDLA and PEG had a pore diameter of 0.5 to 1 micrometers, and the pores were uniformly distributed over the surface of the film. The surfaces of the films prepared from PEG and PLLA also contained pores up to 100 nanometers in diameter, but significantly fewer pores than the blended films prepared from PDLA. However, under conditions of rapid evaporation of chloroform, PEG with a lower MM (PEG6000) did not produce films with holes on the surface and did not form separate phases that can be dissolved in water (Figure 2.13).

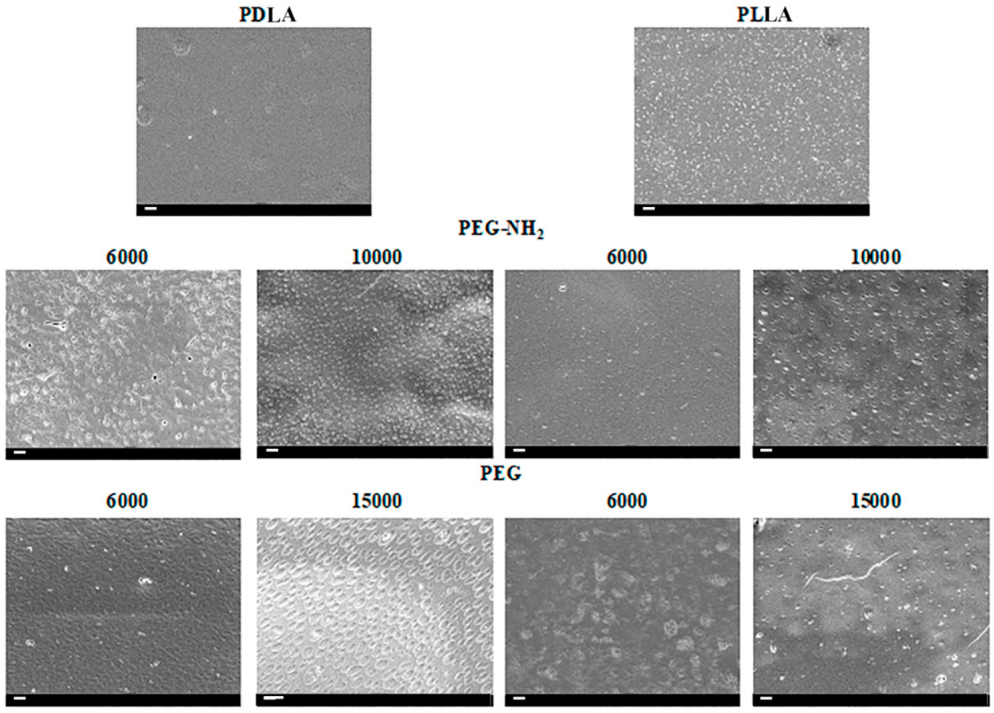

Figure 2.13: SEM images of pure PLA with different isomeric forms PDLA and PLLA. The blend PLA/PEG or PLA/PEG-NH2 with different molecular mass of PEG (6000 or 15 000 g/mol) and PEG-NH2 (6000 or 10 000 g/mol). Scale bar 1 micrometer (taken from [32]).

2.5 Crystallization process

Crystallization has an important effect on the mechanical, optical and thermal properties of polymers. Crystallization of polymers follows the nucleation and growth pathway, which determines the rate of crystallization and the final crystal structures. In industry, a higher crystallization rate and degree of crystallinity are preferred to improve the production rate and thermal stability of polymer products. Acceleration of crystal nucleation is therefore of interest, and numerous techniques have been applied. Let us introduce crystallization in general terms.

Crystallization of polymers consists in a transition of an ensemble of entangled chains from a disordered liquid state to a partially ordered solid semi-crystalline state. Crystallization occurs through a nucleation and growth mechanism. **Nucleation** is the initiation from a solution, liquid, or vapor in which a small number of molecules are arranged in a pattern characteristic of a crystalline solid. Stable molecular nuclei are formed and can grow into macroscopic crystals [42]. It can be either homogeneous or heterogeneous, depending on whether the nuclei consist of polymer chains or impurities. Homogeneous nucleation is less common because polymers usually contain a significant amount of impurities. Heterogeneous nucleation results from impurities such as catalyst residues or added nucleating agents and is triggered by contact with foreign particles and surfaces [43].

Crystal growth is the development of nuclei in visible dimensions and occurs only at temperatures below the melting temperature T_m and above the glass transition temperature T_g. In the absence of a thermal gradient, the growth of a spherulite follows a characteristic pattern. Starting from a primary core as the center, a spherical body is formed, typically consisting of numerous crystalline fibers whose lateral dimensions are remarkably constant and which, through repeated branching, uniformly fill the space throughout the radiating aggregate [44]. Spherulites range in size from about 1 to 100 micrometers and can form the "Maltese cross" pattern and other polarization phenomena, caused by molecular alignment within individual lamellae of a spherulite when viewed between crossed polarizers in an optical microscope [45].

Crystals of different sizes can be formed during the crystallization process. Control of particle size distribution depends on control of nucleation and growth. As can be seen in Figure 2.14, as nucleation increases, the crystal growth rate decreases and smaller spherulites are formed. The fastest crystallization rate is achieved at an intermediate temperature between the preferred temperatures for nucleation and growth [42].

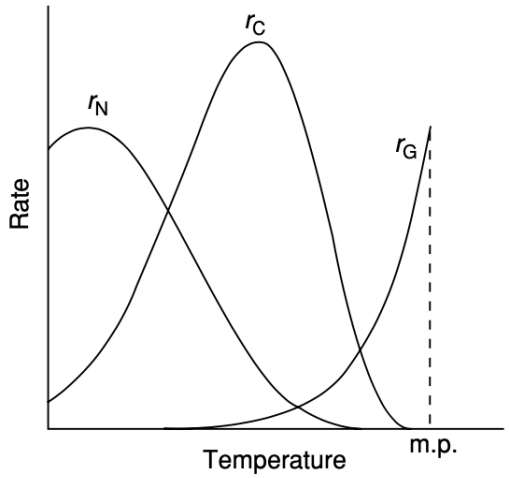

Figure 2.14: Typical temperature dependence of crystallization rate from a single-component melt. r_G, crystal growth rate; r_N, crystal nucleation rate; r_c, overall crystallization rate (taken from [42]).

The thermodynamic driving force for nucleation and growth is supersaturation, in the case of solution crystallization. It is generated in different ways depending on the crystallization technique [42]. Moreover, the same crystallization carried out under different conditions can yield crystals with different properties (i.e., size, morphology, chemical purity, polymorphic form, etc.). Supersaturation can result from solvent evaporation, temperature change, etc.
Cooling crystallization is attractive because most substances are more soluble at higher temperatures than at lower temperatures and almost any solvent can be used. As the temperature drops, the mixture becomes supersaturated and crystallization begins when the cooling rate is

low enough [46]. Melt crystallization differs in that no solvents are used.
Solvent evaporation is the simplest way to grow crystals and works best for compounds that do not respond to ambient conditions in the laboratory. In dilute solutions, the molecular chains have no connection to each other and exist as separate polymer coils in the solution. As the solvent evaporates, the concentration increases, leading to interactions between the molecular chains and possible crystallization [47].
Crystallization can also be **strain-induced**. It occurs, for example, in the extrusion process used to make fibers and films. In this process, the temperature is above T_g and the polymer is forced through a nozzle which creates tensile stress that begins to disentangle, unfold, and straighten the randomly coiled and entangled chains, causing molecular alignment in the stretch direction. This can be considered as crystallization and affects the properties of the material. Due to the formation of crystals, which act as physical reinforcement, a significant increase in modulus is usually observed. This can be of particular interest for certain polymers that do not crystallize from the melt and that can be partially aligned by stretching [48].

Chapter 3

Objectives and strategy

3.1 Context and objectives

As mention in the previous chapter, PLA/PEG blends are increasingly studied. The stiff and brittle nature of PLA can be improved by modifying its physical properties through several approaches including blending with other polymers. This technique is simple and more economic as compared with copolymer synthesis. PEG has been reported to be the most suitable material which has been used to enhance PLA properties, due to its miscibility and biodegradability.
Sheth et al.[33] demonstrated that PLA/PEG blends can be miscible to partially miscible, depending on the PEG concentration. When PEG content increases from 10 to 50 wt%, phase separation occurs and polymers crystallizes independently. Moreover, Baiardo et al.[36] concluded that the miscibility limit moves toward lower PEG contents with increasing PEG molar mass from 4000 g/mol to 10 000 g/mol. Sungsanit et al.[34] and others [39][49] found that phase separation from the PLA/PEG blends occurs when PEG content was higher than 10 wt%, the blends became brittle at relatively high PEG content. Besides, Wang et al.[35] performed thermal analysis and concluded that PLA and PEG form miscible blends in compositions less than 50/50.
PEG content and its molar mass have shown to induce very different properties in PLA/PEG blends. Brittleness, thermal and morphological properties strongly depend on these parameters, it is thus important to balance the PLA/PEG blend properties.
Isothermal crystallization temperature is hardly investigated, compared to the other parameters stated above. However, PEG shows to influence the PLA thermal properties. A study of its influence on the crystallization of PLA as well as its location in the blend would allow to determine which isotherm temperature would achieve the desired morphology.
One of the main applications of these blends is in biology and tissue engineering. Porous scaffolds are essential for cell colonization. As mentioned in Chapter 1, the ability to 3D print them in any shape offers even more possibilities for tissue engineering and organ rehabilitation. However, the challenge is to achieve well-controlled pore sizes, using only biocompatible and sustainable processes. Porosity is an important parameter affecting the behavior of cells. In general, porosity of scaffold range from 20 to 1500 micrometers, depending on the cell type and function desired. Pore size and interconnectivity determine communication between cells, as well as nutrient, gas, and waste diffusion. Necrosis could be induced by too small pores and a lack of interconnection between them [50]. Moreover, the macroscopic morphology of the PLA surface can affect the orientation and morphology of the cells. It can induce cell elongation and change the morphology of the nucleus. Effect of MW, composition, and other parameters on the surface morphology and porosity of PLA were analyzed. Nevertheless, porosity varies a lot depending on the processing parameters and many things need to be investigated.

The specific aim of this thesis is to develop and optimize a method, based on PEG phase

extraction from PLLA/PEG blends for producing porous PLA material with well-controlled and tunable porosity.

3.2 Strategy

PLLA is choosen over PDLA for its harmless degradation in the human body and its superior thermal and mechanical properties, as previously mentioned in last sections. By PEG extraction, porous material will be obtained and analyzed. The extraction method of PEG will be discussed before analysing the porous films. The crystallization and morphology of the semicrystalline blends will be studied to see the impact of the different parameters chosen. The porosity after PEG dissolution will then be evaluated. Finally, a discussion on the applicability of these films, future perspectives and future improvement will be proposed.

The overall strategy to elaborate the desired porous PLA, consists of three main steps. First, PEG and PLA are dissolved in a co-solvent (chloroform) at room temperature, according to the solvent casting method detailed in the following chapter. Second, the blend is casted onto a glass Petri dish so that the solvent evaporates to obtain a thin film. Third, the PEG is removed by water extraction to end up with a porous PLA having the desired shape.

The impact of the following different parameters on the morphology of the blend films before and after PEG removal was carefully studied.

- **Molar mass of PEG**: low MM-3350 g/mol (PEG3K) and high MM-10000 g/mol (PEG10K).
- **Composition of the blends**: as it strongly influence the blend miscibility and properties, mixtures with a ratio of 100/0, 90/10, 70/30 and 50/50 w/w of PLA/PEG will be analyzed for each molar mass.
- **Isotherms**: thermal treatment and a crystallization step will be performed to try to better control the porosity. These isotherms will be at 70, 110 and 130°C; to follow the different stages of the PLA bell-shaped curve.
- **Crystallization time**: as one do not know how long it will take for the blends to crystallise, isotherms will be maintained for 3 different lengths of time: 1, 4 and 18 hours. This will allow to see how the morphology evolves with time and if the porosity is impacted.

Measurements and characterization techniques used to assess the morphology are: polarised microscopy (POM), scanning electron microscopy (SEM) and Fourier-transform infrared spectroscopy (FTIR). These methods will be described in the next chapter. The general scheme of the strategy is shown in Figure 3.1.

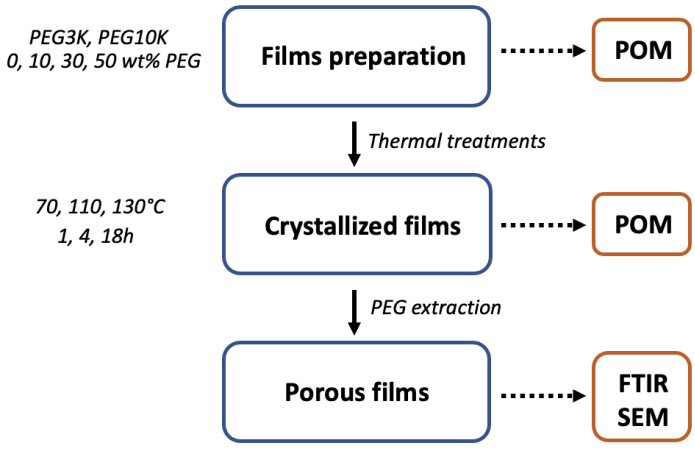

Figure 3.1: Scheme of the overall strategy

Chapter 4

Experimental section

4.1 Materials

Poly(lactic acid) IngeoTM PLA HP2500 in form of pellets was purchased from NatureWorks and used for the fabrication of pure PLA and PLA/PEG blends. PEG powder with M_n 3350 g/mol (PEG3K) and flakes with M_n 10 000 (PEG10K) were obtained from Sigma-Aldrich. Chloroform was also purchased from Sigma-Aldrich and used as acquired.

4.2 Sample preparation

To minimize hydrolytic degradation during melt blending, the PLA and PEG pellets were first vacuum dried overnight at 50°C before processing. Polymer films were prepared by the solvent-casting method as schematized in Figure 4.1. This process was selected because some solvents are known to induce phase separation between the two polymers, even if they are partially miscible in the melt or amorphous state. This method involves dissolving a blend of a polymer and a water-soluble porogen in an organic solvent. Then, the evaporation of the solvent is processed by casting in the desired shape mold. The sample can then be submitted to further thermal treatments (i.e., melting and crystallization). The porogen is removed by leaching in water [30].

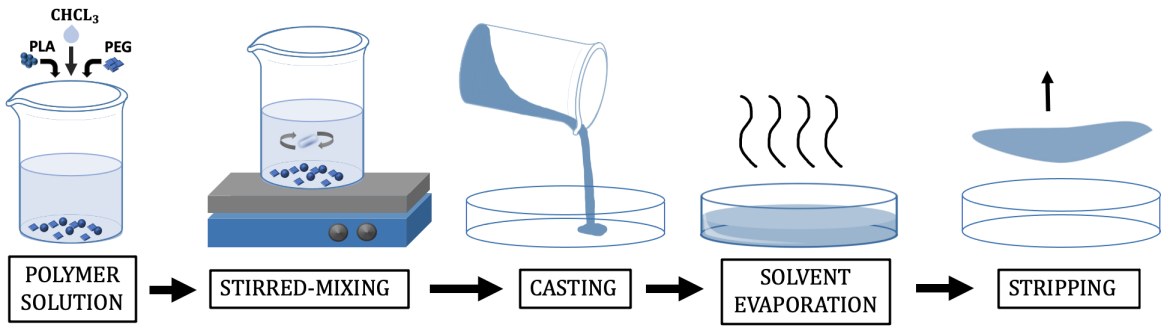

Figure 4.1: Solvent-casting technique

PLA and PEG were blended with the ratio of 100/0, 90/10, 70/30 and 50/50 w/w, where the first and second number represent PLA and PEG by weight percentage, respectively. The desired PLA/PEG content was weighted and placed in a beaker. Chloroform was then added inside the tube to obtain a 40 mg/ml solution. The solution was stirred during 1h at 500 rpm at room temperature, until a homogeneous mixture is obtained. The solution was then poured into a glass Petri dish covered with a beaker, so that the solvent slowly evaporates to obtain a thin film overnight. The films were then peeled off and stored in plastic Petri dishes in a fumehood

in ambient conditions. The thickness of the prepared films was ∼35 µm, measured with a digital micrometer.

4.3 Isothermal crystallization

The isothermal crystallization of the films is performed by a thermal process. One sample of each blends was kept without thermal treatment as reference for later comparison. For blends, three layers of film were superimposed to have enough content. Small PLA and blends samples were placed between two sheets of Kapton to facilitate the removal of the film after treatment and deposited in an aluminum mask. Then, they were melted and pressed between thin metallic sheets in a hot press machine at 200°C for 10 minutes with minimal pressure to erase previous thermal history, and to obtain complete melting without liquid-liquid phase separation. Four pressure cycles between 5 to 0 MPa were done to remove air bubbles before quenching in another oven for isotherms at T_c 70, 110 and 130°C for 1, 4h and 18 hours. (Figure 4.2).

After isotherms, metallic sheets were removed from the press and samples were then cooled down to room temperature for 15 minutes by placing the metal sheets on a non-insulating surface. The samples were peeled off and stored in Petri dishes under ambient conditions before further analysis.

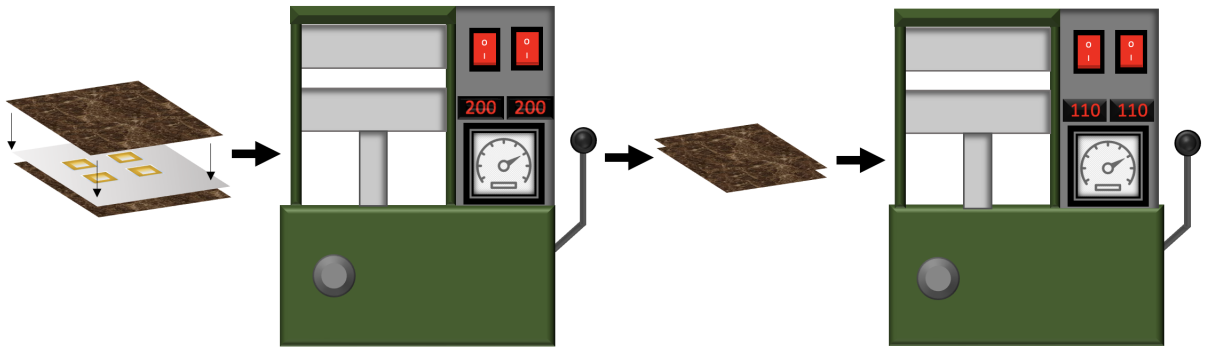

Figure 4.2: Scheme of the thermal process

4.4 Extraction method

Samples were immersed in a beaker containing ultra pure Milli-Q water, covered with aluminum foil to avoid water evaporation. These beakers were placed on a stirring plate at 130 rpm at room temperature. The water was changed after 1, 4 and 24 hours to avoid saturation of the water with PEG. Samples were then dried overnight in a vacuum-oven.

4.5 Characterization techniques

4.5.1 FTIR

The molecular structures and composition of neat PLA, neat PEG and PLA/PEG blend samples were analyzed using FTIR spectra on a Nicolet iN10 FTIR spectrometer (Thermal Scientific, USA) in the wavelength range 600–3200 cm^{-1}, with a high spectral resolution of 4 cm^{-1} and an accumulation of 64 scans. The technique of attenuated total reflectance (ATR) was used for the measurements in order to evaluate the extraction method of PEG. Because ATR only probes the top 10-20 µm of the films, transmission mode was also used to confirm the complete extraction of the PEG from the films.

4.5.2 POM

The polarized light microscope is designed to observe specimens that are optically birefringent. As depicted in Figure 4.3, the microscope is equipped with a first polarizer positioned in the light path before the sample. A second polarizer called "analyzer" is placed in the optical pathway between the objective rear aperture and the camera, perpendicular to the first one. Image contrast arises from the interaction of plane-polarized light with a birefringent sample which acts as if producing two individual wave components that are each polarized in mutually perpendicular plane. These two components travel at different speeds and are then dephased when emerging from the sample. They recombine to form a generally elliptically polarized light. Part of the light is thus trasmitted through the crossed analyzer, except when the incident field is polarized parallel to an optical axis (in which case the polarization of the light is not changed when passing through the sample). Hence, the method allows to check a simple is birefringent, and to detect the orientation of the optical axes.

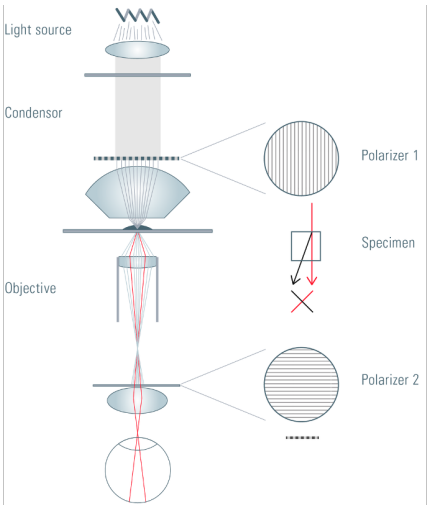

Figure 4.3: Principles of a polarizing microscope [51]

Olympus AX70/Provis equipped with a charge coupled device (CCD) camera was used with polarizing light to observe the crystal morphologies of pure PLLA and its blends. Films were put between a glass slide and a cover slip before observation at room temperature. Objectives of x10 and x50 were used. The crystalline morphology of the samples was recorded using the CCD camera.

4.5.3 SEM

Scanning electron microscopy uses an electron beam to image samples with a resolution down to the ten nanometer scale. The electrons are emitted from a filament and collimated into a beam in the electron source. The beam is then focused on the sample surface by a set of lenses in the electron column, resulting in emission of X-rays, secondary electrons, back-scattered electrons, etc. As secondary electrons are sensitive to surface structure, they provide morphology and topography information. They result from inelastic interactions between the electron beam and the sample, with a lower energy compared to the backscattered electrons.

The morphologies of the porous materials were examined using a JEOL 7600F (Japan). The samples were sputter-coated with a 15 nm-thin layer of gold with a sputter coater (Ted Pella, Cressington208HR High Vacuum Turbo Sputter Coater) prior to examination, to be electrically conductive. The samples were mounted on aluminum foil with double-sided tape and then introduced into the sputtering device. They were then stored in a vacuum dissecator before analysis. All samples were observed in Secondary Electron Imaging (SEI) mode, with either Low Magnification (LM) or higher magnification (SEM) with an acceleration voltage of 5kV at a working distance of 8 mm.

Chapter 5

Results and discussion

5.1 Solvent evaporation

Solvent evaporation is widely used to induce supersaturation and crystallization. It is also an easy way to prepare films. However, thermal treatment is often required afterwards to generate a more defined starting state, as well as to increase the crystallinity of the material and improve its properties.
In order to analyze the effect of isothermal crystallization in the following sections, let us first analyze the film after solvent evaporation at room temperature for low and high MM PEG for comparison.

By its intrinsic slow rate of crystallization, neat PLA does not crystallize at room temperature after evaporation of the solvent (image not shown). In contrast, blends 90/10, 70/30 and 50/50 PLA/PEG crystallize under solvent evaporation as shown in Figure 5.1.

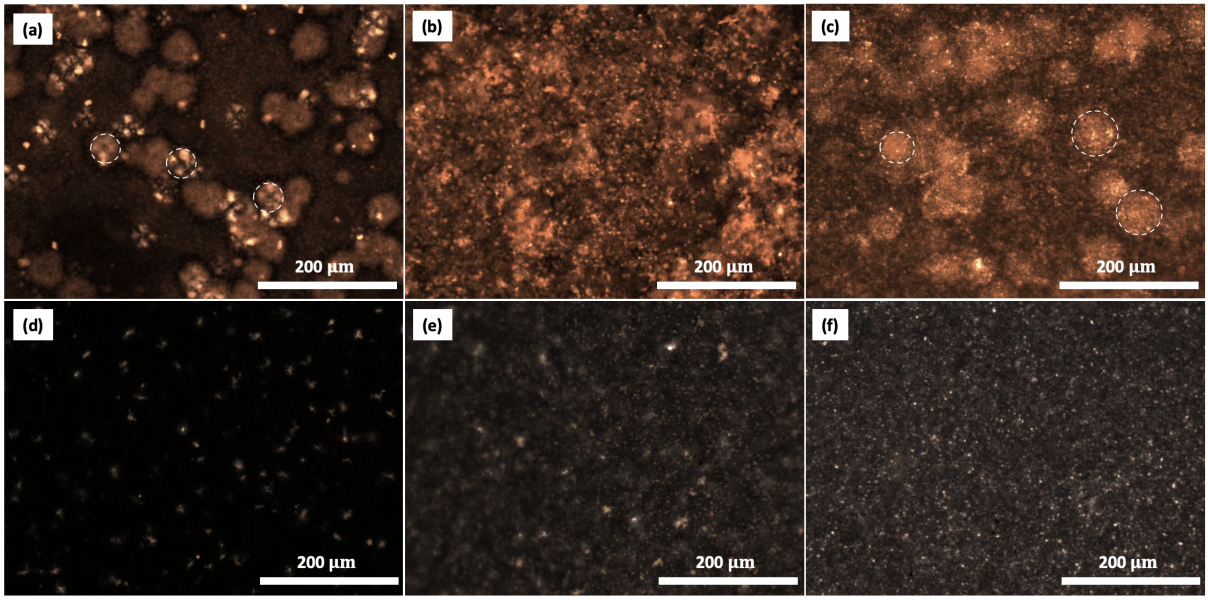

Figure 5.1: POM micrographs after solvent evaporation of PLA/PEG3K 90/10 (a), PLA/PEG3K 70/30 (b), PLA/PEG3K 50/50 (c), PLA/PEG10K 90/10 (d), PLA/PEG10K 70/30 (e), and PLA/PEG10K 50/50 (f).

On the one side, with PEG3K spherulites of $\sim$ 40 µm diameter are observed for the 90/10 blend (see circles in Figure 5.1 (a)) and of $\sim$ 70 µm for a larger PEG content (Figure 5.1 (c)). However, spherulites do not cover the entire surface homogeneously, indicating incomplete spherulitic growth. The completion of spherulitic growth increases with the PEG content.

On the other side, with higher molar mass PEG10K (Figure 5.1 (d), (e), (f)), spherulites are much smaller and less easily distinguishable than with the lower molar mass, but it is still more crystalline than neat PLA, especially for the 30 and 50 wt% of PEG. This can be explained by the fact that the higher the molar mass of PEG, the higher the viscosity of the concentrated solution, resulting in a decrease in the growth rate of PLA spherulites.

This is in line with the work of Li et al.[38], where they concluded that when the molar mass of PEG is 8000 g/mol or above, it causes more resistance to crystallization compared to PEG of lower molar mass.
Likewise, the presence of PEG decreases the blend viscosity compared to pure PLA; therefore the introduction of PEG increases the crystallization of the blends, although it is unclear whether it is the PLA, PEG, or both that crystallize during solvent evaporation.

SEM analysis of the porosity of the films after PEG extraction is shown in Figure 5.2. In LM micrographs of the inserts in Figure 5.2 (a) and (d), homogeneous undulation and depressions on the surface can be noticed. This roughness becomes pores of slightly increasing size with increasing PEG content (Figure 5.2 (b), (c), (e), (f)). However, SEM micrographs in high magnification mode do not show the presence of porosity. Spherical structures may result from partial phase separation between PEG and PLA, or may be due to solvent evaporation. These appear closed, with some slightly open at 50 wt% of PEG in Figure 5.2 (c) and (f). Their size increases by about one micrometer as the molar mass increases.

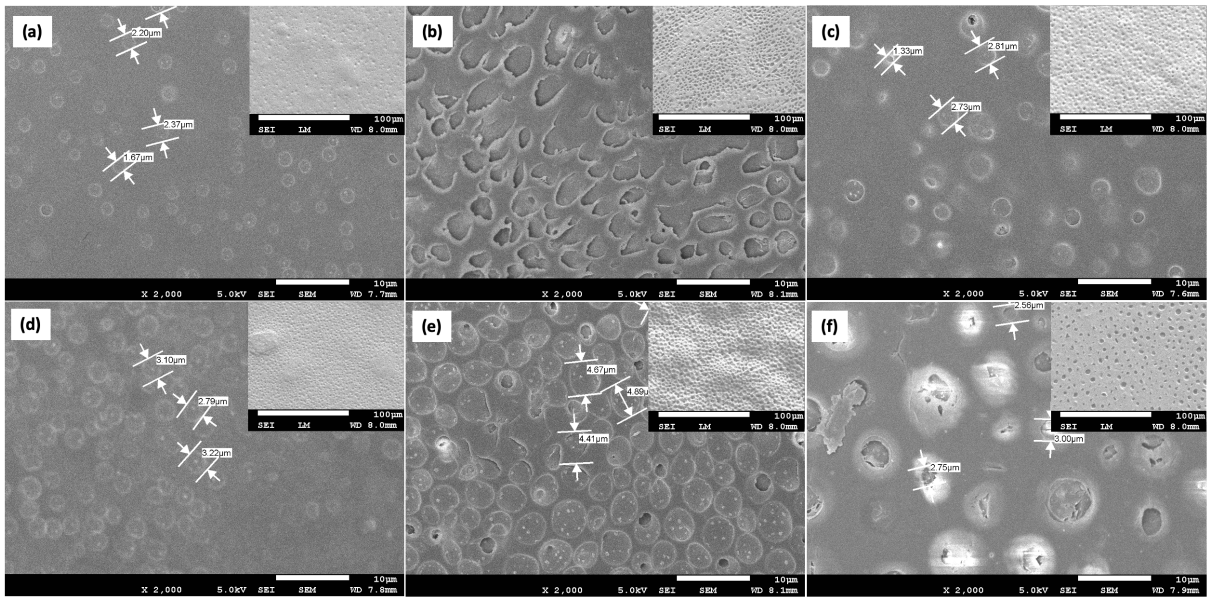

Figure 5.2: SEM micrographs after PEG extraction of PLA/PEG3K 90/10 (a), PLA/PEG3K 70/30 (b), PLA/PEG3K 50/50 (c), PLA/PEG10K 90/10 (d), PLA/PEG10K 70/30 (e), PLA/PEG10K 50/50 (f). Inserted images are the LM images.

The objective of this analysis was to show that the evaporation of the solvent at room temperature allows the blends to crystallize slightly but does not present any exploitable porosity. Indeed, open porosity is necessary for all cell growth in future applications. It also confirmed that PEG increases the crystallinity of the samples compared to neat PLA. However, the evaporation of the solvent is not similar over the whole surface and leads to non-uniform films. In the following analyses, thermal treatment will erase the morphology. Then, isotherms will be applied to control the crystallization and phase separation to determine which parameters might control the porosity.

5.2 Evaluation of the extraction method

To analyze the porosity created by the removal of PEG from PLA/PEG films, it is essential to ensure that PEG is properly extracted. For this purpose, FTIR analyses were performed on samples before and after extraction. As explained in the experimental section, the extraction consists in immersing the films in MilliQ water for 24 hours, with water change after 1 and 4 hours. Table 5.1 summarizes the main absorption peaks observed in Figure 5.3 for neat PLA and neat PEG in the range 600–3100 cm^{-1}.

	Wavenumber (cm^{-1})	**Characteristics**
PLA	1751	C = O stretching
	2942	CH_3 symmetric stretching
	2995	CH_3 asymmetric stretching
PEG	842	CH_2 rocking, C − O and C − C stretching
	958	CH_2 rocking and twisting
	1124	C − O and C − C stretching
	1340	CH_2 wagging
	2883	CH stretching

Table 5.1: Characteristic absorption peaks of FTIR spectrum of neat PLA and PEG [52]

Only the spectra of PLA/PEG10K blends before thermal treatment were analyzed, as previous studies showed no differences in FTIR spectra of PEG10K and PEG3K [52]. Figure 5.3 displays FTIR spectra of neat PLA (grey), neat PEG (blue) and the 50/50 PLA/PEG10K blend films before (yellow) and after extraction (orange). The spectra of the 90/10 and 70/30 blends were also measured and are available in Appendix A.1. Before extraction, the spectrum of the blend shows similar absorption peaks as both PLA and PEG, with lower amplitude. After extraction, its spectrum is similar to neat PLA, the specific peaks of PEG at 2883, 1340, 1124, 958, and 842 cm^{-1} have disappeared (see vertical lines in Figure 5.3). This was also measured for the thermally treated samples.
Transmission spectra were performed to ensure that the PEG was well extracted throughout the film thickness, with film thicknesses of approximately 70 micrometers (after heat treatment). Transmission mode spectra are not showed here, but they confirmed that PEG was indeed extracted in depth, validating that the extraction process by immersion in water is efficient. It also shows that the PEG is not trapped in closed pores, otherwise PEG could not have been extracted.

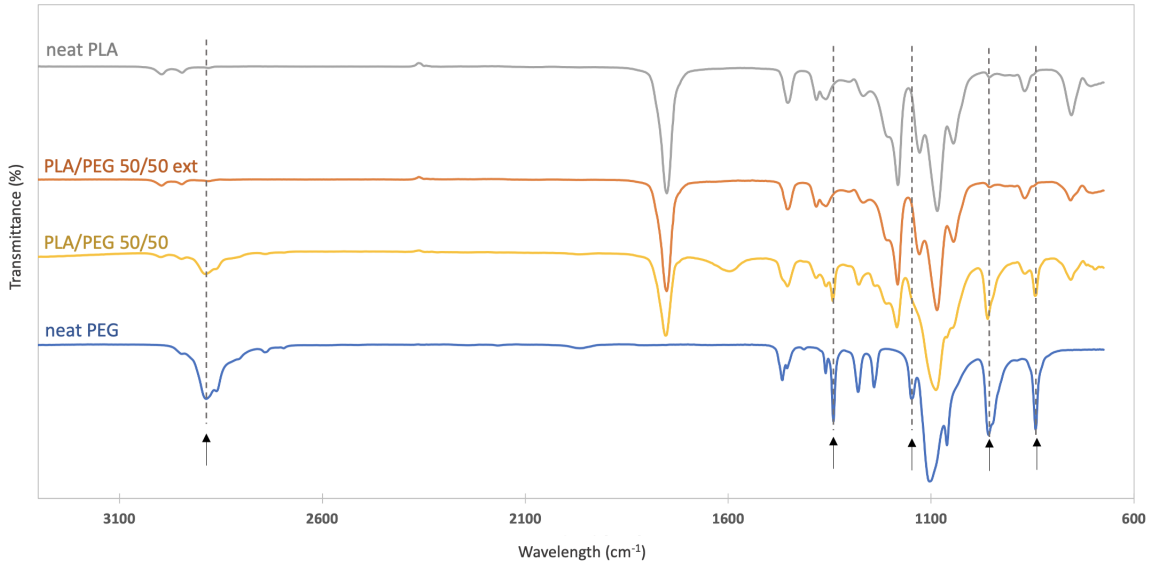

Figure 5.3: FTIR spectra of neat PLA, neat PEG and the blend 50/50 before and after extraction (ext).

To support these results, POM micrographs of the films after PEG extraction were also taken. After extraction, the birefringent character of PEG disappears with the dissolution of PEG, leaving the skeleton of PLA spherulites that are less birefringent (Figure 5.4 (e), (f)). Fibrils are seen within the PLA spherulites, suggesting that PEG crystallizes in the regions between these fibrils in PLA spherulites. In addition, cracked areas between spherulites are frequently observed, suggesting that PEG was also likely repelled from PLA spherulites during PLA crystallization. PEG would therefore be located in inter-and intra-spherulitic regions. This will be confirmed and discussed in the porosity analysis in the following sections.

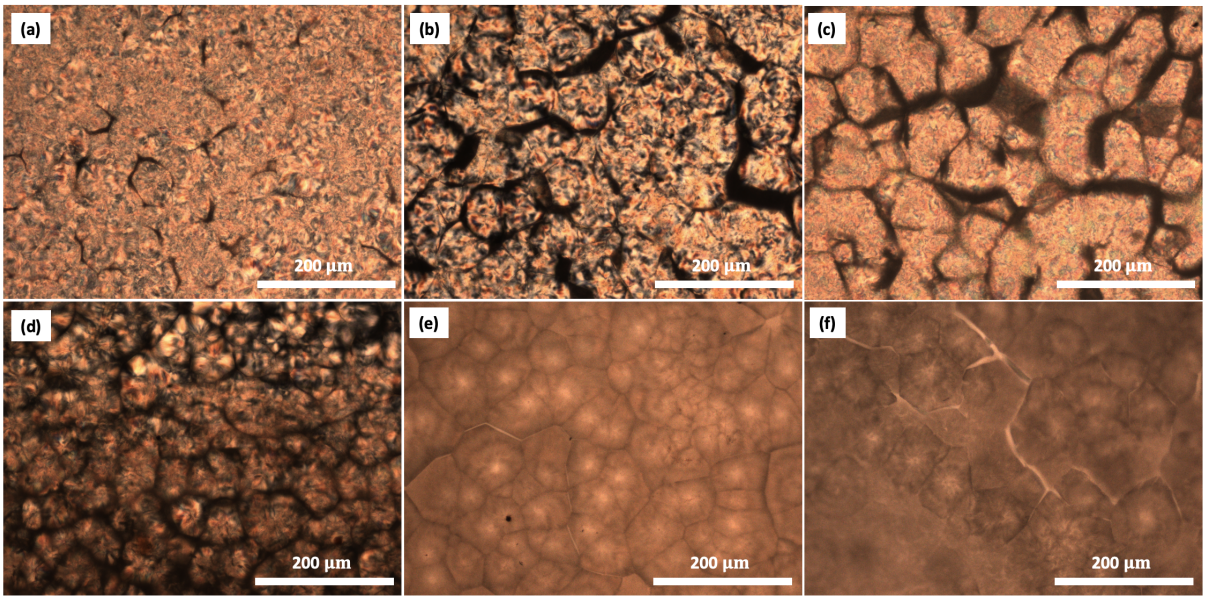

Figure 5.4: POM micrographs before (a, b, c) and after extraction (d, e, f) of PLA/PEG10K 90/10 (a, d), PLA/PEG10K 70/30 (b, e), PLA/PEG10K 50/50 (c, f).

Now that the PEG extraction method has been validated, this ensures that the post-extraction samples that will be observed by SEM will indeed be composed only of PLA. The observed porosity will therefore be due to the removal of PEG. The different parameters can now be studied.

5.3 Characterization of PLLA films

5.3.1 Effect of blend composition

Before analyzing the porosity of the samples, it is important to study the morphology before PEG extraction. To see the effect of the composition of the blends on the morphology of PLA by POM, the samples that were isothermally crystallized for 4 hours at 130°C were selected because they are representative of the general phenomena also observed at isothermal crystallization temperatures of 70 and 110°C. POM micrographs are available for these two crystallization temperatures in the Appendix A.2.

Compared to the films before heat treatment, large differences in film morphology can be observed, depending on the PEG content. Neat PLA (Figure 5.5 (a)) shows spherulites with the Maltese cross pattern. Initially, some nucleation sites appear (forming larger spherulites), while many others appear later and form smaller spherulites. Thus, the process of nucleation is sporadic and not immediate.

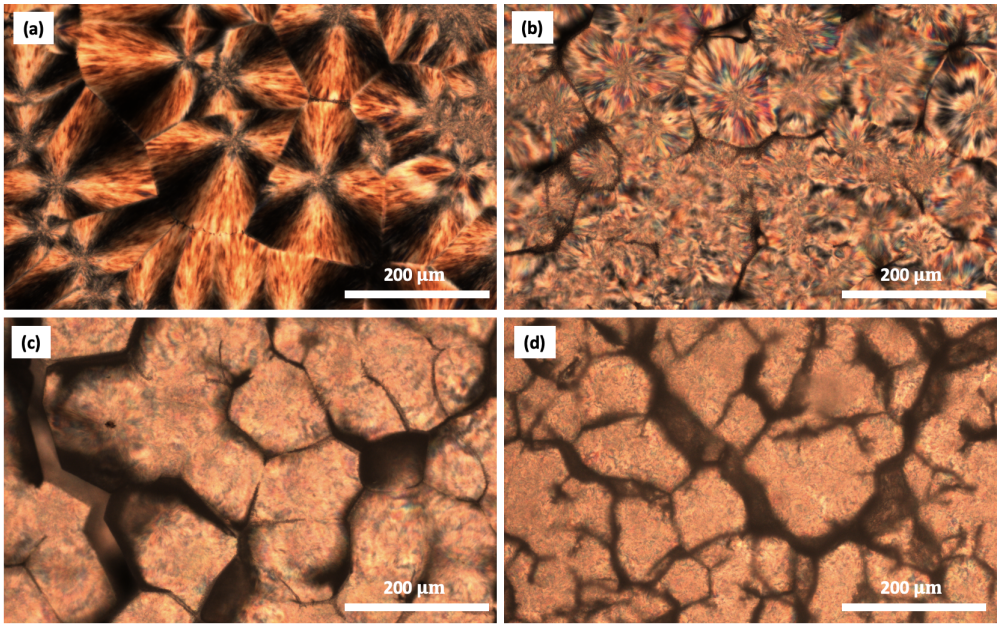

Figure 5.5: POM micrographs before extraction, after 4h at T_c = 130°C of neat PLA (a) and blends PLA/PEG10K 90/10 (b), PLA/PEG10K 70/30 (c), PLA/PEG10K 50/50 (d).

At a PEG content of 10 wt% (Figure 5.5 (b)), an increase in nuclei density and a larger number of spherulites with smaller size can be seen compared to pure PLA. This shows that PEG improves the crystallization ability of PLA, which is probably due to the decrease in viscosity.
At 30 wt% and 50 wt% of PEG (Figure 5.5 (c) and (d)), more and more nuclei appear. As a result, the spherulites tend to impinge on their neighbors and impede further growth, resulting in smaller spherulites. This makes difficult to identify the Maltese cross-extinction patterns. In addition, black aggregates form around the spherulites. To determine the composition of these aggregates, microscopic FTIR in ATR mode allows a probe to be inserted directly into the region of interest using microscopic optics in conjunction with the focused infrared beam. This confirmed that these black areas were PEG-rich phases. Thus, it can be assumed that PEG is found intra- and inter-spherulitically, and the higher its content, the more so. SEM micrographs of the porous films will confirm this in the following explanation.

The LM images in Figure 5.6 depict the surface morphology of the samples crystallized at 110°C after PEG extraction. At lower PEG content, there is no porosity (Figure 5.6 (a)). As the PEG content increases, the surface morphology changes and is less smooth, with spherulite patterns appearing. The spherulites are observed over the entire surface of the film and form polygons as they cross other spherulites growing at the same rate. In Figure 5.6 (b), spherulites are visible at 30 PEG wt%, as in POM images after PEG extraction in Figure 5.4 (e). The size of the spherulites is about 82 µm. Moreover, at a PEG content of 50 wt%, a distinct porosity starts to appear both within the spherulites and between them.

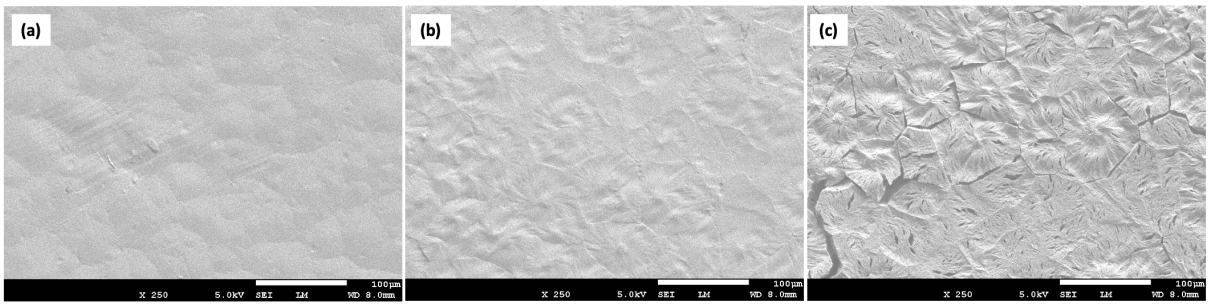

Figure 5.6: SEM micrographs in low magnification of samples after 4h at T_c = 110°C of extracted blends PLA/PEG10K 90/10 (a), PLA/PEG10K 70/30 (b), PLA/PEG10K 50/50 (c).

To observe porosity at greater depth and magnification, SEM micrographs are shown in Figure 5.7. In the first row, the morphology can be seen at lower magnification. Some areas appear bright in the gray matrix. When the surface is scanned, the contrast variations produce an image of the surface. The amount of secondary electrons produced depends on the angle of incidence of the primary beam on the surface: the greater the angle of incidence, the greater the emission and thus the production of secondary electrons. Therefore, large amounts of electrons are produced by the edges and perimeter of the pores, resulting in a lighter color [53].

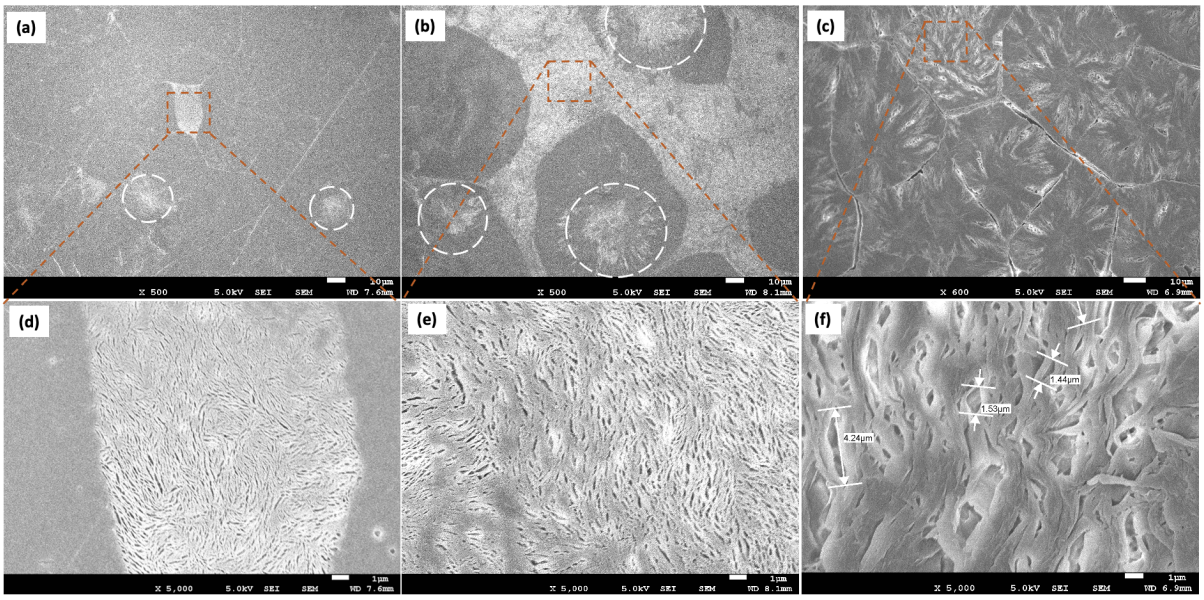

Figure 5.7: SEM micrographs of samples after 4h at T_c = 110°C for extracted blends PLA/PEG10K 90/10 (a, d), PLA/PEG10K 70/30 (b, e), PLA/PEG10K 50/50 (c, f). First row was at lower magnification x500 (a, b, c), second row at larger magnification of x5000 (d, e, f).

At 10 and 30 PEG wt%, the morphology of the samples is very heterogeneous. The clear appearing lines correspond to the interfaces between the spherulites, they are well visible on the

sample in Figure 5.7 (a). Thus, the bright areas correspond to the porosity in which the PEG was before its extraction. Porous spherulites are visible (see circles), showing that PEG was partially intra-spherulitic.
It is important to mention that what is seen on the surface depends on the orientation of the PLA lamellae. If they are parallel to the surface, the porosity created by the extraction of PEG will be visible. Besides, if the lamellae are perpendicular to the surface, the image appears grey and the porosity is not visible. This phenomenon will be discussed later in the general discussion.
Observation of these areas at higher magnification (Figure 5.7 (d), (e)) reveals porosity with a pore size of $\sim$ 1 µm. Between 10 and 30 PEG wt%, the same pore morphology is observed but with more porous zones at higher PEG composition. At lower PEG content, it localizes in the center of the spherulites and covers some of them. An expansion of porosity is observed at 30 PEG wt%.

With a further increase of the PEG content to 50 wt%, the surface morphology becomes increasingly homogeneous. The spherulites are characterized by localized porosity between their lamellae and at the edge between the spherulites. PEG appears to diffuse from the center of the spherulites toward the edge. By increasing the amount of PEG, it increasingly migrates to the interfaces between the spherulites. The porous zones observed at 30 wt% appear to become more and more clustered, creating a fracture between the spherulites.
Regarding the porosity in Figure 5.7 (f), disordered narrow strips of pores with a larger pore size between 1.4 and 4 µm are visible. As suggested by Hsieh et al.[54], this pore morphology can be attributed to the interpenetration of the thin PLLA lamellae with the PEG crystals as they grew before the PEG was extracted. After extraction, most of the PLLA lamellae exposed in the PEG-rich mixture appeared to exhibit edge orientation with occasional twisting.

One might wonder if the gray-looking area around the pores could also be porous or completely smooth. At higher magnification in Figure 5.8 (b), a tiny homogeneous porosity can be seen. The pores are smaller than 1 micron, with a width of $\sim$ 0.16 µm. The question would be whether these pores are due to the extraction of PEG, or whether they were present prior to extraction. To determine the origin of these pores, an image of a pure PLA sample after thermal treatment at 110°C for 4 hours is shown in Figure 5.8 (c). The porosity is also observed, but much more heterogeneously (see circle). The main issue with this sample was that the electron energy damaged the PLA sample rather quickly. Where small pores were observed, they became larger and larger when dwelling on that area for a few seconds. One might therefore wonder if this porosity on the neat PLA sample is not more fragile areas that break in places when imaged at this magnification.

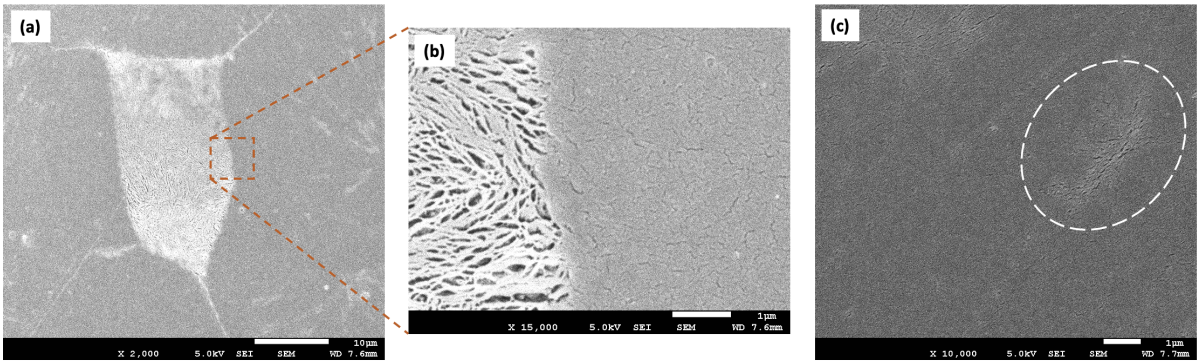

Figure 5.8: SEM micrographs in SEI of samples after 4h at T_c = 110°C of extracted blends PLA/PEG10K 90/10 at x2000 (a) and x15000 (b), and neat PLA (c).

Nevertheless, this porosity is not comparable to the one we observed in the blends after the extraction of PEG. It should also be noted that the porosity may not be visible in some areas due to a flat-on orientation of the PLA lamellae. The flat-on orientation forms near surfaces, which could explain its important presence.
Thus, since this porosity is not usable, it is not analyzed or considered in the next image analysis.

At this stage, it would be interesting to analyze a cross-section of the films to better characterize this porosity. However, since the samples were too brittle, a clean section could not be performed. Nonetheless, Figure 5.9 shows torn zones between the spherulites at 50 PEG wt%, which allows the porosity to be observed deeper in the sample. This porosity is uniformly shaped and more homogeneous than that of the surface in Figure 5.7 (f). Thus, it can be assumed that the porosity is well distributed throughout the thickness of the film. This cannot be confirmed for samples with a lower content of PEG and needs to be further investigated as it is very different from the surface porosity.

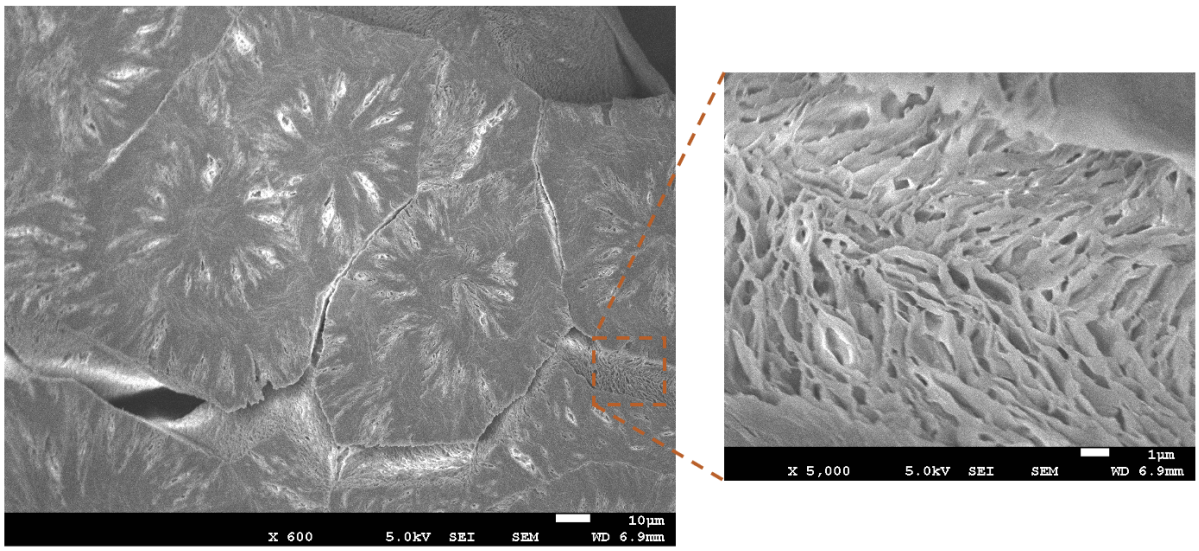

Figure 5.9: SEM image of a PLA/PEG10K 50/50 sample after 4h at T_c = 110°C after extraction. The higher magnification image shows the porosity at the fracture zone.

Based on these observations, the composition of the blends has a significant impact on the morphology before and after the extraction of PEG. With increasing PEG content, the orientation of PLA lamellae on the surface seems to change significantly. Therefore, a strong change in morphology can be observed. SEM micrographs confirmed that PEG is both inter- and intra-spherulitic as its content increases. The morphology of the pores at 10 and 30 wt% is similar, with a pore size of $\sim$ 1 µm. At higher PEG content, the morphology of the pores changes and becomes disordered and twisted, with a larger pore size between 1.4 and 4 µm.
Due to this increasing porosity between grains, the 70/30 and 50/50 samples were brittle and easily disintegrated into small pieces after PEG extraction. This could be a problem for future applications, since the purpose of the thermal treatment is to increase the crystallinity and properties of PLA. However, if the PEG content is too high, the mechanical properties look poor.

5.3.2 Effect of PEG molar mass

PEG is available in a wide range of molecular masses. Therefore, depending on the application, it is important to determine which is more suitable to control the porosity of the films and their influence on crystallinity.

Figure 5.10 shows POM micrographs of blends with PEG3K (first row) and PEG10K (second row) after isothermal crystallization at 110°C for 1 hour.
In Figure 5.10 (a) and (d), PEG3K seems to promote the spherulitic growth of PLA more than PEG10K. At 10 wt% PEG, the PLA spherulites grow in a Maltese cross pattern and are larger at the low molar mass PEG. With PEG10K, the spherulites begin to form and grow but have not yet covered the entire observed surface area. This must be due to the higher viscosity of the blends consisting of the PEG with higher molar mass.

At 30 wt% PEG, the spherulites with the Maltese cross pattern are still visible in the mixture with higher molar mass (Figure 5.10 (e)), while they are no longer visible with decreasing molar mass (Figure 5.10 (b)) as the spherulites become smaller as the nucleation sites increase with decreasing viscosity. However, the spherulites can still be seen thanks to the black areas surrounding them.
During crystallization of PLA, PEG is rejected from the PLA spherulites and forms these black aggregates. As mentioned earlier, Zhang et al.[39] compared PEO/PLA and PEG /PLA bilayer films and showed that both accelerate the spherulitic growth of PLA. However, thanks to the shorter chain length, the spherulitic growth rate of PEG/PLA film was higher than that of PEO. This confirms the observations regarding the increase in nucleation sites thanks to the plasticizing effect of PEG.

At 50 wt% PEG (Figure 5.10 (c) and (f)), there is no longer much difference between the different MM in terms of morphology. With increasing PEG content, the crystallization of PLA is increasingly improved and the molar mass seems to have less influence on the crystallization. The same observations can be made for samples crystallized at 70 and 130°C, but the morphology is different and will be discussed in the next subsection.

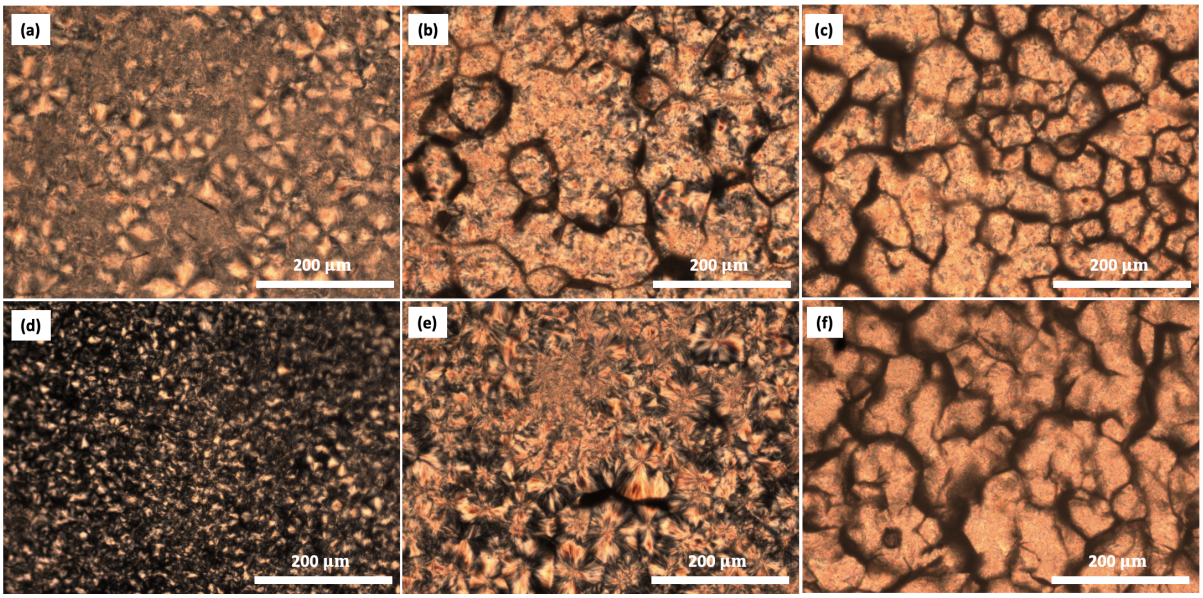

Figure 5.10: POM micrographs of PLA/PEG3K 90/10, PLA/PEG3K 70/30, PLA/PEG3K 50/50 (a, b, c), PLA/PEG10K 90/10, PLA/PEG10K 70/30, and PLA/PEG10K 50/50 (d, e, f) crystallized at T_c=110°C for 1h.

Now that the difference in crystalline morphology has been discussed, the SEM analysis of porosity can be considered. SEM micrographs of the 70/30 blends are depicted in Figure 5.11. Samples crystallized isothermally at 110°C for 1 hour were selected because they show well the differences in microstructure in the POM micrographs.

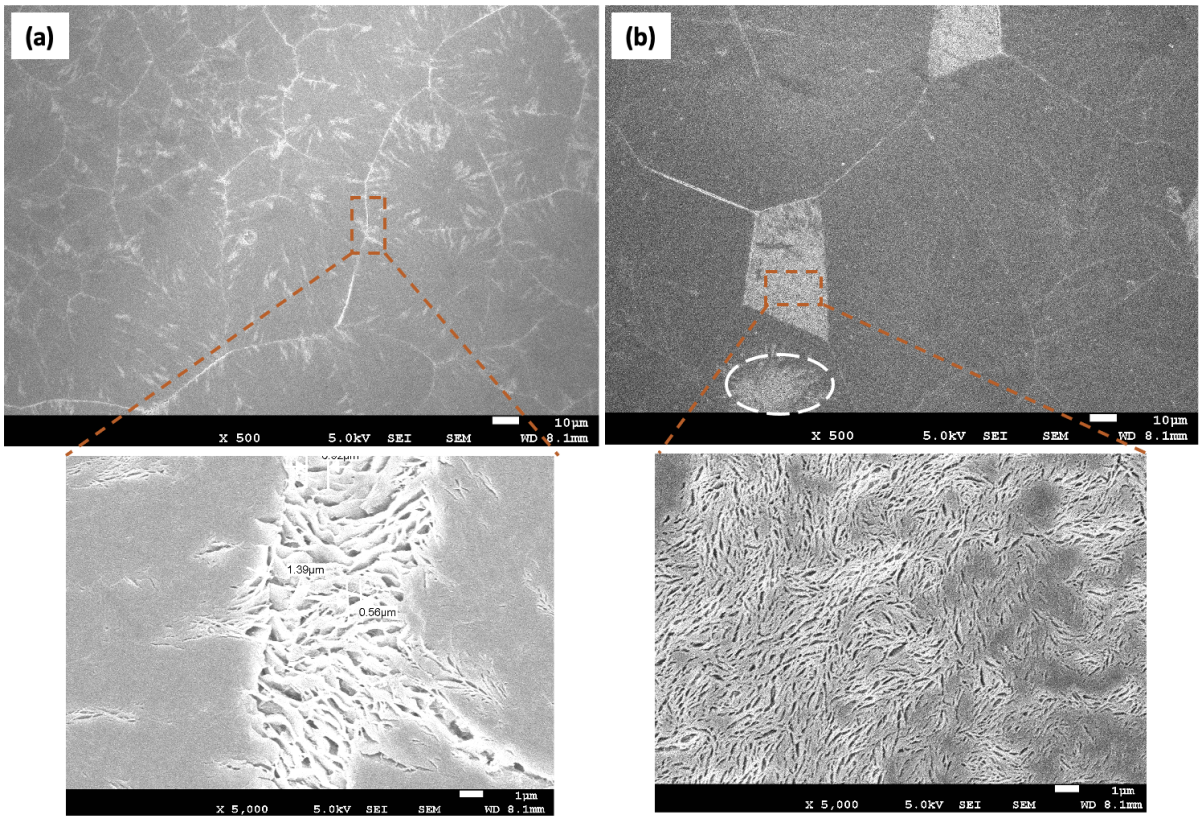

Figure 5.11: SEM micrographs after extraction of PLA/PEG3K 70/30 (a) and PLA/PEG10K 70/30 (b) crystallized at T_c=110°C for 1h.

Morphology changes significantly with molar mass. The porous areas correspond to the areas where the PEG was located before its extraction. In Figure 5.11 (a), porosity due to extraction of PEG3K is mainly localized at the edges of the spherulites with sizes between 0.5 and 1.5 µm. Again, PEG appears to migrate to the interface of adjacent spherulites as crystallization proceeds. In this way, it reveals the interfaces between the them. Nevertheless, porosity is still present around the center of some spherulites. The micrograph below is magnified and shows this porosity, with increasingly interconnected pores accumulating at the interfaces between the spherulites.

With PEG10K in Figure 5.11 (b), the porosity seen in some spherulites is heterogeneously distributed over the entire surface of the film. In some places, the porosity is partially observed in the center of the spherulites (see circle), while the entire surface of some other spherulites is porous. However, at higher magnification, the pores are regular in shape and size of $\sim$ 1 µm. PEG10K does not appear to have diffused from the spherulites to their interfaces as it did with the lower molar mass. Once more, the orientation of the lamellae on the surface shows a very different surface morphology, depending on the molar mass.

POM images show that for the 50/50 blend crystallized at 110°C, no significant differences are observed between the two molar masses. Nevertheless, this is not always the case and SEM micrographs in Figure 5.12 display the blend crystallized at 70°C for 4h after PEG extraction.

Extracted sample PLA/PEG3K in Figure 5.12 (a) exhibits a larger spherulite width size from 10 to 40 µm, ruptured in many places. As the PEG accumulated, there was nothing left after it was removed from these areas, causing the material to break in some places. Porosity is localized both at the interfaces between the spherulites and the center of them, with sizes from 0.2 to 0.7 µm.
Figure 5.12 (b) depicts the blend at the same composition, but after extraction of PEG10K. In agreement with the previous observations, the spherulites are smaller and highly porous with a larger porosity of 1 to 1.5 µm. The entire surface is more porous and pores are located between the lamellae of the spherulites, confirming that PEG was partially there before extraction. There were interstices between the spherulites, probably where the PEG chains met after their migration.

As PLA crystallization is enhanced, PEG appears to diffuse from the spherulites. With decreasing molar mass, the growth rate of the spherulites is higher and the phenomena are observed more rapidly than with higher molar mass. With increasing molar mass, the viscosity of the mixture is higher than that of PEG3K. Therefore, the chains of PEG need more time to diffuse. However, the pore width increases with molar mass, as previously discussed by Tsuji et al.[40].
After 18 hours of isothermal crystallization at that temperature, the blend PLA/PEG10K 50/50 has a similar structure to PLA/PEG3K 50/50 crystallized for 4h (see Appendix A.3). This demonstrates that PEG3K accelerates the crystallization process of PLA, even more than PEG10K, which improves the mobility of PLA chain segments less. The influence of crystallization time will be discussed later.

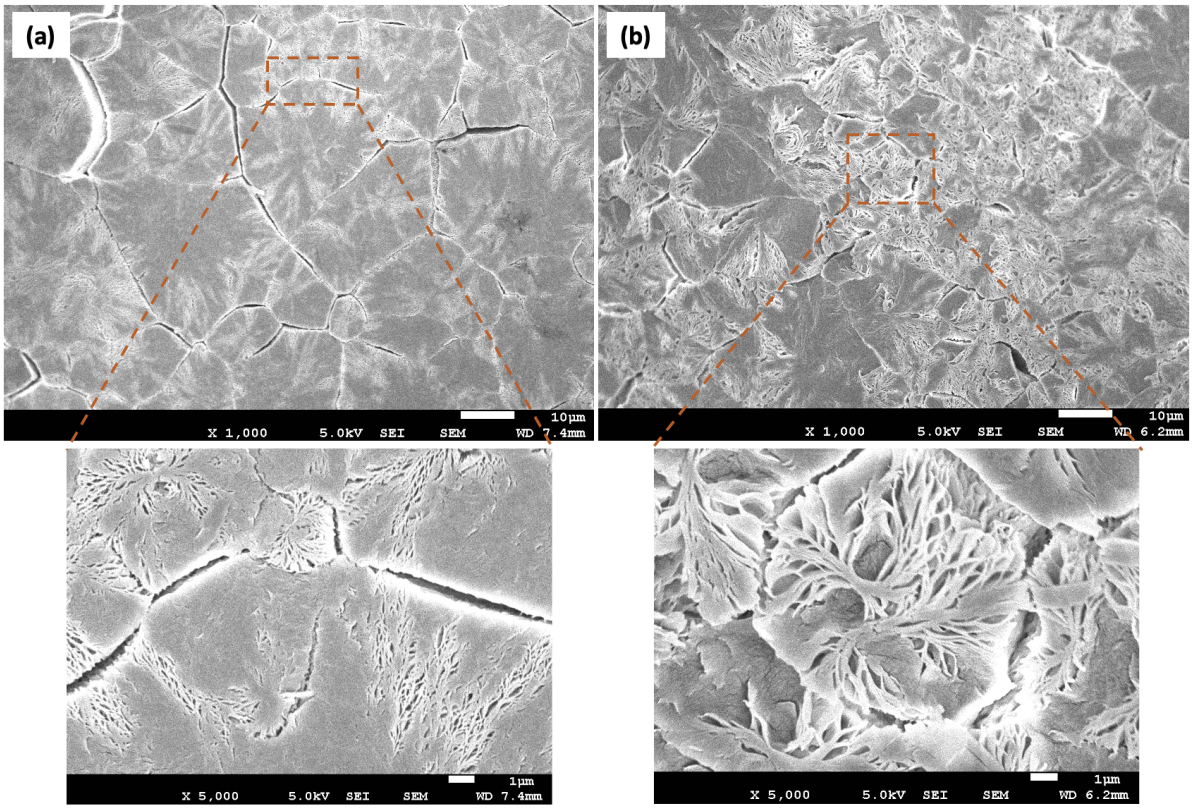

Figure 5.12: SEM micrographs after extraction of PLA/PEG3K 50/50 (a) and PLA/PEG10K 50/50 (b) crystallized at T_c=70°C for 4h.

To conclude, the molar mass of PEG has an effect on porosity. A lower molar mass improves the crystallization process of PLA more than a higher one. Nevertheless, the morphology of

the pores does not change significantly, while their size varies and increases with MM. When the crystallization time is longer, approximately the same pore morphology and distribution are obtained for a given composition. However, the distribution of porosity at the surface changes with accumulation at the interfaces, which is more pronounced at lower MM as PEG seems to diffuse more rapidly.
Migration of PEG to the interfaces between the spherulites could be a problem, because the films are much more brittle and difficult to handle. In the next subsection, the influence of crystallization temperature will be discussed.

5.3.3 Effect of isotherms

Before choosing isothermal temperatures, it was important to verify that the blends can crystallize at these temperatures. Temperatures at three locations in the spherulitic growth rate bell-shaped curve versus temperature of PLA were chosen. The lower selected temperature is close to the T_g of PLA, which slows down the crystallization due to the increasing viscosity of the liquid. The intermediate temperature is close to the maximum spherulitic growth rate. Then, the higher temperature is close to the thermodynamic melting temperature ($T°_m$). At that temperature, crystallization slows down until it stops at T_c=$T°_m$.
As mentioned in Chapter 2, the kinetics of melt crystallization of PLA have been extensively studied and isothermal crystallization temperatures were determined over a wide temperature range from 70 to 165°C with a maximum around 105-120°C [16].

DSC experiments were conducted at 70°C (near T_g), 110°C (near to the optimal growth rate temperature) and 130°C (near $T°_m$). Samples were first heated from 25 to 200°C to erase the thermal history for 5 minutes. Then, they were cooled down to the isothermal temperature at a cooling rate of 10°C/min and maintained for 20 minutes at this isotherm. Then, samples were cooled down to -20°C at same rate, before a second heating from -20 to 200°C at same rate. Measurement were taken during the second heating.

Figure 5.13 shows DSC heating curves of neat PLA and PLA/PEG3K blends after isothermal crystallization at 70°C (light blue), 110°C (medium blue) and 130°C (dark blue).
For the second heating, the PLA curves after isotherms at 70 and 130°C are similar. The T_g of PLA appears about 65°C (circled in the figure). This means that amorphous parts of PLA were present after the isotherm and that PLA does not crystallize or crystallizes poorly at 70 and 130°C. Moreover, a cold crystallization peak (T_{cc}) is observed at 99°C, as the polymer chains gain mobility and can rearrange more easily to form crystals. However, after an isotherm at 110°C, the T_g and T_{cc} of PLA are no longer present. PLA can therefore effectively crystallize at this temperature.

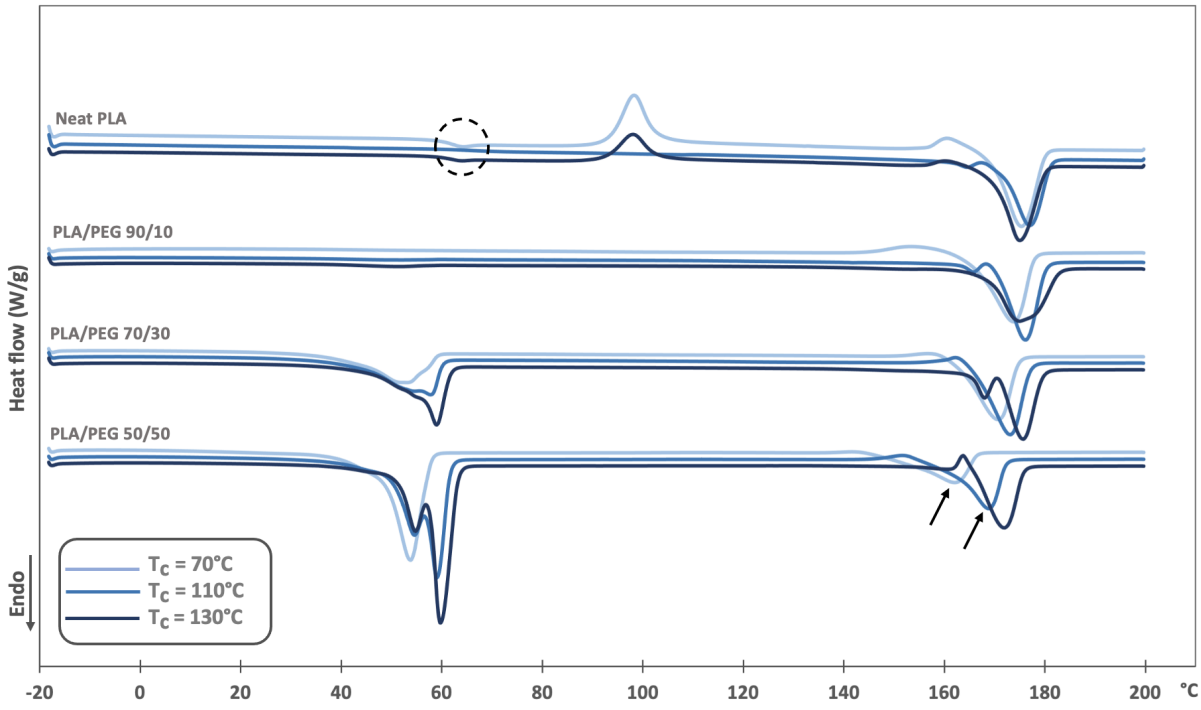

Figure 5.13: DSC heating curves of neat PLA and PLA/PEG3K blends.

From a PEG content of 10wt% and above, the T_g and the T_{cc} of PLA disappear after all isotherms, because PEG chains have mixed with PLA, which increases the mobility of the molecular chains and allows rearrangement of the chains. A small broad exothermic peak appear just before (T_m), because a small remaining amorphous amount crystallizes. The addition of a small amount of PEG enhances the crystallization of PLA. Thus, PLA crystallizes during all isotherms, thanks to the addition of PEG.
At a low PEG content of 10wt%, the melting peak of PEG is absent. PEG does not crystallize either during the isotherm or the cooling. The content is low and the PEG molecules are too dispersed in the PLA to crystallize successfully.

Nevertheless, as the PEG content increases, PEG is able to increasingly crystallize during cooling and melt when heated to $\cong$ 55°C. However, PEG will never crystallize during isotherms because it is above its T_m in the liquid state. PEG improves PLA crystallization at 10 and 30wt% of PEG content, but PLA melting enthalpy decreases slightly when the content reach 50wt% at the lower isothermal temperatures (see arrows). This may be due to the PEG content which segregates from PLA and could increases the viscosity at this PEG content. Consequently, if the temperature is not high enough to allow the viscosity to decrease, PEG will hinder the crystallization of PLA.
In addition, the phase separation of the blends can be discussed. PEG segregates from PLA above 10 wt% of PEG, because the melting peak of PEG and PLA are present. This is consistent with Sungsanit et al.[34] and others [39][49] who found that phase separation from the PLA/PEG blends occurs when PEG content exceed 10 wt%.
These results clearly demonstrate that PEG improves the crystallization of PLA and allows it to crystallize at 70 and 130°C. They also confirm that these three isotherms can be selected for crystallization of the blends. These DSC curves will support the following analysis.

Before analyzing POM micrographs of the blends, images of neat PLA are shown in Figure 5.14. At 70°C, PLA does not crystallize during the isotherm (Figure 5.14 (a)), in agreement with the literature and DSC results. At 110°C, the maximum spherulitic growth rate is reached, many nucleation sites and spherulites of $\sim$ 45-50 µm with the Maltese cross pattern can be observed (see circles in Figure 5.14 (b)). Ma et al.[55] confirmed that higher nucleation density was observed at 100°C and 110°C, which is the fastest crystallization temperature for PLA.
At 130°C, even if PLA does not crystallize during the 20-minutes isotherm in DSC, it crystallizes after 4 hours. The size of the spherulites increased to $\sim$ 200 µm with the increasing crystallization temperature, which can be attributed to the decrease in nucleation density (Figure 5.14 (c)).

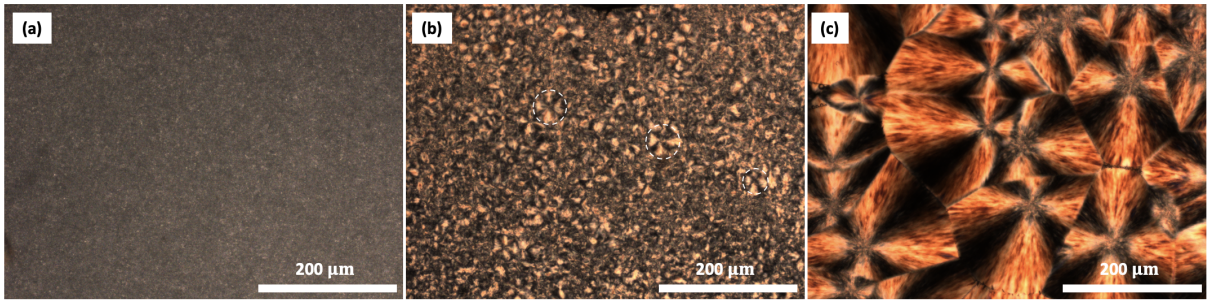

Figure 5.14: POM micrographs of neat PLA crystallized at T_c=70°C (a), T_c=110°C (b), and T_c=130°C (c) for 4h.

As discussed by Zhang et al.[56], nucleation is slower when the samples crystallized at a higher T_c, which gives the polymer enough time to form stable crystals. However, due to the larger size of the spherulites, aggregation of the amorphous PLA chains and formation of coherent amorphous phases occurs. Ma et al.[55] investigated the effects of crystallization temperature

on the mechanical properties and found that the mechanical properties decreased with increasing crystallization temperature, which can be attributed to this phenomenon.

Figure 5.15 shows POM micrographs of PLA/PEG10K blends after 4 hours isotherms. The first, second, and third columns represent the three blend composition after 70, 110, and 130°C isotherms, respectively.
At 70°C, PEG enhances nucleation and allows crystallization of PLA at lower temperatures. The spherulites are more evident in the 70/30 blend (Figure 5.15 (b)), the nucleation density increases with higher PEG content, covering the entire surface (Figure 5.15 (c)).
If the temperature is increased to 110°C, the morphology of the 90/10 and 70/30 blends changes significantly. At 10 wt% PEG, crystallization is already well advanced and nucleation is so advanced that no spherulites can be distinguished (they are too small), while at 70°C crystallization has just started and some nucleation sites are present. As DSC shows, the enthalpy of fusion of PLA after isothermal crystallization at 110°C is already slightly higher after 20 minutes than at other isotherms, leading to a more crystalline morphology over time thanks to the effect of PEG (Figure 5.15 (d)). At 30wt%, black aggregates appear as in the 50/50 blend at 70°C. At 50 wt% PEG, however, there is not much change compared to the isotherm at 70°C, and the aggregates appear to become larger and larger, perhaps because PEG diffuses more and more to the interfaces of the spherulites as crystallization progresses, as mentioned earlier. As the crystallinity of PLA increases, the amorphous regions become smaller, causing PEG to migrate out of the spherulites.
At 130°C the general morphology of the blends remains similar to the isotherm at 110°C.

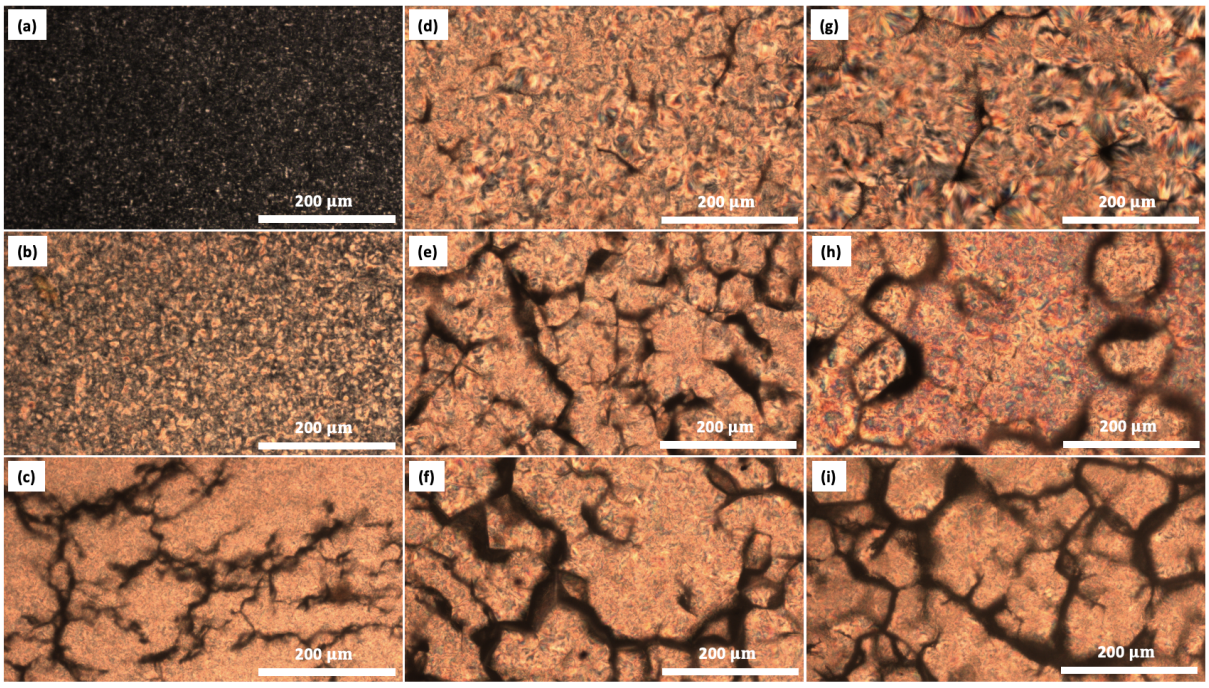

Figure 5.15: POM micrographs of PLA/PEG10K 90/10, PLA/PEG10K 70/30 and PLA/PEG10K 50/50 isothermally crystallized at T_c=70°C (a, b, c), T_c=110°C (d, e, f), and T_c=130°C (g, h, i) for 4h.

The results show that crystallization and crystal morphology are closely related to temperature, which determines the formation and growth of crystal nucleus.
On this basis, SEM micrographs were taken on PLA/PEG10K 70/30 blends isothermally crystallized for 4 hours at 70, 110, and 130°C.
Figure 5.16 (a) depicts the 70/30 blend crystallized at 70°C and after extraction of PEG. In agreement with Figure 5.15 (b), the surface is quite homogeneous with lighter areas resembling

small spherulites. At higher magnification, the porosity is not uniformly distributed, but it is clear that PEG was located in spherulites. The pores are not interconnected at the surface and are difficult to measure, but appear to be about 0.5 to 1 µm wide.
In Figure 5.16 (b), the spherulites are larger after isothermal crystallization at 110°C. As already discussed in the subsection 5.3.1, PEG molecules accumulated more and more, forming large porous regions. In some areas (see circles in Figure), the pores are uniformly distributed with a size of $\sim$ 1 µm; in these areas, the orientation of the lamellae is favorable for observation.
At higher isothermal temperature, more and more such areas are seen. In Figure 5.16 (c), the spherulites show porosity accumulated at the spherulite boundaries, indicating segregation of PEG in inter-spherulitic regions. PEG seems to have diffused more from the center of the spherulites to their boundaries. The pores are larger than at lower isothermal temperatures, and range in size from 1.2 to 2 µm.

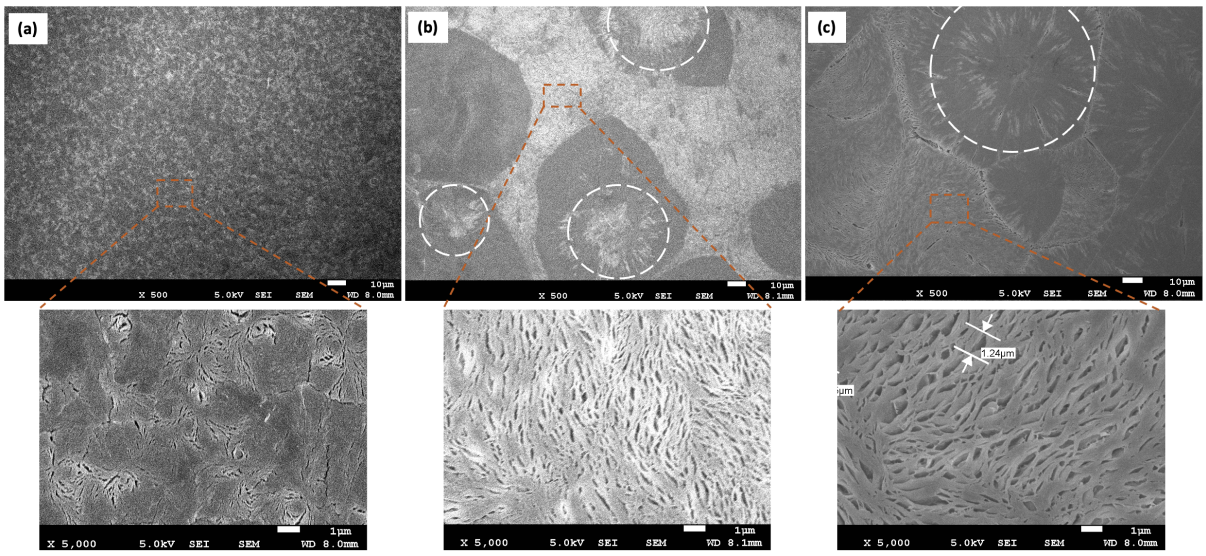

Figure 5.16: SEM micrographs in SEI of extracted blends PLA/PEG10K 70/30 after isotherm of 4h at T_c = 70°C (a), 110°C (b) and 130°C (c). First row is at lower magnification x500, second row at larger magnification of x5000.

The blends crystallize better at higher temperatures. Although the images from POM are not significantly different between 110 and 130°C, the images from SEM are significant after extraction. From SEM observations, the spherulites are much larger after isotherms at 110° and 130°C than at 70°C, in agreement with POM observations. Porosity begins to distribute heterogeneously as temperature increases, because crystallization is more advanced. PEG was clearly segregated intra-and even inter-spherulitically at T_c of 110 and 130°C. The pore size also increases slightly with T_c and the pores become increasingly interconnected at the surface. With increasing temperature, the spherulites appear to increasingly repel the PEG molecules, causing porosity to gather between the spherulites and form large porous aggregates. Consistent with this, Wang et al.[35] showed that the migration rate of PEG was slower at 100°C than at 130°C, because both the PLA molecules and plasticizer have a higher mobility at a higher temperature.

5.3.4 Effect of crystallization time

The last parameter to be analyzed is the crystallization time. As mentioned in Chapter 1, the influence of crystallization time has already been studied. Lie et al.[38] studied the crystal morphology of blends of PDLA-PEG-PDLA triblock copolymer and PLLA, with various MM of PEG from 2000 to 8000 g/mol crystallizing isothermally from 5 minutes to 4 hours at 140 and 180°C. Since it is not known how long it takes PLA to crystallize in the presence of PEG, three isothermal crystallization times were chosen: 1, 4 and 18 hours. This will allow to assess the effects of crystallization time on the crystal morphology of PLA/PEG blends.

POM micrographs are shown in Figure 5.17 for neat PLA (first row), PLA/PEG3K 90/10 (second row) and PLA/PEG10K 90/10 (third row). The samples of the first, second and third columns were crystallized at 110°C for 1, 4, and 18 hours, respectively. These samples were selected because the most significant changes in PLA and 90/10 blends were observed at T_c of 110°C, which is approximately the fastest crystallization temperature of PLA [55]. The micrographs at 70 and 130°C are shown in the appendix A.4.
At 70°C, there is no difference in structure between 1, 4 or 18 hours of crystallization, for both PLA and blends. The final structure seems to be reached after 1 hour. However, it is very difficult for PLA to crystallize at this temperature, so changes may occur after a longer period than 18 hours. It is interesting to note that the samples at 30 wt% PEG and above are crystallized with many small spherulites, in contrast to the 90/10 blends, which are not very crystalline. At 130°C, the same conclusion emerges. For both for PEG3K and PEG10K, there are no morphological changes with time. However, since the PLA already crystallizes effectively at this temperature, all blends above 10 wt% PEG are crystalline.

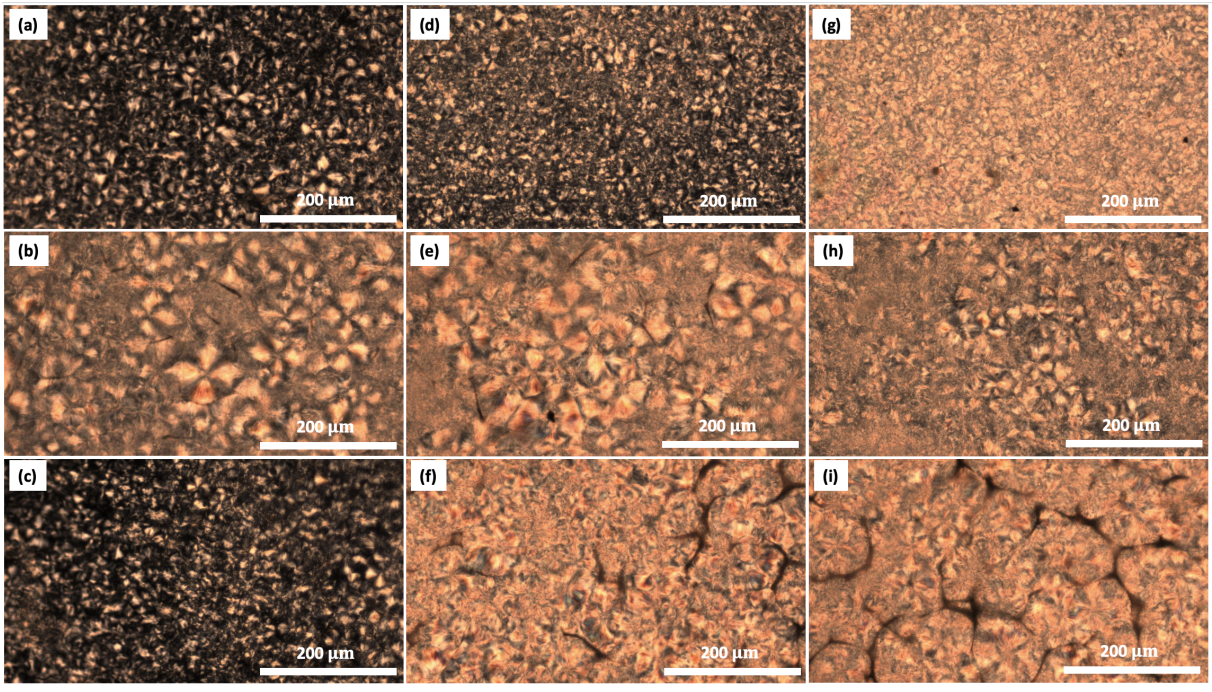

Figure 5.17: POM micrographs of neat PLA (first row), PLA/PEG3K 90/10 (second row), PLA/PEG10K 90/10 (third row) crystallized at T_c=110°C for 1h (a, b, c), 4h (d, e, f), and 18h (g, h, i).

PLA has an intrinsically slow crystallization rate; it takes time to complete its crystallization. At 110°C, between 1 and 4 hours (Figure 5.17 (a) and (d)), spherulites do not appear numerous, but smaller. If the crystallization time is extended to 18 hours, the crystals fill the entire surface (Figure 5.17 (g)) and the cross extinction pattern is no longer visible. The number of nucleation sites appears to increase with time at this temperature.

With the introduction of PEG3K, the spherulites become much larger, reaching a diameter of 100 µm (Figure 5.17 (b) and (e)). However, with time, smaller spherulites of 50 µm form with increasing PLA nucleation sites (Figure 5.17 (h)). The surface is heterogeneous and the spherulites are imperfect.
PEG 10K does not change the crystal morphology of the blend after 1 hour (Figure 5.17 c). At 10 PEG wt%, the PEG chains diffuse slowly. Therefore, there is no difference in the crystalline structure after 1 hour for this composition. In the DSC curves, PEG in 90/10 blends did not crystallize after 20 minutes isotherm, which could explain the unchanged morphology compared to neat PLA. Nevertheless, tiny spherulites form rapidly, and the nucleation density increases dramatically between 1 and 4 hours (Figure 5.17 (c) and (f)). PEG increases the nucleation density and inhibits the growth of large spherulites after 4 and 18 hours. As mentioned in the section on the effect of molar mass 5.3.2, the longer molecular chains with higher molar mass PEG are less likely to decrease viscosity compared to lower MM, so they tend to accumulate more at the boundaries of PLA spherulites. Because of this phenomenon, PEG could hinder the growth of larger spherulites, as observed with PEG3K, resulting in tiny crystals with PEG10K..

Blends based on PEG3K did not show significant structural differences in POM. Therefore, the analysis of the effect of crystallization time by SEM is performed on the samples after the extraction of PEG10K. Figure 5.18 (a) and (b) show extracted blends 90/10 after crystallization time of 1 and 4 hours, respectively. With time, porosity is much less present in the spherulites and appears to decrease at these sites. The pore width seems to be the same except at the interface where the pores are interconnected and slightly larger. It can therefore be assumed that the location of the porosity corresponds to the black aggregates that begin to form around the crystal structure of the mixture in the POM micrograph in Figure 5.17 (f). When measuring the width of these aggregated in the POM and SEM micrographs (white porous aggregate in Figure 5.18 (b)), the same width of about 10 µm is observed.

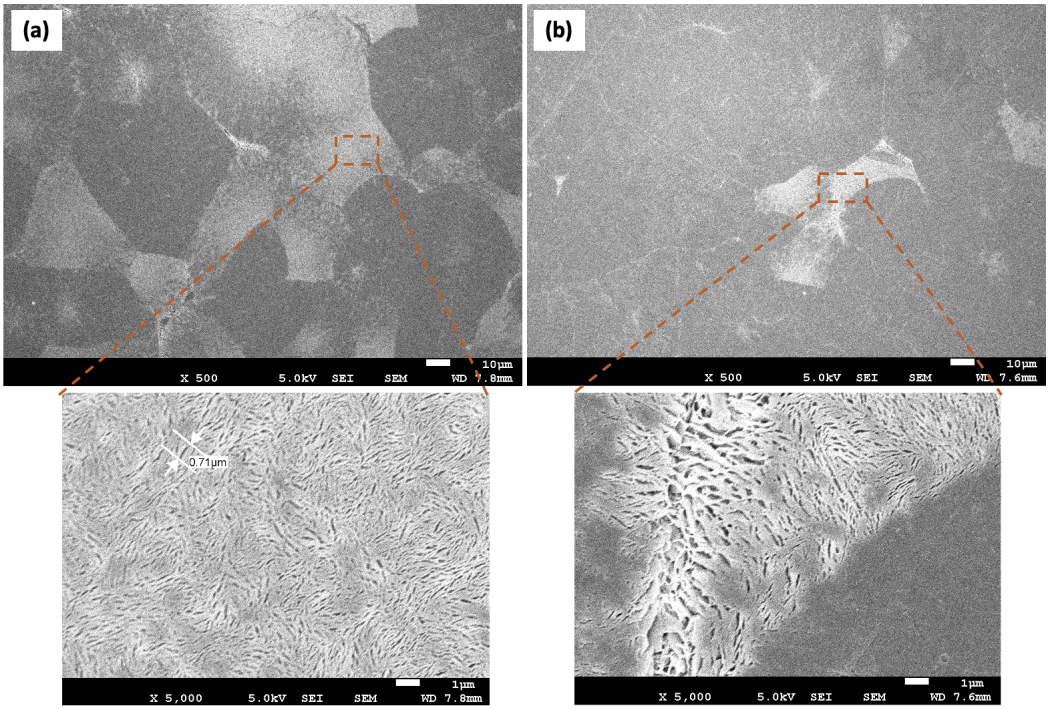

Figure 5.18: SEM micrographs after extraction of PLA/PEG10K 90/10 crystallized at T_c=110°C for 1h (a) and 4h (b).

Significant changes in the porous structure can also be seen on SEM micrographs of the extracted PLA/PEG10K 70/30 blends. Before discussing them, the POM micrographs before extraction are shown in Figure 5.19 (a) and (b). Between 1 and 4 hours of crystallization, the main difference is in the crystalline structure. In Figure 5.19 (a), the spherulitic pattern can still be seen in some parts of the sample. However, as time progresses, the spherulites impinge each other and form a crystalline structure in which the pattern can no longer be seen. In addition, black aggregates form with time and their width appears to increase, which is due to PEG migration from the spherulites during crystallization of PLA.

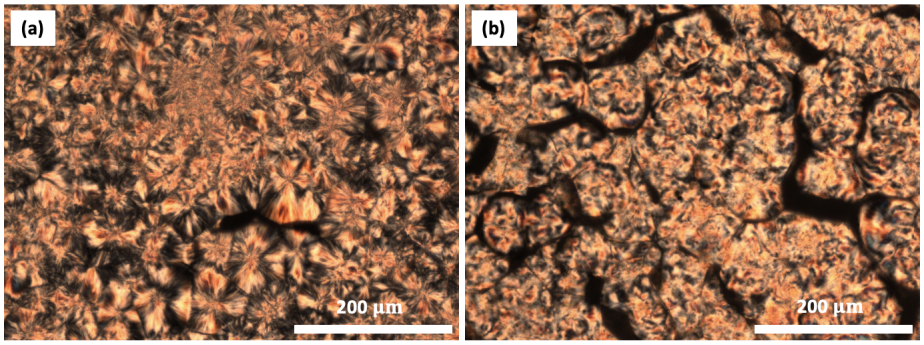

Figure 5.19: POM micrographs of PLA/PEG10K 70/30 crystallized at T_c=110°C for 1h (a) and 4h (b).

At 30 wt% PEG after 1 hour of crystallization, porosity can be observed in some fully porous spherulites with a homogeneous pore size of $\sim$ 1 µm. However, as circled in Figure 5.20 (a), porosity is also found in localized regions in the center of the spherulites. With a longer crystallization time (Figure 5.20 (b)), the porosity is more distributed on the surface, so it is more difficult to distinguish the boundaries of spherulites (represented by the white lines in Figure 5.20 (a)) . The PEG appears to migrate from one spherulites to another, forming large porous areas. However, the pore size remains the same after 1 hour of crystallization. Porosity is still found in the center of the spherulites, as circled in Figure 5.20 (b). These observations are consistent with POM micrographs. The porous structure appears to correspond to the black aggregates accumulated at the interfaces between the spherulites, as mentioned above.

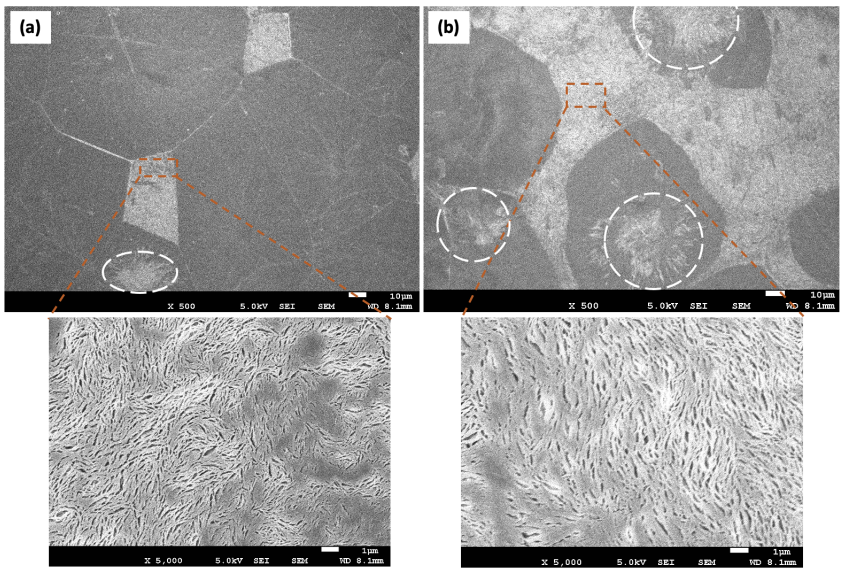

Figure 5.20: SEM micrographs after extraction of PLA/PEG10K 70/30 crystallized at T_c=110°C for 1h (a) and 4h (b).

While the number of nucleation sites and the size of the spherulites increase with crystallization time, the formed spherulites are increasingly in contact with each other and become indistinguishable. PEG partially segregates at the interfaces of the spherulites during the crystallization process, forming these large porous zones observed in SEM. With PEG3K, the crystallization process was practically complete in 1 hour for all isotherms, no changes were observed with increasing time (see Appendix A.4).
The effect of crystallization time is much greater with increasing molar mass of PEG. Some changes were observed in the general structure of the sample with PEG10K. However, the morphology and size of the porosity do not vary much with time for a given composition. The crystallization time affects the crystalline structure of the blends and, consequently, the location of PEG. Thus, the distribution of pores on the surface varies. It is also important to note that the time does not show significant changes depending on the composition, especially for the 50/50 blends.

5.4 General discussion

Now that the different parameters have been studied independently, let us summarize the results. To this end, Figures 5.21 and 5.22 show all the micrographs after solvent evaporation (first column) and after isothermal crystallization at 110°C for 1, 4 and 18 hours, respectively.

Thermal treatment improves the crystallization of blends and PLA. After evaporation of the solvent, the samples were birefringent but very few spherulites with the Maltese cross pattern were observed (first column of Figure 5.21 and 5.22). Annealing at the crystallization temperature between T_g and T_m allows the chains to arrange in crystals thanks to the mobility acquired at this temperature.

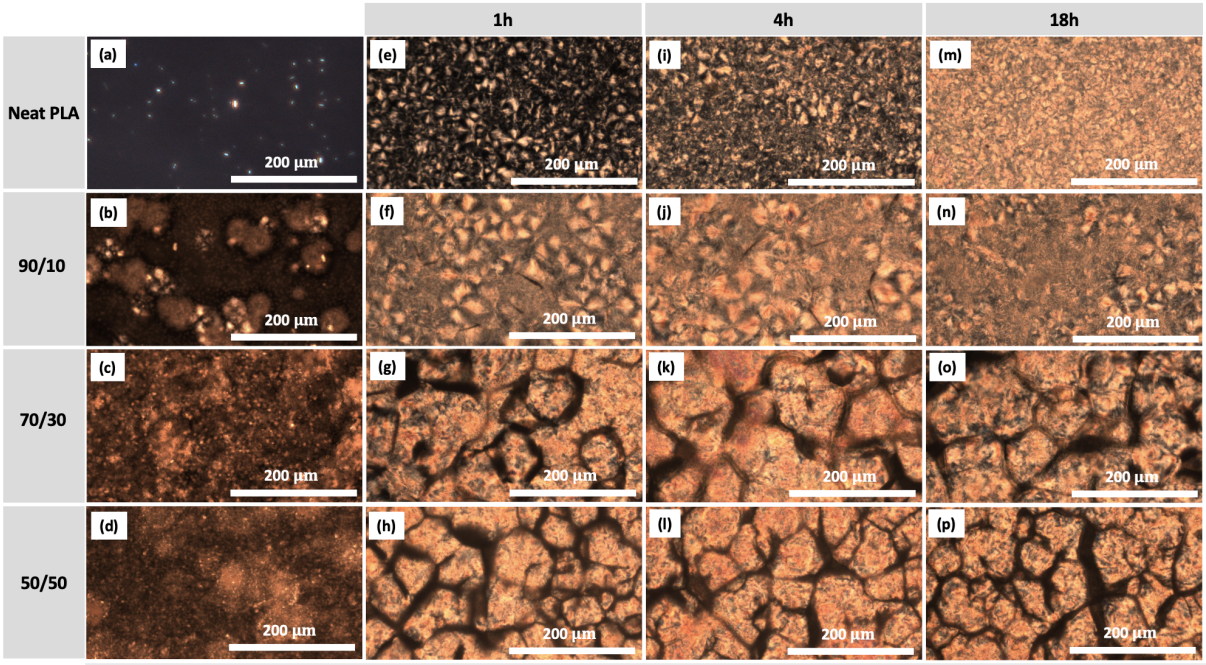

Figure 5.21: POM micrographs of blends after solvent evaporation (first column) and isotherms at 110°C for 1h (second column), 4h (third column) and 18h (fourth column). First, second, third, fourth rows are the neat PLA samples, PLA/PEG3K 90/10, PLA/PEG3K 70/30 and PLA/PEG3K 50/50, respectively.

The **composition** of the blends has a significant effect on the morphology. DSC curves have shown that the addition of a small amount of PEG enhances the crystallization of PLA. Thus, PLA crystallizes during all isotherms, thanks to the addition of PEG. This confirms the observations in POM micrographs. By increasing the PEG content, the viscosity and PLA chain entanglements decrease, leading to easier movement of PLA chains and an increase in the number of nucleation sites, both for PEG3K and PEG10K. This reduces the size of the spherulites. Black aggregates start to form at 30 wt% PEG and surround the spherulites more and more as the content increases. This phenomenon is more pronounced at low molar mass PEG (Figure 5.21 (g), (k), (o)). The chains are smaller and therefore diffuse more easily to surround the spherulites as they migrate to the interfaces while the PLA continues to crystallize. At larger molar mass, they can also surround the spherulites, but less individually and locally, as diffusion takes more time at higher viscosity (Figure 5.22 (g), (k), (o)). Therefore, the spherulitic morphology and subsequent porosity after PEG extraction, is less homogeneously distributed over the surface at larger molar mass. This may indicate that PEG segregates inter-spherulitically and this becomes more so with increasing PEG content. Evidence that PEG is included in the intra-spherulitic region of PLA has been mentioned in previous studies [57]. Nazari et al.[58] also pointed out that when the PEG domains are interconnected, especially in the 50/50 mixture,

PEG chains easily find a way to emerge from the crystalline PLA domains, which could explain the aggregates in POM micrographs.
SEM micrographs confirm that PEG is located in both inter- and intra-spherulitic regions as its content increases. They show that the pores are similar for 10 and 30 wt% PEG extracted blends with a pore size of $\sim$ 1 µm. With increasing PEG content, the same type of morphology is observed, but with more porous areas for the same pore size. However, at 50 wt%, the porous morphology changes and becomes disordered narrow pore strips, with a larger pore width between 1.4 and 4 µm. The distribution of pores on the surface becomes more homogeneous with this composition.
For all these reasons, an intermediate blend composition seems to be of interest. If the PEG content is too high, it segregates inter-spherulitically, the mechanical properties are poor, and the samples become brittle and easily disintegrate into small pieces after PEG removal. If it is too low, the porosity distribution is heterogeneous and insufficient. However, with an intermediate composition of 30 wt% PEG, the samples are less brittle and have higher porosity. It may be interesting to also analyze blends at 20 and 40 wt% PEG to determine if they might have a better porosity distribution after extraction and are less brittle than the 50/50 blends.
Athanasoulia et al.[59] studied the isothermal crystallization of extruded PLLA/PEG blends containing 10, 20 and 30 wt% PEG10K at 110, 115, 120, and 125°C. The crystallization activation energy of PLLA decreased by 56% after the addition of 10 wt% PEG and then increased with a further increase in PEG content. They found that the blends became brittle when the PEG content exceeded 20 wt% (i.e., the tensile strain and the elongation at break decreased). They concluded that the optimum PEG concentration is between 20 and 30 wt% to improve crystallization ability and achieve optimum mechanical and thermal properties.

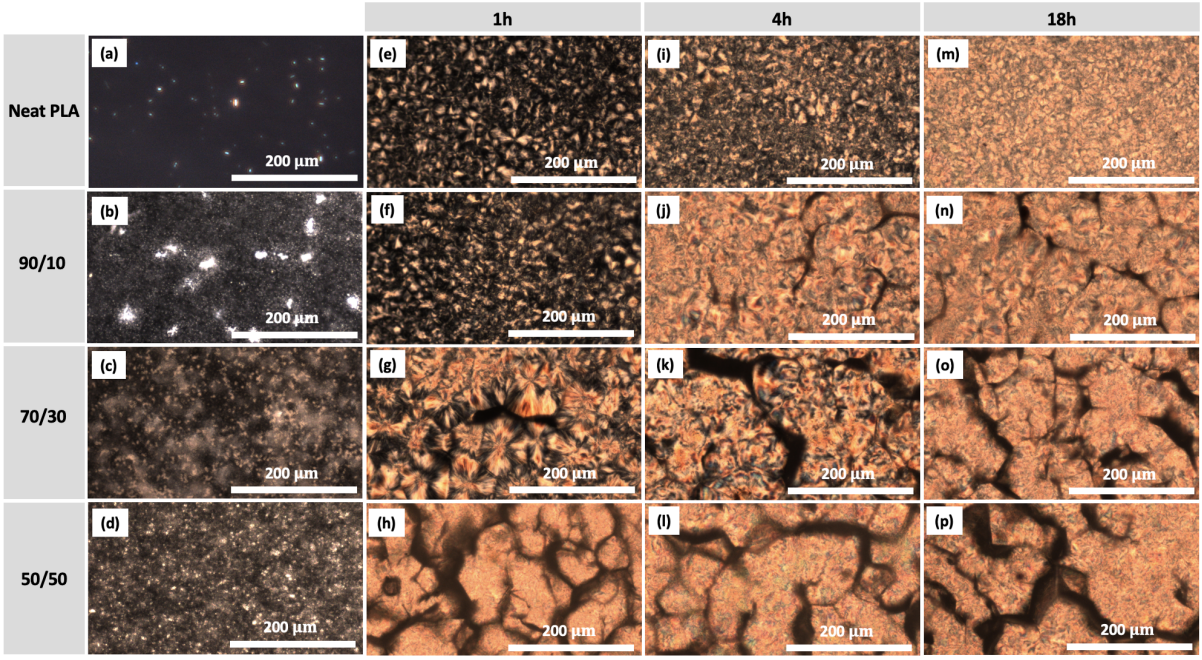

Figure 5.22: POM micrographs of blends after solvent evaporation (first column) and isotherms at 110°C for 1h (second column), 4h (third column) and 18h (fourth column). First, second, third, fourth rows are the neat PLA samples, PLA/PEG10K 90/10, PLA/PEG10K 70/30 and PLA/PEG10K 50/50, respectively.

As addressed in the subsection 5.3.1, PLA crystals have two orientations on a surface: edge-on and flat-on orientation. When there is homogeneous nucleation on the surface of a film, the edge-on orientation is preferred, while the flat-on orientation is favored when there is heterogeneous nucleation. Wang et al.[60] concluded that this depends that this was highly dependent on many parameters: polymer chain mobility, temperature, film thickness, etc. During the

isotherms, the PLA and PEG were in contact with Kapton. Depending on the interfacial energy, PLA lamellae appear in edge-on or flat-on orientation. In the case of edge-on lamellae, porosity can be seen after extraction of PEG, while it is not visible in the case of flat-on lamellae. This explains the heterogeneous porosity seen in SEM micrographs. In addition, the orientation of the lamellae seems to change with PEG content, at 50 wt% PEG extracted samples appear more porous at the surface.

Besides, the **molar mass** also has an important influence. Although their distribution is less homogeneous and does not surround the small crystals, the aggregates appear faster at 10 wt% PEG10K (Figure 5.22 (j), (n)). As mentioned in the previous sections, the longer molecular chain of PEG diffuses more slowly with increasing molar mass. At 10 wt% PEG content, the PEG chains separate from the PLA and are more inter-spherulitically arranged. Due to the higher viscosity at this molar mass, the PEG gets stuck in these areas and cannot diffuse to other sites.
When crystallizing from the melt, the components of a binary mixture must redistribute during crystallization, and co-crystallization is rare. If one component (A) crystallizes first, the other component (B) (which is crystallizable but at a lower temperature than A) could be excluded and may be between the spherulites of A, between the growth arms of A within the spherulite, or between the crystalline lamellae of A within the spherulite [61][62]. Keith et al.[44] pointed out that the localization of this component is controlled by δ, which is defined as the ratio between the diffusion coefficient (D) of the amorphous component and the crystal growth rate (G). This parameter is proportional to the size of the amorphous regions. On the one hand, at a lower D and a higher G, the amorphous component is confined by the crystal lamellae, leading to an enrichment of the inter-lamellar domains (Figure 5.23 (a)). On the other hand, a larger δ leads to a strong diffusivity of the amorphous component when it has enough time to diffuse away as the spherulites grow slowly (Figure 5.23 (b)). To make the analogy with this work, PEG was liquid (as component B) during the isotherm, while PLA crystallized (A).
At lower molar mass, POM micrographs do not show these aggregates at 10wt% PEG (Figure 5.21 (j), (n)). The spherulitic growth rate may have been too high to allow PEG diffusion over long distances. This is confirmed by SEM micrographs where the porosity is localized in the spherulites and not at the boundaries (image not shown).
PEG3K enhances the crystallization process of PLA, even more than PEG10K, which reduces the mobility of PLA chain segments. As shown in the previous sections, the SEM structure after extraction of PEG10K is similar to that of PEG3K after a longer crystallization time, allowing the PEG10K more time to diffuse. The pore size increases with molar mass from 0.5 to 1.5 µm, but the morphology does not change significantly.

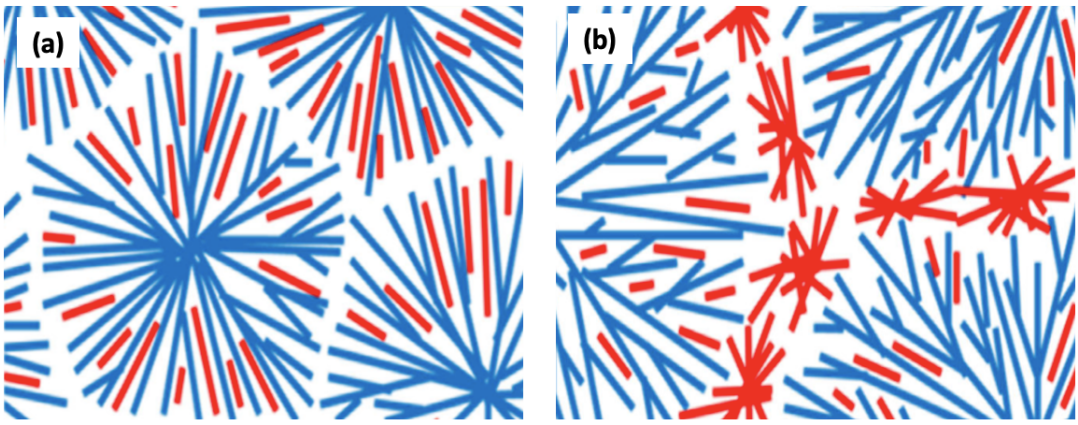

Figure 5.23: Schematic diagram of PEG (red) location during PLA (blue) crystallization. PEG can be intra-spherulitic (a), or inter-spherulitic when phase separate (b) (adapted from [62]).

As the **crystallization time** increases, the spherulites become smaller. PEG has sufficient time to diffuse out of the spherulites, especially for PLA/PEG10K blends at 10 wt% (Figure 5.22 (j) and (n)). However, the effect of time on PLA/PEG3K blends is much less obvious, and the morphology is stable after 1 hour. Even if the crystal structure no longer changes, PLA may still crystallize, but at a much slower rate. SEM showed that the morphology and size of the pores do not vary much with time for a given composition. Nevertheless, the pore distribution varies with PEG location, depending on the crystallization time. Moreover, depending on the composition of the mixture, time does not always have an influence. The higher the content of PEG, the shorter the crystallization time and the more stable the final structure after 1 hour. Li et al.[38] compared two molar masses of PEG in PEG-PDLA/PLLA blends, but also the morphology after different crystallization times from 5 minutes to 4 hours at two isothermal temperatures (140°C and 180°C). With increasing crystallization time, the crystal size was found to increase gradually between 5 minutes and 4 hours. At a crystallization time of 4 hours, crystal growth was essentially complete. This can also be observed for the PLA/PEG10K 90/10 blends between Figure 5.22 (f) and (j). Thus, a longer crystallization time is no longer of interest after 4 hours.

Crystallization temperature is also an essential parameter to consider. As the temperature increases, the viscosity decreases, which allows for better diffusion. As a result, the diffusion coefficient also increases, and the PEG aggregates subsequently diffuse more readily into the inter-spherulitic region, for both PEG3K and PEG10K (images not shown). Thus, the morphology does not change much with time during the 130°C isotherm, reaching a stable structure after 1 hour. However, at a low isothermal temperature of 70°C, viscosity increases and PEG takes longer to diffuse, changing morphology over time. This shows that the different parameters are interdependent.
The spherulites increase in size with increasing temperature as the probability of forming stable nuclei decreases. Therefore, each nucleation site had more space to grow before the spherulites impinge on each other.
Porosity began to distribute heterogeneously with increasing temperature as crystallization was more advanced. As the crystallinity of PLA increases, the amorphous regions become smaller, leading to the migration of PEG from the spherulites. The pores size also increases slightly with T_c and becomes increasingly interconnected. As the temperature increases, the spherulites repel more and more PEG, creating porosity between them and forming large porous aggregates. This shows that a too high crystallization temperature seems to accelerate PEG diffusion, forming a fracture zone between the spherulites.

Chapter 6

Conclusions and perspectives

The aim of this work was to produce a porous material that can be further used as a cell scaffold. On the one hand, good mechanical properties, mainly determined by crystallinity, are required to achieve good mechanical support. On the other hand, porosity is crucial to promote the transport of nutrients and cells in the scaffold. To obtain these materials, PLA and PEG were blended. Porosity was obtained by extraction of the PEG phase. Also, the effects of various parameters such as blend composition, crystallization temperature, PEG molar mass and crystallization time on crystallinity and porosity were investigated.

Films with different composition of 10, 30, and 50 wt% of PEG were prepared. Solvent casting was chosen for its efficiency in forming a homogeneous blend and thin films. After evaporation of the solvent, thermal treatment was performed to erase this non-uniform morphology and control the crystallization process. The PEG extraction method in water could be validated by FTIR spectra and could be reused for future studies on films.

Analysis of the effects of composition on crystallization and porosity of the blends demonstrates that by increasing the PEG content, crystallization of PLA was improved and a final morphology was achieved more quickly. Moreover, porosity and pore size increase with the content of PEG. Although the pore morphology was similar at 10 and 30 wt%, it changes significantly at 50 wt% with disordered narrow strips of pores resulting from the interpenetration of the thin PLLA lamellae with the PEG crystals as they grew before the PEG was extracted. This is due to the orientation of the lamellae on the film surface. At 30 wt%, black aggregates begin to appear around the spherulites. This is consistent with DSC measurements, which showed that PEG and PLA separate at this content, as described in the literature. Plus, these observations were confirmed: at low PEG content, the porosity of the extracted films was located in the PLA spherulites, while it became increasingly inter-spherulitic with increasing PEG content. This is due to the fact that with increasing PEG content, the PEG domains become interconnected and the chains easily find a way out of the PLA crystal domains.

Two molar masses of PEG were compared. When PEG10K was used, it took longer for the long chains to diffuse and improve the mobility of PLA chain segments. They could even hinder the crystallization of PLA by diffusing too slowly out of the spherulites. Besides, PEG3K reduces the viscosity and changed the crystalline morphology, which significantly improved the crystallization of PLA. The morphology of the pores does not change importantly, while their size varies and increases slightly with MM from 0.5 to 1.5 micrometers. Therefore, molar masses close to 3000 g/mol seem to be a good choice to promote the crystallization of PLA and to obtain a crystal structure stable faster. However, depending on the application, a higher MM could allow a slow diffusion of PEG, which would then be exclusively intra-spherulitic.

The results show that crystallization and crystal morphology are closely related to temperature, which determines crystal nucleus formation and growth. As mentioned in Chapter 1, when nucleation increases, crystal growth rate decreases, forming smaller spherulites. The fastest crystallization rate is achieved at an intermediate temperature between the preferred temperatures for nucleation and growth. DSC experiments show that PEG allows PLA to crystallize at a lower temperature. At 70°C, this temperature is too close to the T_g of PLA which cannot crystallize. However, by introducing PEG, which is liquid at this temperature, the viscosity can be lowered and the crystallization of PLA can be improved by the plasticizing affect of PEG.
The pores increase in size and the porosity becomes more heterogeneous with increasing temperature. As the PLA spherulites size grow with T_c, PEG appears to separate and localize between the spherulites.
The size of the spherulites is larger at 130°C, but Ma et al.[55] found that the spherulites of PLA were imperfect after crystallization at this temperature. The distribution of crystalline and amorphous phases was heterogeneous, resulting in deterioration of mechanical performance. Therefore, large spherulites are not conducive to mechanical performance and tend to fracture easily. This is an important parameter to consider when studying mechanical properties.
Based on this and the observations of this work, the best temperature to obtain an appropriate spherulite size for good mechanical properties seems to be the midway between T_g and T_m, the temperature at which the spherulite growth rate is highest (near 110°C in the case of PLA).

The crystallization time affects the observed crystalline morphology. However, at low MM PEG3K, the PEG molecules diffuse faster and reach a stable PLA crystalline structure quickly than with PEG10K. Over crystallization time, PEG accumulates at the interface of the spherulites as crystallization progresses. Thus, the porosity distribution varies, while the pore morphology and size do not vary a lot with time for a given composition.
A crystallization time of 4 hours seems to be sufficient to crystallize the samples and reach a complete morphology, both for PEG 3K and for PEG10K. But, it also depends on the composition of the blend; a shorter time might be required for 30 and 50 wt% PEG. However, this depends on the type of porosity targeted.

Although porosity increases slightly with parameters (i.e., composition, MM, T_c), it does not vary greatly, ranging only from 1 to 4 microns. Depending on the desired pore size, the idea is to control the pore size by refining these parameters. As mentioned in Chapter 3, the porosity of the scaffold generally ranges from 20 to 1500 microns, depending on the cell type and desired function. However, it was not possible to vary the pore size that much using the polymer blending method and by changing the parameters studied. Nevertheless, greater porosity was obtained in the literature with PEO of larger MM than those used in this work.
In addition, interconnectivity is of critical importance. In the subsection 5.3.1, it was shown that the 50 wt% PEG was fragile. Thus, the porosity of the 50/50 blend could be observed at greater depths thanks to the fracture zones between the spherulites. This porosity seems to be more interconnected. This raises the question of whether the interconnectivity is also present at the depth of the films. Interestingly, the extraction method shows that PEG was well extracted at depth, which indicate open porosity at depth. PEG is not trapped in closed pores, otherwise PEG could not have been extracted. In addition, the porosity could be greater at depth.
SEM micrographs show the surface porosity of the films after PEG extraction. The structures observed on them depend on the orientation of the PLA lamellae (i.e. edge-on, flat-on), which depends on the interfacial energy with the surface during the thermal treatment. Thus, what was observed is not representative of what is present at depth. However, as mentioned earlier, looking at the cross-section is essential to determine the distribution of porosity at depth. Although pores may be heterogeneously distributed and poorly connected at the surface, they may be well connected at depth. In this work, an attempt was made to obtain a cross-section of the

film after cooling in liquid nitrogen. Since this method was not conclusive, more precise devices such as a microtome could be used.
In addition, other measurement techniques could be used to better characterize porosity. Mercury intrusion porosimetry is a reliable method for determining pore size distribution. Nitrogen sorption analysis is also commonly used and allow determination of specific surface area and pore volume. Another simple pore measurement is the extracted weight ratio, which gives an idea of void volume fraction. However, since the samples broke into small pieces during PEG extraction in water, this value could not be measured.
Besides, other techniques could be used to create porosity in a polymer material. 3D printing technologies are increasingly emerging and would allow precise control of pore size. 3D models can be created based on noninvasive imaging technologies such as computed tomography and magnetic resonance imaging, which provide 3D images of tissues and organs. These models are then sent to the 3D printer, which prints complex geometries after computer processing.

As raised in each sections, the samples were brittle, especially at 30 and 50wt% PEG. Removal of the PEG, which was located between the interfaces of the spherulites, caused the film to break into small pieces. For future applications, a ratio of PLA to PEG closer to 30wt% of PEG, would be more interesting to avoid the film becoming too fragile.
Heat treatment was performed in hot press machines, one to melt the samples, another to quench them to isotherms. The temperature sensors indicated that the temperature varied slightly between the upper and lower presses with time. The isotherms lasted between 1 and 18 hours, so these small temperature differences could be neglected. Nevertheless, this could be a problem for the reproducibility of the manipulations and could be remedied with a more precise intrument. Even though no pressure was applied to the metal plates, they could have exerted a mechanical stress on the liquids and affected crystallization. This could also explain the heterogeneity of the surface of the film, with edge-on and flat-on orientations. Comparing the obtained images, the crystals are more imperfect than in other works, possibly due to the thermal process or the observation conditions (sample not flat enough, not optimal microscope settings, etc.). Moreover, it would be interesting to control the cooling rate of the samples, always with the goal of reproducing these experiments more accurately.
The samples were observed in POM after cooling at room temperature and could be compared to the samples before cooling. POM combined with a hot stage would allow to be observe the samples during the isotherms and at their end, before the PEG crystallizes.

The crystalline morphology and surface porosity were analyzed for these promising PLA/PEG blends. The objectives of this thesis were partially achieved. The influence of PEG on PLA crystallization is successful and shows the different nature of segregation of PEG (i.e., intra and inter-spherulitic). From the analysis of the different experimental parameters, it can be concluded that all parameters have an influence. However, it remains difficult to establish a protocol with the different parameters to be chosen to obtain a very accurate porosity until it is know how the internal morphology is affected. In addition, many parameters still need to be investigated for future use in 3D printing. Dynamic mechanical analysis and tensile tests could be used to measure the mechanical properties of the blends before and after extraction with the different parameters used in this work.

Appendices

A.1 FTIR spectra

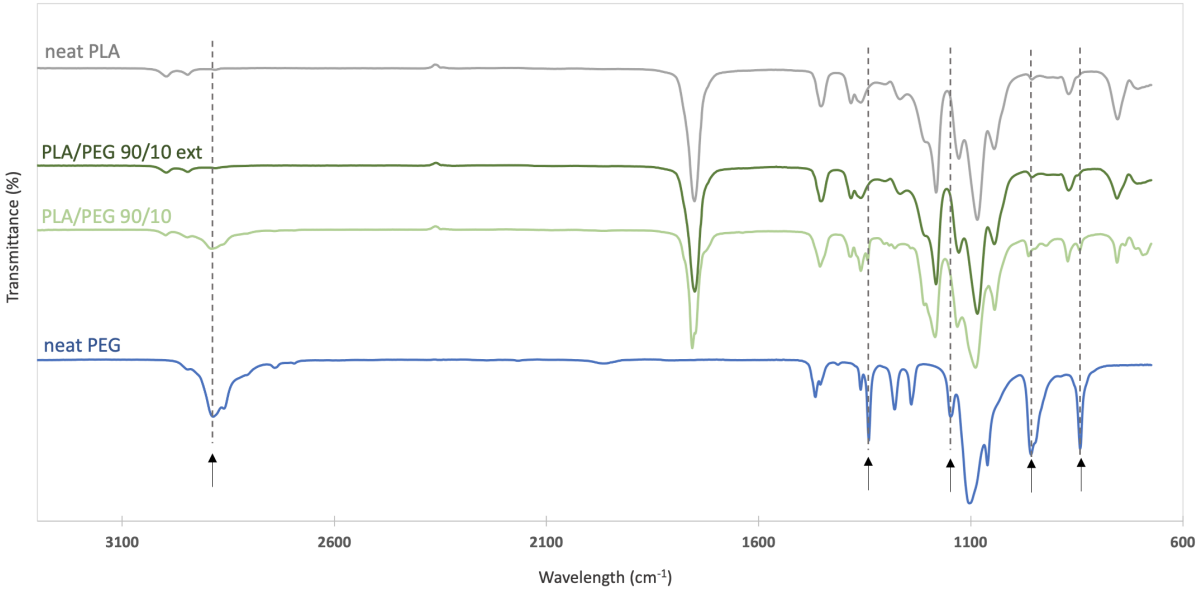

Figure A1: FTIR spectra of PLA/PEG10K 90/10.

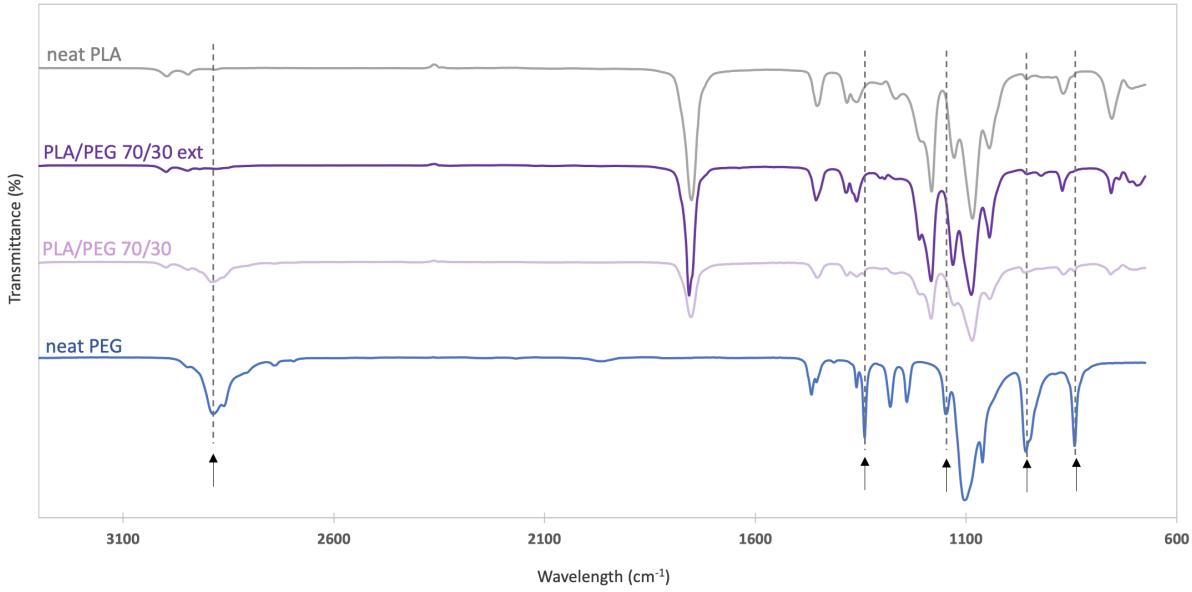

Figure A2: FTIR spectra of PLA/PEG10K 70/30.

A.2 Effect of composition

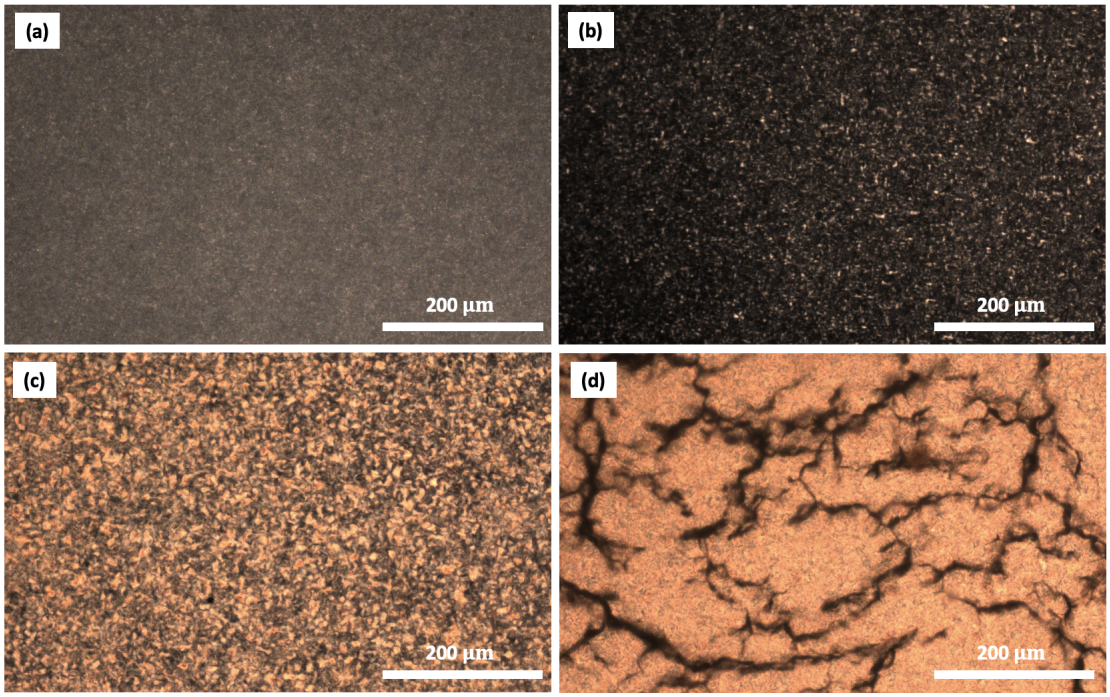

Figure A3: POM micrographs before extraction, after 4h at T_c = 70°C of neat PLA (a) and blends PLA/PEG10K 90/10 (b), PLA/PEG10K 70/30 (c), PLA/PEG10K 50/50 (d).

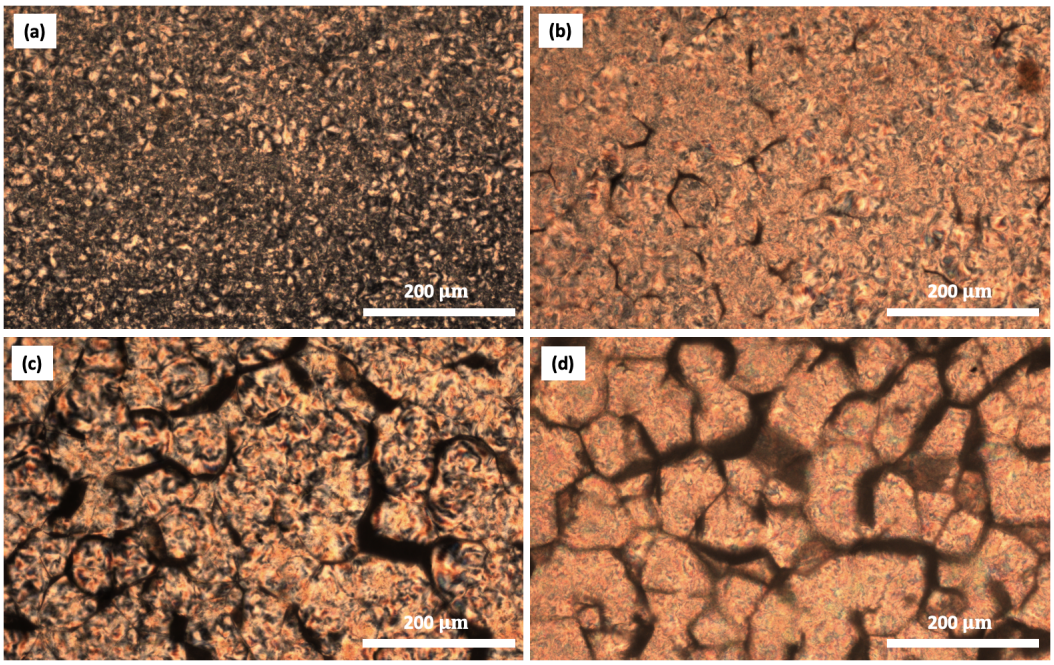

Figure A4: POM micrographs before extraction, after 4h at T_c = 110°C of neat PLA (a) and blends PLA/PEG10K 90/10 (b), PLA/PEG10K 70/30 (c), PLA/PEG10K 50/50 (d).

A.3 Effect of molar mass

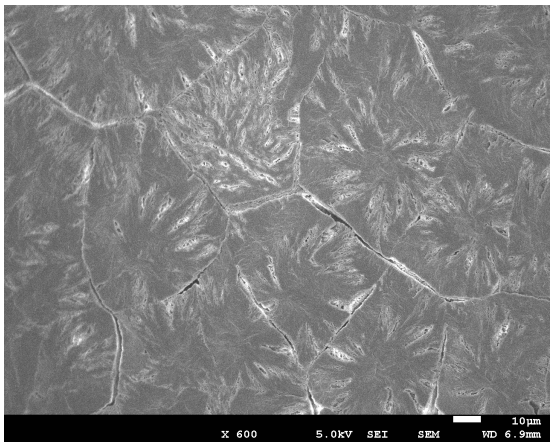

Figure A5: SEM micrograph of PLA/PEG 10K 50/50 crystallized at 110° for 4h.

A.4 Effect of crystallization time

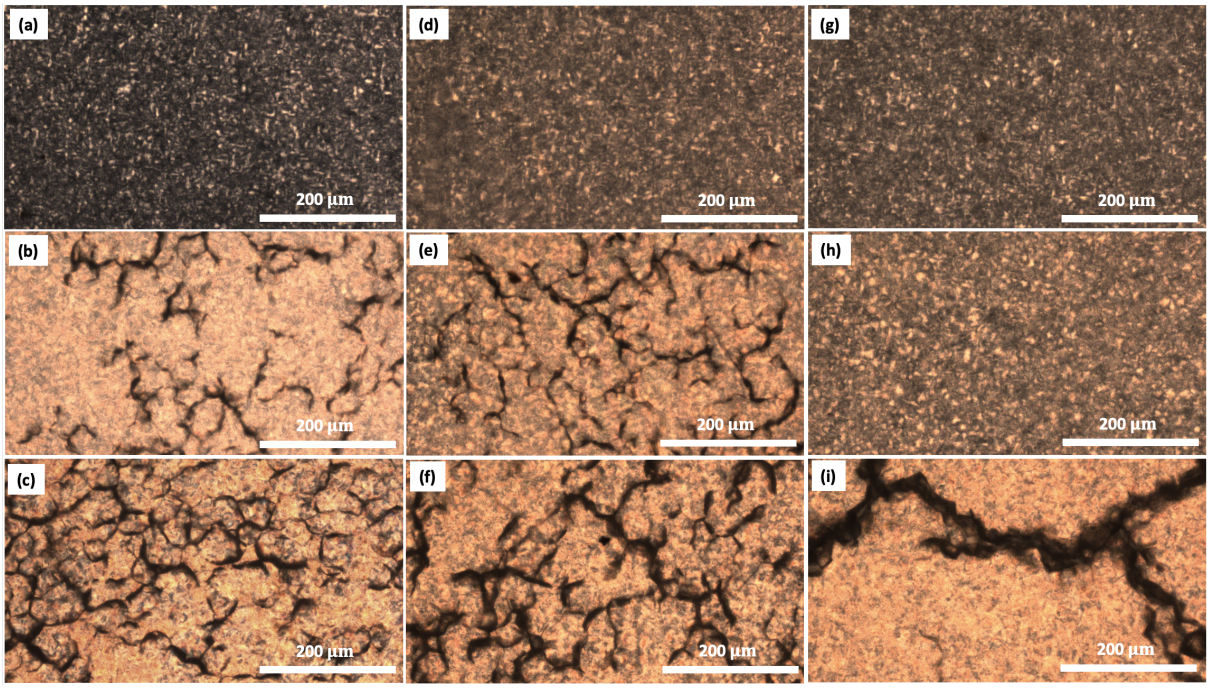

Figure A6: POM micrographs of PLA/PEG3K 90/10 (first row), 70/30 (second row) and 50/50 (third row) crystallized at T_c=70°C for 1h (a, b, c), 4h (d, e, f), and 18h (g, h, i).

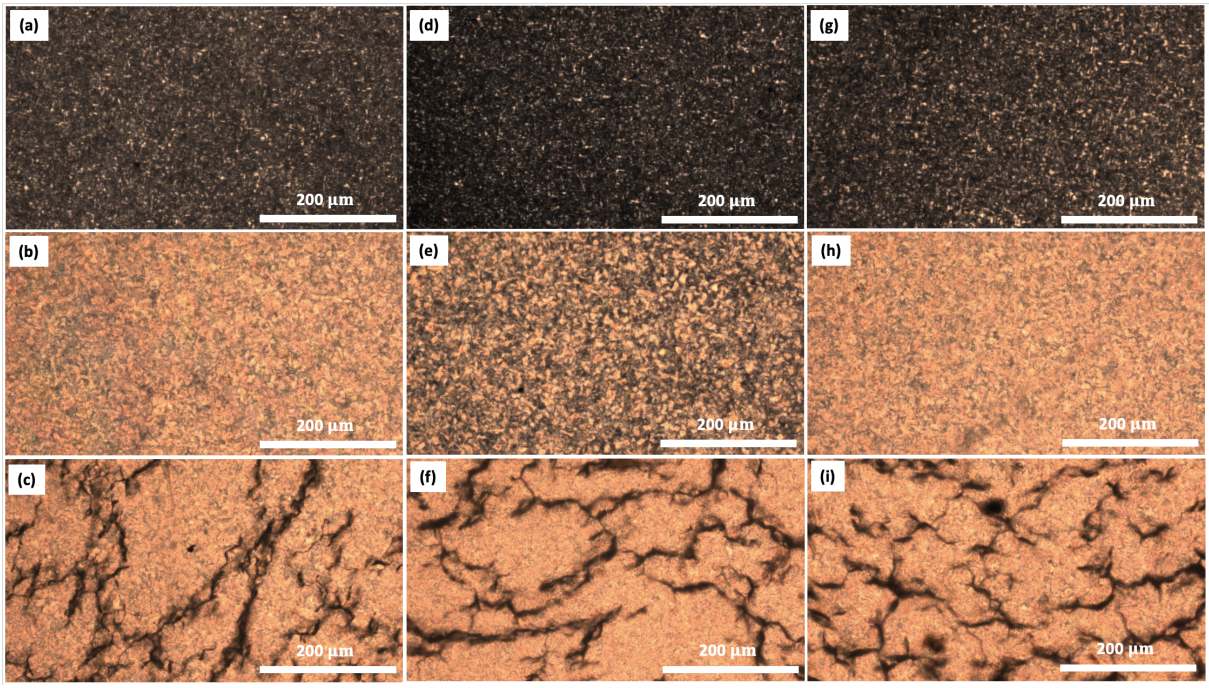

Figure A7: POM micrographs of PLA/PEG10K 90/10 (first row), 70/30 (second row) and 50/50 (third row) crystallized at T_c=70°C for 1h (a, b, c), 4h (d, e, f), and 18h (g, h, i).

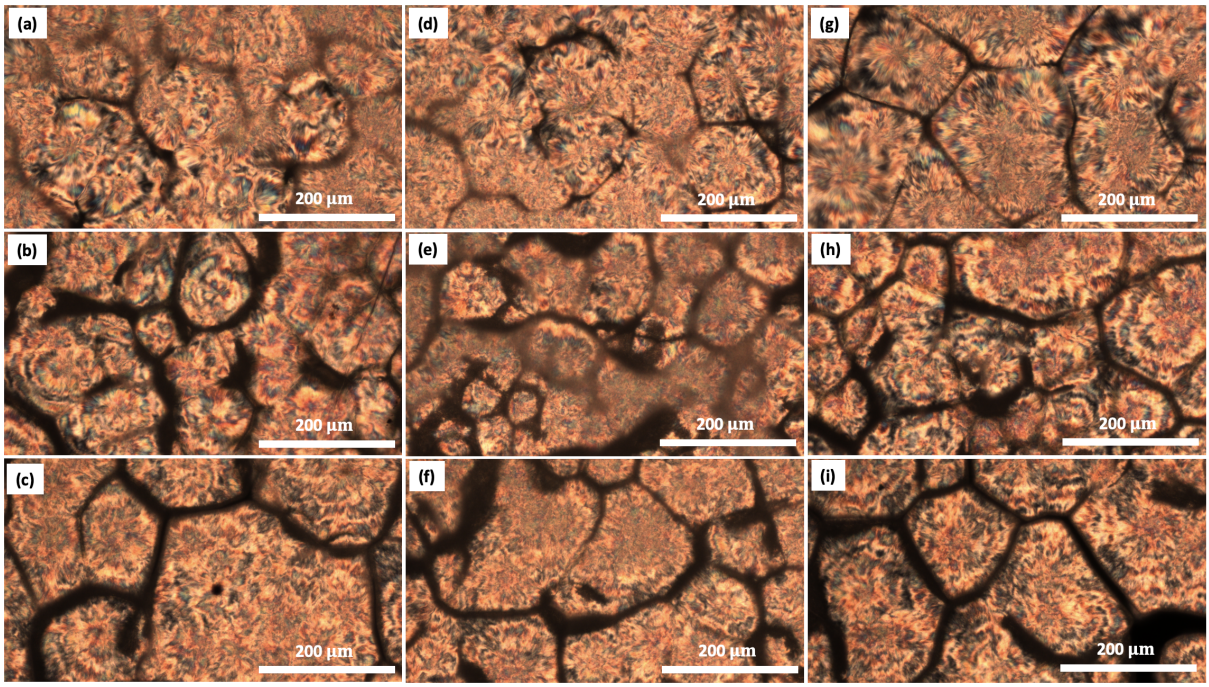

Figure A8: POM micrographs of PLA/PEG3K 90/10 (first row), 70/30 (second row) and 50/50 (third row) crystallized at T_c=130°C for 1h (a, b, c), 4h (d, e, f), and 18h (g, h, i).

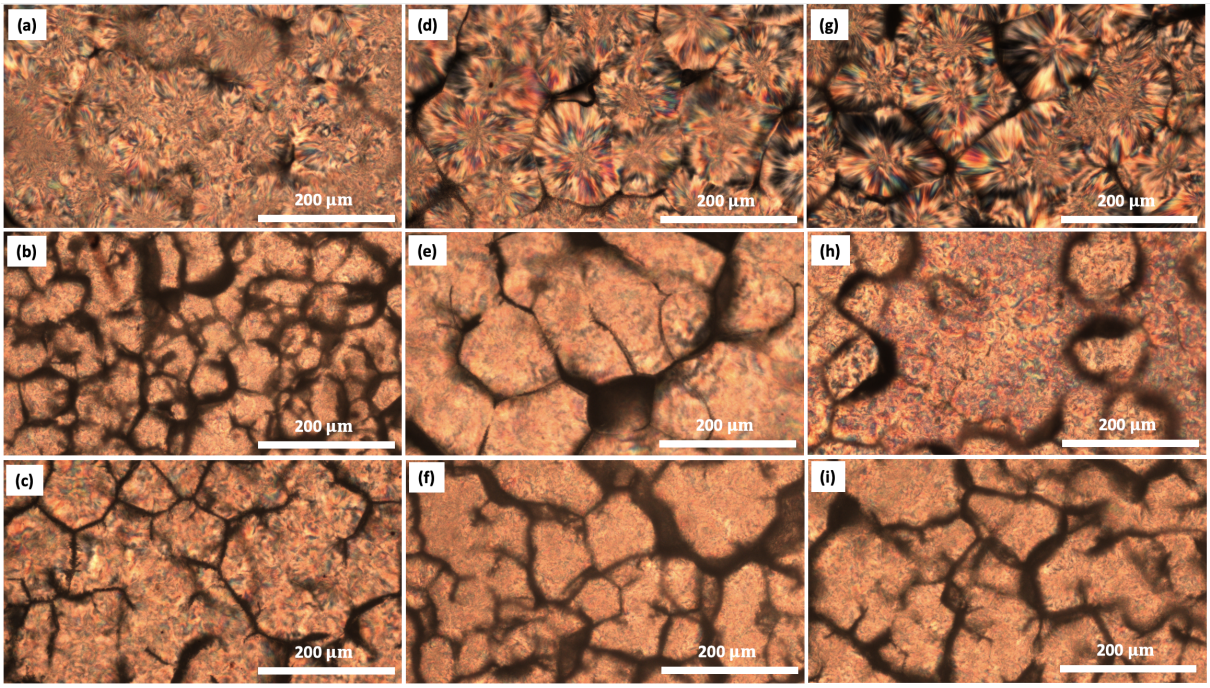

Figure A9: POM micrographs of PLA/PEG10K 90/10 (first row), 70/30 (second row) and 50/50 (third row) crystallized at T_c=130°C for 1h (a, b, c), 4h (d, e, f), and 18h (g, h, i).

Bibliography

[1] S. Yang et al. "The Design of Scaffolds for Use in Tissue Engineering. Part I. Traditional Factors". In: *Tissue engineering* 7 (Jan. 2002), pp. 679–89. DOI: 10.1089/107632701753337645.

[2] M. S. Lopes, A. Jardini, and R. M. Filho. "Poly (Lactic Acid) Production for Tissue Engineering Applications". In: *Procedia Engineering* 42 (2012). CHISA 2012, pp. 1402–1413. ISSN: 1877-7058. DOI: https://doi.org/10.1016/j.proeng.2012.07.534.

[3] V. Pérez Puyana et al. "Polymer-Based Scaffolds for Soft-Tissue Engineering". In: *Polymers* 12 (July 2020), p. 1566. DOI: 10.3390/polym12071566.

[4] K. M. Nampoothiri, N. Nair, and R. P John. "An overview of the recent developments in polylactide (PLA) research". In: *Bioresource technology* 101 (Nov. 2010), pp. 8493–501. DOI: 10.1016/j.biortech.2010.05.092.

[5] M. Nofar et al. "Poly (lactic acid) blends: Processing, properties and applications". In: *International Journal of Biological Macromolecules* 125 (Dec. 2018), pp. 307–360. DOI: 10.1016/j.ijbiomac.2018.12.002.

[6] S. Farah, D. G. Anderson, and R. Langer. "Physical and mechanical properties of PLA, and their functions in widespread applications — A comprehensive review". In: *Advanced Drug Delivery Reviews* 107 (2016), pp. 367–392. ISSN: 0169-409X. DOI: https://doi.org/10.1016/j.addr.2016.06.012.

[7] B. Gupta, N. Revagade, and J. Hilborn. "Poly(lactic acid) fiber: An overview". In: *Progress in Polymer Science* 32.4 (2007), pp. 455–482. ISSN: 0079-6700. DOI: https://doi.org/10.1016/j.progpolymsci.2007.01.005.

[8] D. Henton et al. "Polylactic Acid Technology". In: *Natural Fibers, Biopolymers, and Biocomposites* (Apr. 2005), pp. 1841–1846. DOI: 10.1201/9780203508206.ch16.

[9] R. Naseem et al. "Strategies for Enhancing Polyester-Based Materials for Bone Fixation Applications". In: *Molecules* 26 (Feb. 2021), p. 992. DOI: 10.3390/molecules26040992.

[10] Polylactide. *PDLA/Poly(D-Lactide)*. https://polylactide.com/polyd-lactide/.

[11] A. Lasprilla et al. "Poly-lactic acid synthesis for application in biomedical devices — A review". In: *Biotechnology Advances* 30.1 (2012). Systems Biology for Biomedical Innovation, pp. 321–328. ISSN: 0734-9750. DOI: 10.1016/j.biotechadv.2011.06.019.

[12] D. Garlotta. "A Literature Review of Poly(Lactic Acid)". In: *Journal of Polymers and the Environment* 9 (Apr. 2001), pp. 63–84. DOI: 10.1023/A:1020200822435.

[13] M. S. Singhvi, S. S. Zinjarde, and D. V. Gokhale. "Polylactic acid: synthesis and biomedical applications". In: *Journal of Applied Microbiology* 127 (6 Dec. 2019), pp. 1612–1626. ISSN: 13652672. DOI: 10.1111/jam.14290.

[14] S. Målberg, A. Finne-Wistrand, and A.-C. Albertsson. "The environmental influence in enzymatic polymerization of aliphatic polyesters in bulk and aqueous mini-emulsion". In: *Polymer* 51 (Oct. 2010), pp. 5318–5322. DOI: 10.1016/j.polymer.2010.09.016.

[15] M. Kuterbekov et al. “Solvent-free preparation of porous poly(L-lactide) microcarriers for cell culture”. In: *Acta Biomaterialia* 75 (June 2018), pp. 300–311. DOI: 10.1016/j.actbio.2018.06.009.

[16] R. Androsch, C. Schick, and M. L. Di Lorenzo. “Kinetics of Nucleation and Growth of Crystals of Poly(l-lactic acid)”. In: *Advances in Polymer Science* (May 2017), pp. 235–272. DOI: 10.1007/12_2016_13.

[17] M. Teboho et al. “Thermoplastic Processing of PLA/Cellulose Nanomaterials Composites”. In: *Polymers* 10 (Dec. 2018), p. 1363. DOI: 10.3390/polym10121363.

[18] T. Kawai et al. “Crystallization and Melting Behavior of Poly (l-lactic Acid)”. In: *Macromolecules* 40 (Nov. 2007), pp. 9463–9469. DOI: 10.1021/ma070082c.

[19] M. A. Elsawy et al. “Hydrolytic degradation of polylactic acid (PLA) and its composites”. In: *Renewable and Sustainable Energy Reviews* 79 (2017), pp. 1346–1352. ISSN: 1364-0321. DOI: https://doi.org/10.1016/j.rser.2017.05.143.

[20] M. L. Di Lorenzo and R. Androsch. “Synthesis, Structure and Properties of Poly(lactic acid)”. In: *Advances in Polymer Science* (Jan. 2018), pp. 153–195. DOI: 10.1007/978-3-319-64230-7.

[21] A. Moetazedian et al. “Mechanical performance of 3D printed polylactide during degradation”. In: *Additive Manufacturing* 38 (Dec. 2020), p. 101764. DOI: 10.1016/j.addma.2020.101764.

[22] X. Pang et al. “Polylactic acid (PLA): Research, development and industrialization”. In: *Biotechnology Journal* 5 (11 Nov. 2010), pp. 1125–1136. ISSN: 18606768. DOI: 10.1002/biot.201000135.

[23] A. A. D’souza and R. Shegokar. “Polyethylene glycol (PEG): a versatile polymer for pharmaceutical applications”. In: *Expert Opinion on Drug Delivery* 13 (9 Sept. 2016), pp. 1257–1275. ISSN: 17447593. DOI: 10.1080/17425247.2016.1182485.

[24] K. Knop et al. “Poly(ethylene glycol) in drug delivery: Pros and cons as well as potential alternatives”. In: *Angewandte Chemie - International Edition* 49 (36 Aug. 2010), pp. 6288–6308. ISSN: 14337851. DOI: 10.1002/anie.200902672.

[25] X.-F. XIAO, X.-Q. JIANG, and L.-J. ZHOU. “Surface Modification of Poly Ethylene Glycol to Resist Nonspecific Adsorption of Proteins”. In: *Chinese Journal of Analytical Chemistry* 41 (Mar. 2013), pp. 445–453. DOI: 10.1016/S1872-2040(13)60638-6.

[26] M. Puthumana, P. S. G. Krishnan, and S. K. Nayak. “Chemical modifications of PLA through copolymerization”. In: *International Journal of Polymer Analysis and Characterization* 25 (8 Nov. 2020), pp. 634–648. ISSN: 15635341. DOI: 10.1080/1023666X.2020.1830650.

[27] V. DeStefano, S. Khan, and A. Tabada. “Applications of PLA in modern medicine”. In: *Engineered Regeneration* 1 (Jan. 2020), pp. 76–87. ISSN: 2666-1381. DOI: 10.1016/J.ENGREG.2020.08.002.

[28] S. Bose, S. Robertson, and A. Bandyopadhyay. “Surface Modification of Biomaterials and Biomedical Devices using Additive Manufacturing”. In: *Acta Biomaterialia* 66 (Nov. 2017), pp. 6–22. DOI: 10.1016/j.actbio.2017.11.003.

[29] Y. Cheng et al. “Polylactic acid (PLA) synthesis and modifications: A review”. In: *Frontiers of Chemistry in China* 4 (Sept. 2009), pp. 259–264. DOI: 10.1007/s11458-009-0092-x.

[30] S. Selvam et al. “Microporous Poly(L-Lactic Acid) Membranes Fabricated by Polyethylene Glycol Solvent-Cast/Particulate Leaching Technique”. In: *Tissue engineering. Part C, Methods* 15 (Feb. 2009), pp. 463–74. DOI: 10.1089/ten.tec.2008.0431.

[31] Q. L. Loh and C. Choong. "Three-Dimensional Scaffolds for Tissue Engineering Applications: Role of Porosity and Pore Size". In: *Tissue engineering. Part B, Reviews* 19 (May 2013), pp. 485–502. DOI: 10.1089/ten.TEB.2012.0437.

[32] Y. Nashchekina et al. "Functional polylactide blend films for controlling mesenchymal stem cell behaviour". In: *Polymers* 12 (9 Sept. 2020), pp. 1–11. ISSN: 20734360. DOI: 10.3390/polym12091969.

[33] M. Sheth et al. "Biodegradable polymer blends of poly(lactic acid) and poly(ethylene glycol)". In: *Journal of Applied Polymer Science* 66 (Dec. 1998), pp. 1495–1505. DOI: 10.1002/(SICI)1097-4628(19971121)66:8<1495::AID-APP10>3.0.CO;2-3.

[34] K. Sungsanit, N. Kao, and S. Bhattacharya. "Properties of linear poly(lactic acid)/polyethylene glycol blends". In: *Polymer Engineering Science* 52 (Jan. 2012), pp. 108–116. DOI: 10.1002/pen.22052.

[35] B. Wang et al. "Thermal, crystallization, mechanical and decomposition properties of poly(lactic acid) plasticized with poly(ethylene glycol)". In: *Journal of Vinyl and Additive Technology* 24 (Jan. 2018), E154–E163. DOI: 10.1002/vnl.21619.

[36] M. Baiardo et al. "Thermal and mechanical properties of plasticized poly(L-lactic acid)". In: *Journal of Applied Polymer Science* 90 (Nov. 2003), pp. 1731–1738. DOI: 10.1002/app.12549.

[37] I. G. Athanasoulia and P. A. Tarantili. "Preparation and characterization of polyethylene glycol/poly(L-lactic acid) blends". In: *Pure and Applied Chemistry* 89 (1 Jan. 2017), pp. 141–152. ISSN: 13653075. DOI: 10.1515/pac-2016-0919.

[38] R. Li et al. "Effect of molecular weight of polyethylene glycol on crystallization behaviors, thermal properties and tensile performance of polylactic acid stereocomplexes". In: *RSC Advances* 10 (Nov. 2020), pp. 42120–42127. DOI: 10.1039/D0RA08699A.

[39] Y. Zhang et al. "Effect of miscibility on spherulitic growth rate for double-layer polymer films". In: *Soft Matter* 9 (May 2013), pp. 5771–5778. DOI: 10.1039/C3SM50542A.

[40] H. Tsuji et al. "Porous biodegradable polyesters. I. Preparation of porous poly(L-lactide) films by extraction of poly(ethylene oxide) from their blends". In: *Journal of Applied Polymer Science* 75 (Jan. 2000), pp. 629–637. DOI: 10.1002/(SICI)1097-4628(20000131)75:5<629::AID-APP5>3.0.CO;2-A.

[41] K. Nakane et al. "Porous poly(L-lactic acid)/poly(ethylene glycol) blend films". In: *Journal of Applied Polymer Science* 94 (3 Nov. 2004), pp. 965–970. ISSN: 00218995. DOI: 10.1002/app.20959.

[42] L. Yu and S. Reutzel-Edens. "Crystallization - Basic Principles". In: *Encyclopedia of Food Sciences and Nutrition* (Dec. 2003), pp. 1697–1702. DOI: 10.1016/B0-12-227055-X/00313-8.

[43] A. Jonas. "LMAPR2019A - Polymer Science and Engineering A: Physics". In: (Nov. 2020), pp. 163–164.

[44] H. Keith and F. Padden. "A Phenomenological Theory of Spherulitic Crystallization". In: *Journal of Applied Physics* 34 (Sept. 1963), pp. 2409–2421. DOI: 10.1063/1.1702757.

[45] L. Sawyer, D. Grubb, and G. Meyers. "Polymer microscopy: Third edition". In: *Polymer Microscopy: Third Edition* (Jan. 2008), pp. 5–10. DOI: 10.1007/978-0-387-72628-1.

[46] T. Kinetics. *Evaporative Vs. Cooling Crystallization Systems*. https://thermalkinetics.net/evaporative-vs-cooling-crystallization-systems/.

[47] C. Jr. "Seymour/Carraher's Polymer Chemistry". In: (Apr. 2003), pp. 43–45. DOI: 10.1201/9781420051032.

[48] P. Database. *Polymer physics, Crystallization polymer physics*. https://www.polymerdatabase.com. 2015-2020.

[49] I. Pillin, N. Montrelay, and Y. Grohens. "Thermomechanical characterization of plasticized PLA: Is the miscibility the only significant factor?" In: *Polymer* 47 (June 2006), pp. 4676–4682. DOI: 10.1016/j.polymer.2006.04.013.

[50] X. Chen et al. "Recent Progress on 3D-Printed Polylactic Acid and Its Applications in Bone Repair". In: *Advanced Engineering Materials* 22 (Nov. 2019). DOI: 10.1002/adem.201901065.

[51] W. Ockenga. *Polarization Contrast: an introduction*. https://www.leica-microsystems.com/science-lab/polarization-contrast/. May 2011.

[52] N. Vrandečić et al. "Kinetic analysis of thermal degradation of poly(ethylene glycol) and poly(ethylene oxide)s of different molecular weight". In: *Thermochimica Acta* 498 (Jan. 2010), pp. 71–80. DOI: 10.1016/j.tca.2009.10.005.

[53] U. o. W.-M. JEOL. *A Guide to Scanning Microscope Observation*. https://www.jeol.co.jp/en/applications/pdf/sm/844_en.pdf. 2021.

[54] Y.-T. Hsieh, S. Nurkhamidah, and E. Woo. "Lamellar orientation and interlamellar cracks in co-crystallized poly(ethylene oxide)/poly(L-lactic acid) blend". In: *Polymer Journal* 43 (July 2011), pp. 762–769. DOI: 10.1038/pj.2011.63.

[55] B. Ma et al. "Effect of poly(lactic acid) crystallization on its mechanical and heat resistance performances". In: *Polymer* 212 (2021), p. 123280. ISSN: 0032-3861. DOI: https://doi.org/10.1016/j.polymer.2020.123280.

[56] C. Zhang et al. "Melt Crystallization Behavior and Crystalline Morphology of Polylactide/Poly(-caprolactone) Blends Compatibilized by Lactide-Caprolactone Copolymer". In: *Polymers* 10 (Oct. 2018), p. 1181. DOI: 10.3390/polym10111181.

[57] A. K. Pandey and S. Sakurai. "Recent Developments in the Crystallization of PLLA-Based Blends, Block Copolymers, and Nanocomposites". In: *Crystallization and Applications*. Ed. by Y. B. Smida and R. Marzouki. Rijeka: IntechOpen, 2021. Chap. 5. DOI: 10.5772/intechopen.97088.

[58] T. Nazari and H. Garmabi. "Thermo-rheological and interfacial properties of polylactic acid/polyethylene glycol blends toward the melt electrospinning ability". In: *Journal of Applied Polymer Science* 133 (July 2016). DOI: 10.1002/app.44120.

[59] I.-G. Athanasoulia et al. "The effect of PEG mixed with PLLA on the crystallization characteristics and properties of their blends". In: *Polymer International* 68 (Jan. 2019), pp. 788–804. DOI: 10.1002/pi.5769.

[60] Y. Wang, C.-M. Chan, and K. ng. "What Controls the Lamellar Orientation at the Surface of Polymer Films during Crystallization?" In: *Macromolecules* 41 (Mar. 2008), pp. 2548–2553. DOI: 10.1021/ma7021309.

[61] J. Schultz. "The crystallization and morphology of melt-miscible polymer blends". In: *Frontiers of Chemistry in China* 5 (Sept. 2010), pp. 262–276. DOI: 10.1007/s11458-010-0211-8.

[62] C. Ye et al. "Inter-spherulitic/inner-spherulitic localization of PBSU during crystallization of PVDF in PVDF/PBSU blend". In: *Journal of Polymer Science* 58 (May 2020), pp. 1699–1706. DOI: 10.1002/pol.20190232.

UNIVERSITÉ CATHOLIQUE DE LOUVAIN
École polytechnique de Louvain
Rue Archimède, 1 bte L6.11.01, 1348 Louvain-la-Neuve, Belgique | **www.uclouvain.be/epl**